Eur. Phys. J. C (2025) 85:1434
https://doi.org/10.1140/epjc/s10052-025-14695-9

THE EUROPEAN PHYSICAL JOURNAL C

Regular Article - Experimental Physics

Measurement of high-mass $t\bar{t}\ell^+\ell^-$ production and lepton flavour universality-inspired effective field theory interpretations at $\sqrt{s} = 13$ TeV with the ATLAS detector

The ATLAS Collaboration*

CERN, 1211 Geneva 23, Switzerland

Received: 9 April 2025 / Accepted: 28 August 2025

Abstract Measurements of $t\bar{t}\ell^+\ell^-$ production in the region of high dilepton invariant mass with effective field theory (EFT) interpretations are presented. They are performed using final states with three isolated leptons (electrons or muons) and are based on $\sqrt{s} = 13$ TeV proton–proton collision data with an integrated luminosity of 140 fb^{-1}, recorded from 2015 to 2018 with the ATLAS detector at the Large Hadron Collider. Measurements of the $t\bar{t}\,\ell^+\ell^-$ signal strength and cross-section upper-limits are performed inclusively in lepton flavour and separately for electrons and muons. The study also aims to probe anomalous four-fermion interactions including to test for possible lepton flavor universality violation. No significant deviations from the Standard Model predictions are observed and the measurements are interpreted through the EFT formalism to provide new constraints on the relevant operators.

Contents

P. Dervan, J. Khubua, U. Mallik, I. P. J. Shipsey: Deceased.

* e-mail: atlas.publications@cern.ch

1 Introduction

The top quark as the heaviest fundamental particle has a unique role in testing the Standard Model (SM) and electroweak (EW) symmetry breaking. The study of rare processes involving the production of top quarks and heavy bosons is interesting in its own right as a test of the SM electroweak sector at high energy. This also offers a window on to couplings between top quarks and bosons that cannot be directly tested elsewhere in particle collisions. The production of a top–antitop quark pair in association with a Z boson, $t\bar{t}\,Z$, is an example of such a process. One of the cleanest signatures of this process is where the Z boson decays leptonically, $t\bar{t}\,Z \to t\bar{t}\,\ell^+\ell^-$. Measurements of this process, where the Z boson is on-shell, $O(10)$ GeV from the Z mass, have recently been performed at the Large Hadron Collider (LHC) [1] by ATLAS and CMS [2–4] inclusively and at the differential level. This process gives direct sensitivity to the t–Z coupling, which is important as deviations from the SM could be a sign of new physics effects in the EW symmetry breaking mechanism. Several beyond the SM (BSM) models predict such deviations [5–12].

Off-shell $t\bar{t}\,\ell^+\ell^-$ production, where the opposite-sign same-flavour lepton pair originates from the Z/γ^* decay, has not yet been measured by ATLAS. This process is also highly interesting as it gives sensitivity to the effective $t\bar{t}\,\ell^+\ell^-$ cou-

Published online: 18 December 2025

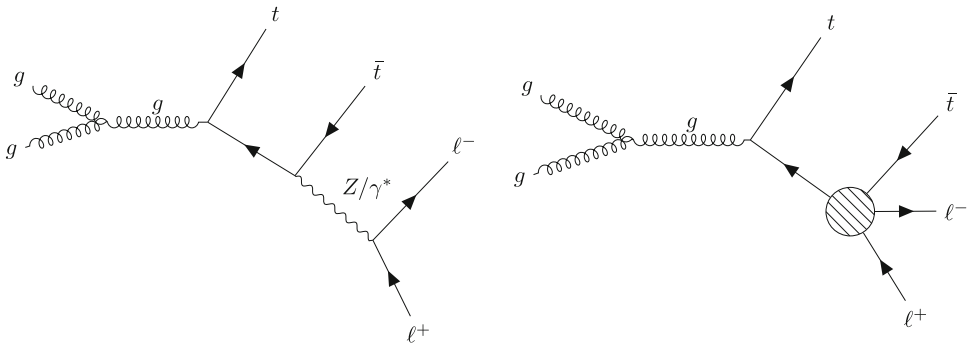

Fig. 1 Representative Feynman diagrams for $t\bar{t}\,\ell^+\ell^-$ **a** in the SM and **b** with an effective vertex

Table 1 Definitions are given of the relevant dimension-6 SMEFT operators. The convention for notation used follows that of Ref. [30], where relevant $SU(2)_L$ indices are represented by k and p, r represent flavour indices. The `top` flavour assumptions are used. Relevant for this measurement is that each of the seven top–lepton operators have corresponding three flavour-diagonal Wilson Coefficients (WCs) denoted $c_{X,i}$ with $i = 1, 2, 3$ an index running over the lepton generations, for a given operator, X. The handedness, left (L) and right (R), of the quarks and leptons in the interaction vertices is given

Operator	Definition	Description
O_{te}	$(\bar{e}_p\gamma_\mu e_r)(\bar{t}\gamma^\mu t)$	R-handed leptons and R-handed quarks in the $t\bar{t}\ell^+\ell^-$ vertex
O_{Qe}	$(\bar{Q}\gamma_\mu Q)(\bar{e}_p\gamma^\mu e_r)$	R-handed leptons and L-handed quarks in the $t\bar{t}\ell^+\ell^-$ and $b\bar{b}\ell^+\ell^-$ vertices
O_{tl}	$(\bar{l}_p\gamma_\mu l_r)(\bar{t}\gamma^\mu t)$	L-handed leptons and R-handed quarks in the $t\bar{t}\ell^+\ell^-$ vertex
O^1_{Ql}	$(\bar{l}_p\gamma_\mu l_r)(\bar{Q}\gamma^\mu Q)$	L-handed leptons and L-handed quarks in the $t\bar{t}\ell^+\ell^-$ and $b\bar{b}\ell^+\ell^-$ vertices, weak-singlet
O^3_{Ql}	$(\bar{l}_p\sigma^i\gamma_\mu l_r)(\bar{Q}\sigma^i\gamma^\mu Q)$	L-handed leptons and L-handed quarks in the $t\bar{t}\ell^+\ell^-$ and $b\bar{b}\ell^+\ell^-$ vertices, weak-triplet
O^1_{leQt}	$(\bar{l}^j_p e_r)\epsilon_{jk}(\bar{Q}^k t)$	Mixed L-/R-handed quarks and leptons in the $t\bar{t}\ell^+\ell^-$, $t\bar{b}\ell^+\ell^-$ and $b\bar{b}\ell^+\ell^-$ vertices, scalar
O^3_{leQt}	$(\bar{l}^j_p\sigma_{\mu\nu}e_r)\epsilon_{jk}(\bar{Q}^k\sigma^{\mu\nu}t)$	Mixed L-/R-handed quarks and leptons in the $t\bar{t}\ell^+\ell^-$, $t\bar{b}\ell\nu$, $\bar{t}b\ell\nu$ and $b\bar{b}\ell^+\ell^-$ vertices, tensor

pling. It is possible to more generically probe possible BSM contributions to these kinds of couplings in the context of effective field theories (EFTs) [13,14]. Figure 1 shows Feynman diagrams for $t\bar{t}\,\ell^+\ell^-$ production in the SM and a possible effective vertex that affects the coupling of interest. The $t\bar{t}\,\ell^+\ell^-$ type of coupling is poorly constrained in existing measurements probing EFT couplings relating to the top quark [15]. High-mass $t\bar{t}\,\ell^+\ell^-$ events are particularly sensitive to such couplings, the impact of the relevant EFT operators strongly increasing with energy [14], motivating a dedicated measurement.

Furthermore, some of the most intriguing evidence for new physics has come from anomalies observed in lepton flavour universality (LFU) tests in B-hadron decays into a D^* and lepton-neutrino pair [16–23]. These measurements have highlighted the importance of probing LFU in general, and there is a commonality in couplings which means anomalies in the B-sector could also be manifest in the top quark sector [24–29].

Therefore, the target of this analysis is to make dedicated measurements of $t\bar{t}\,\ell^+\ell^-$, $(\ell = e, \mu)$, with a focus on the high dilepton invariant mass region. This is achieved by selecting events with three isolated leptons with additional requirements on jet activity to provide a region pure in $t\bar{t}\,\ell^+\ell^-$ production. The three-lepton selection provides a balance between high purity, worsened with a two-lepton selection, and reasonable data statistics, worsened by a four-lepton selection. Many aspects of the analysis are built upon the previous ATLAS measurement of $t\bar{t}\,Z$ production [2] with several extensions to deal with the relatively larger background contributions away from the Z boson mass peak. Measurements of the $t\bar{t}\,\ell^+\ell^-$ signal strength, $\mu(t\bar{t}\,\ell^+\ell^-) = \sigma\,(\text{obs})/\sigma\,(\text{SM})$, and cross-section upper limits are made inclusively in lepton flavour and separately for electrons and muons. These measurements are used to search for new physics entering via four-fermion top quark–lepton EFT operators in the SMEFT [30] formalism, with the `top` flavour assumptions. The relevant operators, considering only those of dimension-6, are shown in Table 1 and the effect of these operators is parameterised as a function of their corresponding Wilson Coefficients (WCs) assuming a mass scale, $\Lambda = 1$ TeV, that characterizes the beyond the SM dynamics. The operators, and WCs, can be treated as flavour-inclusive (no differentiation between lepton flavours), or flavour-split (with individual operators per lepton flavour). Both interpretations are considered in this measurement. Additionally, to probe any possible LFU violation that could be present, an analysis of the flavour-relative WCs, the dif-

ference between the flavour-split electron and muons WCs, is tested for the first time at the LHC. The final outcome is measurements of the relevant WCs in flavour-inclusive, flavour-split and flavour-relative scenarios looking for deviations from the SM and setting limits on possible new physics.

The paper is structured as follows: Sect. 2 outlines the ATLAS detector, Sect. 3 provides an overview of the data and MC samples used in the measurements, and Sect. 4 details the object reconstruction and selection. Section 5 describes the signal region definitions and provides a description of the strategy to estimate backgrounds, an overview of the systematic uncertainties is given in Sect. 6, the results are presented in Sect. 7 and conclusions are given in Sect. 8.

2 ATLAS detector

The ATLAS detector [31] at the LHC covers nearly the entire solid angle around the collision point.[1] It consists of an inner tracking detector surrounded by a thin superconducting solenoid, electromagnetic and hadronic calorimeters, and a muon spectrometer incorporating three large superconducting air-core toroidal magnets.

The inner-detector system (ID) is immersed in a 2 T axial magnetic field and provides charged-particle tracking in the range of $|\eta| < 2.5$. The high-granularity silicon pixel detector covers the vertex region and typically provides four measurements per track, the first hit generally being in the insertable B-layer (IBL) installed before Run 2 [32,33]. It is followed by the SemiConductor Tracker (SCT), which usually provides eight measurements per track. These silicon detectors are complemented by the transition radiation tracker (TRT), which enables radially extended track reconstruction up to $|\eta| = 2.0$. The TRT also provides electron identification information based on the fraction of hits (typically 30 in total) above a higher energy-deposit threshold corresponding to transition radiation.

The calorimeter system covers the pseudorapidity range $|\eta| < 4.9$. Within the region $|\eta| < 3.2$, electromagnetic calorimetry is provided by barrel and endcap high-granularity lead/liquid-argon (LAr) calorimeters, with an additional thin LAr presampler covering $|\eta| < 1.8$ to correct for energy loss in material upstream of the calorimeters. Hadronic calorimetry is provided by the steel/scintillator-tile calorimeter, segmented into three barrel structures within $|\eta| < 1.7$, and two copper/LAr hadronic endcap calorimeters. The solid angle coverage is completed with forward copper/LAr and tungsten/LAr calorimeter modules optimised for electromagnetic and hadronic energy measurements respectively.

The muon spectrometer (MS) comprises separate trigger and high-precision tracking chambers measuring the deflection of muons in a magnetic field generated by the superconducting air-core toroidal magnets. The field integral of the toroids ranges between 2.0 and 6.0 T m across most of the detector. Three layers of precision chambers, each consisting of layers of monitored drift tubes, cover the region $|\eta| < 2.7$, complemented by cathode-strip chambers in the forward region, where the background is highest. The muon trigger system covers the range $|\eta| < 2.4$ with resistive-plate chambers in the barrel, and thin-gap chambers in the endcap regions.

The luminosity is measured mainly by the LUCID–2 [34] detector that records Cherenkov light produced in the quartz windows of photomultipliers located close to the beampipe.

Events are selected by the first-level trigger system implemented in custom hardware, followed by selections made by algorithms implemented in software in the high-level trigger [35]. The first-level trigger accepts events from the 40 MHz bunch crossings at a rate below 100 kHz, which the high-level trigger further reduces in order to record complete events to disk at about 1.25 kHz.

A software suite [36] is used in data simulation, in the reconstruction and analysis of real and simulated data, in detector operations, and in the trigger and data acquisition systems of the experiment.

3 Data and simulated event samples

The full Run 2 data sample, collected in pp collisions during the years 2015–2018 and corresponding to a luminosity of 140 fb^{-1} is used. Only events from time periods in which LHC beams were stable and all ATLAS detectors were operational are selected [37]. The uncertainty in the combined 2015–2018 integrated luminosity is 0.83% [38], obtained using the LUCID-2 detector [34] for the primary luminosity measurements, complemented by measurements using the inner detector and calorimeters The average number of interactions per bunch crossing, $\hat{\mu}$, ranges from 0.5 to approximately 80 and has a mean of 33.7.

The data were collected using a combination of single-electron and single-muon triggers, with requirements on the lepton candidates to maintain high efficiency across the full momentum range while controlling the trigger rates [35,39–41]. For electrons the trigger thresholds were $p_{\mathrm{T}} = 26$, 60 and 140 GeV, whereas for muons the thresholds were $p_{\mathrm{T}} = 26$ and

[1] ATLAS uses a right-handed coordinate system with its origin at the nominal interaction point (IP) in the centre of the detector and the z-axis along the beam pipe. The x-axis points from the IP to the centre of the LHC ring, and the y-axis points upwards. Polar coordinates (r, ϕ) are used in the transverse plane, ϕ being the azimuthal angle around the z-axis. The pseudorapidity is defined in terms of the polar angle θ as $\eta = -\ln\tan(\theta/2)$ and is equal to the rapidity $y = \frac{1}{2}\ln\left(\frac{E+p_z}{E-p_z}\right)$ in the relativistic limit. Angular distance is measured in units of $\Delta R \equiv \sqrt{(\Delta y)^2 + (\Delta\phi)^2}$.

Table 2 The configurations used for event generation of signal and background processes. The samples in black indicate those used as the nominal configurations, those in grey and parentheses are used to estimate the systematic uncertainties

Process	Generator	ME order	Parton shower	PDF	Tune
$t\bar{t}\ell^+\ell^-$	MG5_aMC	NLO	Pythia 8	NNPDF3.0nlo	A14
	(MG5_aMC)	(NLO)	(Herwig 7)	(NNPDF3.0nlo)	(H7-UE-MMHT)
	(MG5_aMC)	(NLO)	(Pythia 8)	(NNPDF3.0nlo)	(A14 Var3c)
$t\bar{t}W$	Sherpa 2.2.10	MePs@Nlo	Sherpa	NNPDF3.0nnlo	Sherpa default
	(MG5_aMC)	(FxFx NLO)	(Pythia 8)	(NNPDF3.0nlo)	(A14)
	(Powheg)	(NLO)	(Pythia 8)	(NNPDF3.0nlo)	(A14)
	(Powheg)	(NLO)	(Herwig 7)	(NNPDF3.0nlo)	(H7-UE-MMHT)
$t\bar{t}W$ (EW)	Sherpa 2.2.10	LO	Sherpa	NNPDF3.0nnlo	Sherpa default
	(MG5_aMC)	(LO)	(Pythia 8)	(NNPDF3.0nlo)	(A14)
$t\bar{t}H$	MG5_aMC	NLO	Pythia 8	NNPDF3.0nlo	A14
$t\bar{t}t\bar{t}$	MG5_aMC	NLO	Pythia 8	NNPDF3.1nlo	A14
$t\bar{t}$	Powheg-BOX	NLO	Pythia 8	NNPDF3.0nlo	A14
	(Powheg-BOX)	NLO	(Herwig 7)	(NNPDF3.0nlo)	(H7-UE-MMHT)
	(Powheg-BOX $2h_{\text{damp}}$)	NLO	(Pythia 8)	(NNPDF3.0nlo)	(A14)
	(Powheg-BOX)	NLO	(Pythia 8 $p_{\text{T,hard}} = 1$)	(NNPDF3.0nlo)	(A14)
$t\bar{t}t$	MG5_aMC	LO	Pythia 8	NNPDF2.3lo	A14
$V, VV, qqVV, VVV$	Sherpa 2.2.2(1)	MePs@Nlo	Sherpa	NNPDF3.0nnlo	Sherpa default
$Z \to \ell^+\ell^-$	Sherpa 2.2.1	MePs@Nlo	Sherpa	NNPDF3.0nnlo	Sherpa default
$Z\gamma$	Sherpa 2.2.4	MePs@Nlo	Sherpa	NNPDF3.0nnlo	Sherpa default
VH	Pythia 8	LO	Pythia 8	NNPDF2.3lo	A14
$t\bar{t}WW$	MG5_aMC	LO	Pythia 8	NNPDF2.3lo	A14
$t\bar{t}\gamma$	MG5_aMC	NLO	Pythia 8	NNPDF3.0nlo	A14
$t\bar{t}Z(\to qq, \nu\nu)$	MG5_aMC	NLO	Pythia 8	NNPDF3.0nlo	A14
$t\ell^+\ell^- q, tWZ$	MG5_aMC	NLO	Pythia 8	NNPDF2.3lo	A14

50 GeV. Isolation requirements were applied to the triggers with the lowest p_{T} thresholds of 26 GeV for electrons and muons.

Samples of simulated events are produced using Monte Carlo (MC) techniques to model the different SM processes. The estimate of the $t\bar{t}\,\ell^+\ell^-$ signal and most considered backgrounds is based upon these simulations. More details of the event generation are given in the following paragraphs and are summarised in Table 2, with the samples in black, or in parentheses, indicating those used as the nominal configurations, or to estimate the systematic uncertainties, respectively. Several data-driven corrections are applied to the estimated backgrounds and detailed in Sect. 5.

After generating events for each process of interest, the detector response was modelled by either a full simulation of the ATLAS detector based on Geant4 [42,43] or a fast simulation (AtlFast 2) relying on parameterised showers in the calorimeter [44]. The latter was only used for the modelling of some rare background processes and the modelling of processes with alternative generators (see Sect. 6). Additional simulated pp collisions, generated with Pythia8.186 [45] using parameter values from the A3 tune [46], are overlaid to model the effects of both the in-time and out-of-time pile-up. Events are weighted such that the pile-up distribution reflect the number of additional interactions observed in data. All simulated events are processed using the same reconstruction algorithms and analysis chain as the data. Corrections are applied so that the object reconstruction and identification efficiencies, energy scales and energy resolutions in simulation match those determined from data, with uncertainties described in Sect. 6.

The SM signal process, associated production of a top–antitop pair with a pair of same-flavour opposite-charge leptons, is modelled using the MadGraph5_aMC@NLO 2.8.1 [47] (MG5_aMC) generator that provides matrix elements (MEs) at next-to-leading-order (NLO) in the strong coupling constant α_{s} with the `NNPDF3.0NLO` [48] parton distribution function (PDF) set. The functional form of the renormalization and factorization scales (μ_{r}, μ_{f}) is set to the default scale $0.5 \times \sum_i \sqrt{m_i^2 + p_{\text{T},i}^2}$, where the sum runs over all the particles generated from the matrix element calculation. Top quarks are decayed at leading-order (LO) using MadSpin [49,50] to preserve all spin correlations. The top-quark mass is set to 172.5 GeV, in this sample and for all other samples involving top-quarks. The events are interfaced with Pythia 8.244 [51] for the parton shower and its hadronization, using the `A14` set of tuned parameters [52] and the `NNPDF2.3LO` PDF set. The decays of bottom and charm hadrons are simulated using the EvtGen 1.7.0 package [53], as are all other samples in the measurement showered using Pythia. The (on-shell) $t\bar{t}\,Z$ cross-section is calculated at NLO quantum chromodynamics (QCD) and NLO EW accuracy using MadGraph5_aMC@NLO and reported in Ref. [54]. The γ^* contribution and the Z/γ^* interference are taken into account with an off-shell (down to $m(\ell^+\ell^-) = 5$ GeV) correction calculated in Ref. [55].

The predicted value at 13 TeV is $0.88^{+0.09}_{-0.10}$ pb, where the uncertainties arise from variations of renormalization and factorization scales, PDF uncertainties, and α_s variations.

For top-quark–antiquark pair production with a Wboson ($t\bar{t}W$), the SHERPA 2.2.10 [56,57] generator and default parton shower are used at NLO accuracy in QCD, with multi-leg merging of up to one additional parton at NLO and up to two additional partons at LO (MEPS@NLO setup [58–61] with a merging scale of 30 GeV). The NNPDF3.1NNLO [62] PDF set is used. Additionally a LO QCD sample is also generated with SHERPA 2.2.10 but for the electroweak production of the $t\bar{t}Wj$ final state. The cross-sections of these QCD and EW $t\bar{t}W$ samples are scaled separately to the predictions of Ref. [63].

Events featuring the production of a $t\bar{t}$pair in association with a SM Higgs boson with a mass of 125 GeV ($t\bar{t}H$) are simulated using NLO matrix elements in MADGRAPH5_AMC@NLO 2.6.0 with the NNPDF3.0NLO PDF set. The samples are showered with PYTHIA 8.230 using the A14 tune.

The production of single top quarks in association with a Z/γ^* in the dileptonic decay mode, including off-shell effects down to $m(\ell^+\ell^-) = 5$ GeV, $t\ell^+\ell^-q$, is modelled using the MADGRAPH5_AMC@NLO 2.9.5 generator at NLO. The production of single top quarks in association with a $W$and a Zboson (tWZ) is modelled using MADGRAPH5_AMC@NLO 2.2.2 at NLO [64], both using the NNPDF3.0NLO PDF set. The $t\ell^+\ell^-q$ events are interfaced with PYTHIA 8.245 and the tWZ events with PYTHIA 8.212, using the A14 tune and the NNPDF2.3LO PDF set. The $t\ell^+\ell^-q$ sample is simulated in the four-flavour scheme (therefore including an additional b-quark in the final state) and normalised to a cross section obtained in the five-flavour scheme.

The possible overlap between events in the $t\bar{t}Z$ sample and tWZ sample, which can occur when a NLO real emission is included in the latter, must be removed. The tWZ sample follows the "diagram removal 1" (DR1) scheme described in Ref. [64] and ignores any Feynman diagrams containing two resonant top quarks for the overlap removal.

The background production of $t\bar{t}$events is modelled using the POWHEG BOX 2 generator [65] at NLO with the NNPDF3.0NLO PDF set and the damping factor h_{damp} set to 1.5 times the top quark mass. The events are interfaced with PYTHIA 8.230 using the A14 tune and the NNPDF2.3LO PDF set.

Diboson plus jets processes featuring the production of three charged leptons and one neutrino or four charged leptons (denoted by WZ+jets or ZZ+jets, respectively) are simulated using the SHERPA 2.2.2 generator. Multiple matrix elements are matched and merged with the SHERPA parton shower based on the Catani–Seymour dipole factorisation scheme [66,67] using the MEPS@NLO prescription. The virtual QCD correction for matrix elements at NLO accuracy are provided by the OPENLOOPS library [68–70]. The production of $W$and Zbosons with multiple jets (V+jets) is simulated similarly but with the SHERPA 2.2.1 generator.

Smaller backgrounds featuring Higgs boson production in association with a Wor Z(VH), four top-quark production ($t\bar{t}t\bar{t}$), triple top-quark production ($tt\bar{t}$), the production of a $t\bar{t}$pair with two Wbosons ($t\bar{t}WW$), the production of a $t\bar{t}$pair with two neutrinos or two jets and processes with three heavy gauge bosons (WWW, WWZ, WZZ and ZZZ) are simulated with the settings shown in Table 2.

Additional MC samples encapsulating EFT effects are produced at LO in QCD for the $t\bar{t}\ell^+\ell^-$ process, using the MADGRAPH 2.9.3 generator and PYTHIA 8.245 parton shower (with the default A14 tune settings). They include the SMEFTsim 3.0 model [30] as the Universal Feynman Output (UFO) model, in the M_W electroweak input scheme [71] with the top flavour restrictions (5FS). The nominal events are generated according to the SM, and the MADGRAPH reweighting module [72] is used to compute a large number of alternative event weights corresponding to the inclusion of dimension-6 EFT vertices and propagators in the production Feynman diagrams.

4 Object identification and reconstruction

Two categories of leptons are defined in the analysis: a looser category referred to as *pre-selected* leptons used for object overlap removal, described later in this section, and to define background-enriched regions; and a tighter category of *signal* leptons used in the selection requirements for most regions, including the signal regions.

Electron candidates are reconstructed from clusters of energy deposits in the electromagnetic calorimeter that are matched to a track in the ID. They are required to satisfy $p_{\text{T}} > 7$ GeV, $|\eta| < 2.47$ and a likelihood-based electron identification [73] is required. Further requirements for pre-selected electrons and signal electrons used in the analysis are summarised in the following. For pre-selected electrons, the LooseAndBLayerLH identification is used, while for the signal electrons used in one of the analysis regions, MediumLH is required. Electrons in the LAr transition region ($1.37 < |\eta| < 1.52$) are rejected and requirements on the transverse (d_0) and longitudinal (z_0) impact parameter are applied to mitigate the contribution from electrons from reducible backgrounds and pile-up. To suppress electrons with incorrect charge assignment, a boosted decision tree (BDT) discriminant based on calorimeter and tracking quantities is applied and finally a procedure to resolve ambiguities between overlapping reconstructed objects is applied. The electron energy scale is calibrated using data [73,74]. The associated scale factors (SFs) for electron reconstruc-

tion, identification, and isolation are applied in MC, to correct for the efficiency differences between data and simulation [75]. The associated scale factors (SFs) for electron reconstruction, identification, and isolation are applied in MC, to correct for the efficiency differences between data and simulation. The selection criteria above largely suppress the contribution from non-prompt leptons arising from hadron decays that contain bottom- or charm-quarks (referred to as "heavy-flavour (HF) non-prompt leptons"). However, as this measurement is particularly sensitive to such backgrounds, signal electrons have a further selection requirement from a non-prompt lepton BDT discriminant [76], based on isolation and lifetime information about a track-based jet that matches the selected light lepton.

Muon candidates are reconstructed from MS tracks matched to ID tracks in the pseudorapidity range of $|\eta| < 2.5$ and are required to have $p_{\mathrm{T}} > 7$ GeV. Both the pre-selected and signal muons are required to satisfy `Medium` identification requirements defined in Refs. [77,78]. Selections on the longitudinal and transverse impact parameters are applied as for the electrons and also, as with electrons, the pre-selected muons have no isolation requirements, while the signal muons selected for the analysis need to satisfy the non-prompt lepton BDT isolation working point requirements. The associated SFs for identification and isolation are applied as multiplicative factors to the MC event weight, to correct for the efficiency differences between data and MC.

Jets are reconstructed using the anti-k_t jet algorithm [79] as implemented in the FastJet package [80] with the distance parameter R set to 0.4. Topological clusters are used [81] along with ID tracks as input to the particle flow reconstruction algorithm [82]. The algorithm removes calorimeter energy deposits due to charged hadrons and uses more precise measurements of their momenta from tracks instead. Jets are calibrated [83] with the `EMPFlow` scheme applying the jet area pile-up corrections. The jets are kept only if they have $p_{\mathrm{T}} > 25$ GeV and are inside a pseudorapidity range of $|\eta| < 2.5$. The `JetVertexTagger` (JVT) [84] is employed to mitigate pile-up effects, and specifically rejects any selected jets after the overlap removal procedure with $p_{\mathrm{T}} < 60$ GeV, $|\eta| < 2.4$ and for which `JVT` < 0.5 (`Tight` working point).

Jets containing a b-hadron, referred to as b-jets, are identified with the `DL1r` b-tagging algorithm [85]. A working point (WP) corresponding to an 85% b-tagging efficiency is used in most regions for pre-selections. Exclusive bins in the b-tagging discriminant corresponding to different b-tagged jet identification efficiencies are also used, as pseudo-continuous b-tagging (PCBT). This allows the possible use of different calibrated b-tagging WPs in defining regions.

The missing transverse momentum $\vec{p}_{\mathrm{T}}^{\,\mathrm{miss}}$ (with magnitude $E_{\mathrm{T}}^{\mathrm{miss}}$) is defined as the negative vector sum of the p_{T} of all selected and calibrated objects in the event, including a term to account for the momenta of soft particles that are not associated with any of the selected objects [86]. This soft term is calculated from inner-detector tracks matched to the primary vertex, which makes it more resilient to contamination from pile-up interactions.

After the identification, overlaps between objects are resolved to avoid double-counting of physics objects. Pre-selected leptons and jets are used for this procedure. The sequence of operations that are performed to solve these ambiguities, referred to as the overlap removal (OR) procedure, is applied in the following steps. First, the lowest p_{T} of any electron pair found with a shared track or an overlapping calorimeter cluster is removed. Next, any muon matched with significant calorimeter energy deposits and found to share a track with an electron is removed, then any subsequent electron found to share a track with a muon is removed. Any jet found within a ΔR of 0.2 of an electron is removed, then any electron found within a ΔR of 0.4 of a jet is removed. Any jet with fewer than three tracks associated with it and found within a ΔR of 0.2 of a muon is removed. Any jet with fewer than three tracks associated with it that has a muon inner-detector track ghost-associated [85,87] to it, is removed. Finally, any muon later found within a ΔR of 0.4 of a jet is removed.

5 Analysis strategy

Regions enriched in the signal of $t\bar{t}\,\ell^+\ell^-$ at high invariant mass of the $\ell^+\ell^-$ pair are defined to obtain sensitivity to the targeted four-fermion EFT operators. The three-lepton final state is utilised due to the high $t\bar{t}\,\ell^+\ell^-$ purity that can be obtained.

Several aspects of the analysis are built on a previous ATLAS measurement of $t\bar{t}\,Z$ production [2]. The main changes are to deal with the relatively larger background contributions away from the Z boson mass peak. These changes are the use of a tighter lepton isolation requirement and the addition of new control regions defined to target the relevant backgrounds.

Background contamination in the signal regions (SRs) is due to contributions from several SM processes which can feature the same final state particles as the signal process. These are broadly split into two categories based on the source of the reconstructed leptons: backgrounds where the three final state leptons are prompt (discussed in Sect. 5.3), and those where at least one of the leptons is labelled as *fake* as it originates from a non-prompt source (described in Sect. 5.4).

Dedicated control regions (CRs) enriched in the dominant backgrounds are defined to constrain these backgrounds from data. There are in total thirteen of these CRs. In eight of them only the overall normalisation enters into the fit: three

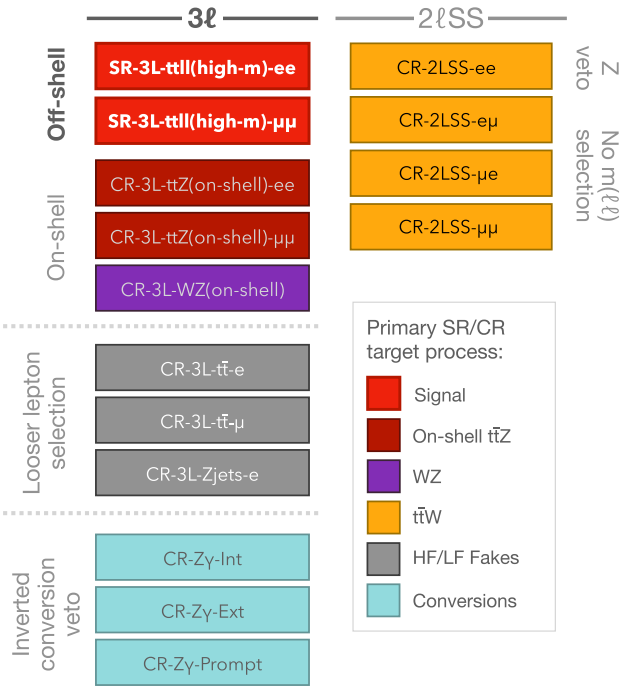

Fig. 2 Schematic diagram of the signal and control regions in the fits. Labelled are their main defining features and the signal or background process they are primarily targetting

that target the normalisation of the events with a fake electron from photon conversions (F-e-IntConv, F-e-ExtConv); two to constrain events with non-prompt fake electrons and muons originating from heavy-flavour hadrons (F-e-HF, F-m-HF); and three targeting on-shell $t\bar{t}Z$ and diboson (VV) production. There are five further CRs which are binned in a dedicated observable: one to constrain electrons from light-flavour hadrons (F-e-LF); and four primarily sensitive to $t\bar{t}W$, $t\bar{t}H$ and electrons with misidentified charge (charge-flip) in addition to the previous backgrounds. The charge-flip background is estimated by using a data-driven approach in the 2LSS CRs and all other backgrounds are estimated purely from simulation. An overview of the signal and CRs is provided schematically in Fig. 2 and comparisons to data are provided in Fig. 3c.

The binned yields (templates) of some simulated processes, namely on-shell $t\bar{t}Z$ and the $t\bar{t}W$, VV, F-e-HF, F-m-HF, F-e-LF, F-e-IntConv, F-e-ExtConv backgrounds are adjusted via normalisation factors that are determined by performing a likelihood fit to data across these dedicated CRs simultaneously with the signal regions.

5.1 Event categorisation

In the following, simulated events are categorised according to different criteria. If all leptons in the events are categorised as prompt, the event is classified according to its process (rare processes are grouped as 'Other', including $t\bar{t}t\bar{t}$, $tt\bar{t}$, VH, WW, VVV, $t\bar{t}WW$, $t\bar{t}qq$ and $t\bar{t}\nu\nu$). If one lepton is categorised as non-prompt, the event is classified according to the type of the non-prompt lepton.

Leptons are categorised as prompt if generator-level information, using a ΔR matching between generator- and detector-level information, identifies them as electrons or muons originating from a τ-lepton or W, Z or H boson. Otherwise the leptons are categorised as fake and attributed to one of the following categories using their generator-level information. Heavy flavour fakes are those identified as originating from a strange, charmed or bottom hadron. Light flavour fakes are similarly those originating from a light baryon or meson, for example from pions. Charge-flip fakes are prompt electrons with mis-identified charge. Conversion electrons are those from photon conversion and are further categorised into two sub-categories; internal photon conversions, from $\gamma^* \to e^+e^-$, and external conversions, photon conversions in the detector material. Finally, conversion muons are those originating from a muon internal photon conversion.

5.2 Signal selection

Events entering the signal region are required to contain exactly three signal leptons with transverse momentum greater than 27 GeV, 20 GeV and 15 GeV and least one opposite-sign (charge) same-flavour (OSSF) lepton pair. Additionally all OSSF pairs are required to have a minimal invariant mass of 10 GeV in order to remove contributions from low mass resonances. Finally at least three jets including at least one b-tagged jet at the 85 % efficiency b-tagging working point are required. The mass of the OSSF pair closest to the Z mass (referred to as $m(\ell^+\ell^-)$ in the following) has to be above 101.2 GeV, targeting specifically the high-mass $t\bar{t}\,\ell^+\ell^-$ region. Additionally none of the leptons should be flagged as conversion candidates as described in Sect. 5.4.

To increase the sensitivity to the flavour specific EFT WCs, the SR is split into two regions corresponding to $t\bar{t}\,e^+e^-$ and $t\bar{t}\,\mu^+\mu^-$ by requiring at least two electrons or two muons respectively.

The resulting SRs (summarised in Table 3 and shown in Fig. 4) with the event yields for each process detailed in Table 4 are then binned in the $m(\ell^+\ell^-)$ distribution. This variable is found to give the highest sensitivity to the four-fermion EFT operators. As the impact of these EFT operators grows with energy, an optimised binning in the highest $m(\ell^+\ell^-)$ bins increases the sensitivity.

5.3 Prompt backgrounds

The dominant background in the SRs is from the $t\bar{t}W$ process, for which the normalisation is treated as a free floating parameter in the fit mainly constrained by dedicated CRs (detailed in Table 5). These regions require events to contain exactly

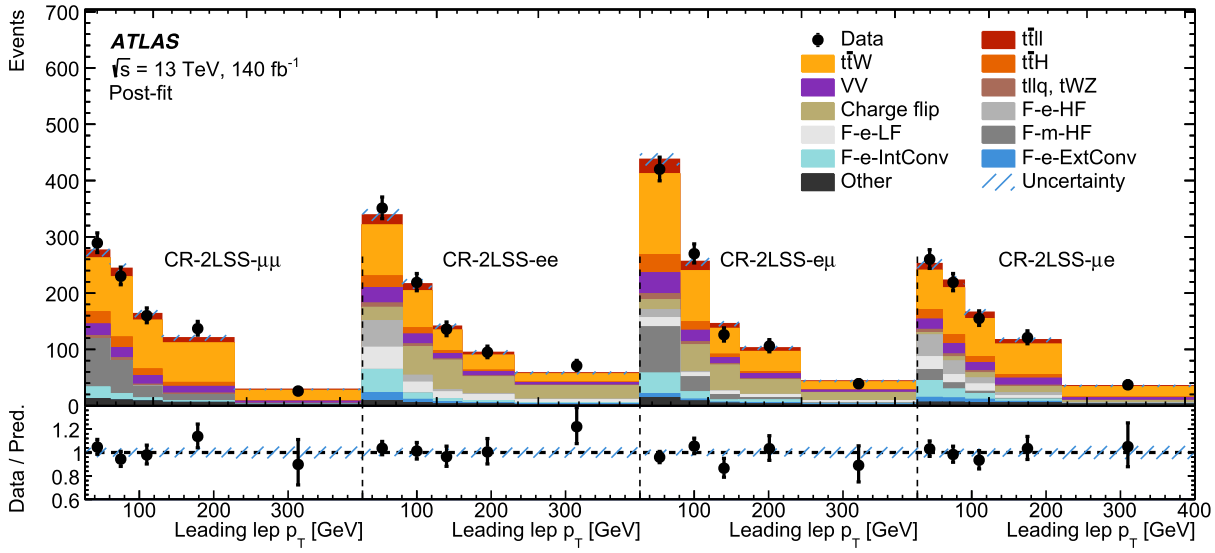

(a)

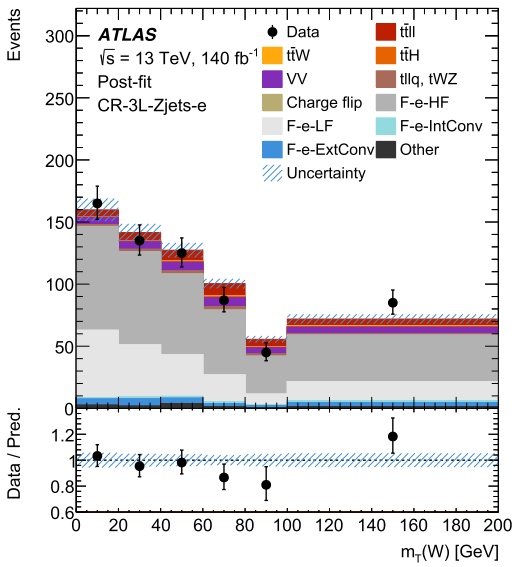

(b)

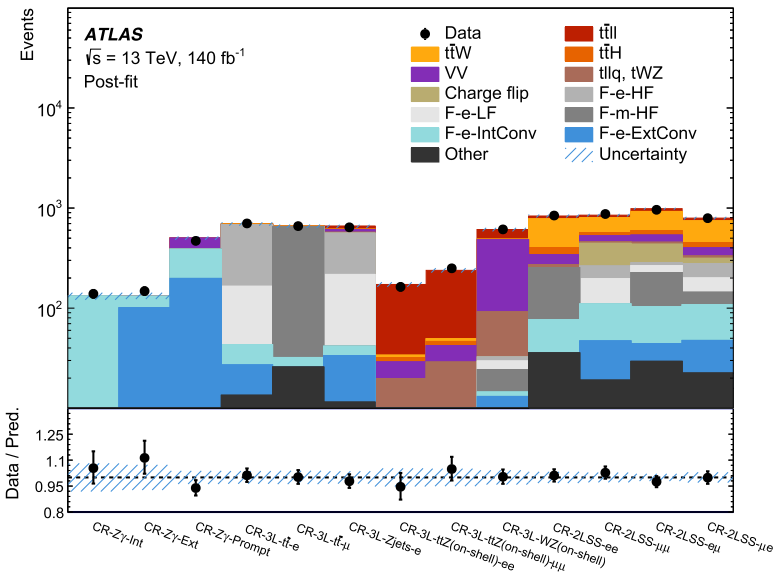

(c)

Fig. 3 Event yields as a function of the relevant kinematic variables in **a** the CR-2LSS CRs, **b** the CR-3L-Zjets-e CR, and **c** inclusively in all CRs considered in the analysis after the fit to data. The uncertainty band includes the statistical as well as the systematical components. In figures **a** and **b** the highest bin is inclusive and contains events above the bin edge

two same-sign (SS) leptons that do not fulfill the conversion criteria and satisfy $p_{\mathrm{T}} > 27\,\mathrm{GeV}$ and $p_{\mathrm{T}} > 20\,\mathrm{GeV}$ respectively. Additionally at least three jets are required, where at least one is b-tagged at the 85 % efficiency WP. Events are split into 2μ, $2e$, $e\mu$ and μe regions, where for the latter two regions the order defines the flavour of the leading and subleading p_{T} leptons respectively. For the $2e$ regions events with an invariant mass of the two leptons around the Z peak are vetoed to suppress backgrounds containing charge-flip leptons. The 2LSS CRs are binned in leading lepton p_{T} as this leads to additional EFT sensitivity from high-mass $t\bar{t}\,\ell^+\ell^-$ events where one lepton is not reconstructed, with the p_{T} of the leading lepton characterising the energy of the event well.

Additionally two CRs targeting contributions from the $t\bar{t}\,Z$ and the WZ+jets processes are obtained by using the SR selection requirements, but requiring the invariant mass of the OSSF pair within the Z peak, $81.2\,\mathrm{GeV} < m(\ell^+\ell^-) <$

Table 3 Summary of the selection criteria for the 3L SRs and CRs. The neural network used for the splitting the $t\bar{t}\,Z$ CR and the WZ+jets CR is introduced in Sect. 5.3

$t\bar{t}\ell^+\ell^-$	$t\bar{t}Z$	WZ+jets
exactly 3 signal leptons $p_T(\ell_1) > 27$ GeV, $p_T(\ell_2) > 20$ GeV, $p_T(\ell_3) > 15$ GeV ≥ 1 OSSF pair $m(\ell^+\ell^-) > 10$ GeV for all OSSF pairs $N_{\text{jets}} \geq 3$ and $N_{b-\text{tagged jets}} \geq 1$ at the 85% efficiency WP none of the leptons passes the conversion cuts		
$m(\ell^+\ell^-) > m_Z + 10$ GeV for $m(\ell^+\ell^-)$ closest to m_Z	$\lvert m(\ell^+\ell^-) - m_Z\rvert \leq 10$ GeV for $m(\ell^+\ell^-)$ closest to m_Z	
—	$DNN(VV) < 0.22$	$DNN(VV) \geq 0.22$
—	$DNN(t\ell^+\ell^-q) < 0.43$	—
SR-3L-ttll(high-m)-ee SR-3L-ttll(high-m)-$\mu\mu$	CR-3L-ttZ(on-shell)-ee CR-3L-ttZ(on-shell)-$\mu\mu$	CR-3L-WZ(on-shell)

101.2 GeV. The $t\bar{t}\,Z$ and the WZ+jets region are split by a requirement on a Deep Neural Network (DNN) output score, classifying how likely it is that an event is a diboson event. This DNN is the same as that used in the on-shell $t\bar{t}\,Z$ analysis [2]. It corresponds to a 3-class DNN discrimination among $t\bar{t}\,Z$, $t\ell^+\ell^-q$ and diboson events and the requirements used for splitting the regions were defined by optimising the signal sensitivity. In this analysis, the $t\ell^+\ell^-q$ region is disregarded. As in the $t\bar{t}\,Z$ analysis, events entering the $t\bar{t}\,Z$ CR are required to satisfy the $DNN(t\ell^+\ell^-q) < 0.43$ and $DNN(VV) < 0.22$ requirements, while events entering the WZ+jets CR need to satisfy the $DNN(VV) \geq 0.22$ requirement. Compared with the $t\bar{t}\,Z$ analysis, the tighter requirement of a b-tagged jet at the 60 % tagging working point is removed in the WZ+jet CR (while still requiring at least one b-tagged jet at 85 %), in order to get a WZ+jets CR targetting all flavour contributions instead of a specific $WZ + b$ CR to better match the composition in the high-mass SR. Similar to the SR, the $t\bar{t}\,Z$ region is split into $t\bar{t}\,e^+e^-$ and $t\bar{t}\,\mu^+\mu^-$. All three of these CRs only contain one bin, with the selections summarised in Table 3.

5.4 Non-prompt backgrounds

This measurement is sensitive to events containing non-prompt fake leptons as they constitute a reducible background in the two same-sign lepton and three-lepton regions. Even after dedicated object selection criteria to reduce them, the large $t\bar{t}$ cross-section relative to the rare top-quark pro-

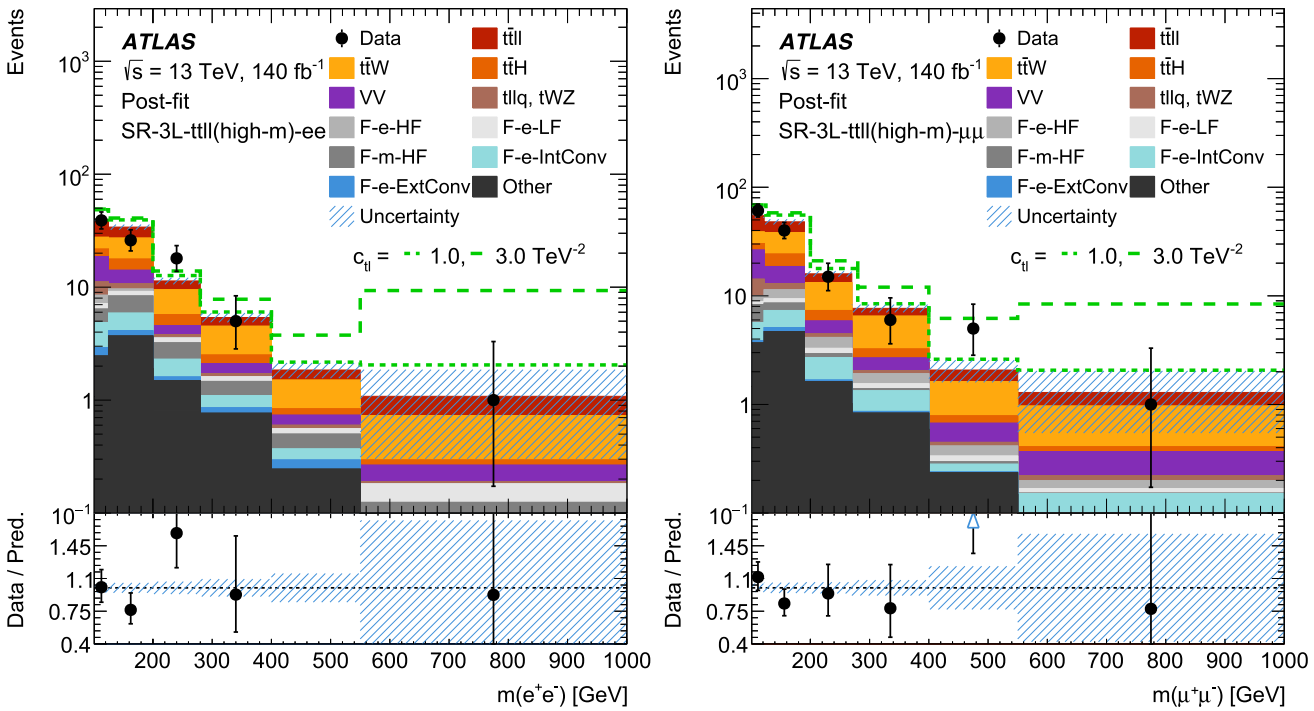

(a) (b)

Fig. 4 Distribution of **a** the $t\bar{t}\,e^+e^-$ and **b** the $t\bar{t}\,\mu^+\mu^-$ SRs binned in the dilepton invariant mass closest to the Z mass after the fit to data where the c_{tl} WC is the primary parameter of interest. The uncertainty bands include statistical and systematical uncertainties. In both figures the highest bin is inclusive and contains events above the bin edge. The green dotted and dashed lines show the total expectation in the presence of an EFT signal corresponding to $c_{tl} = 1.0$ and $c_{tl} = 3.0$ respectively. The triangle symbol in the ratio panel indicates that a data point is above the limit of the frame

Table 4 Expected yields from MC of the different processes in the $t\bar{t}\,e^+e^-$ and $t\bar{t}\,\mu^+\mu^-$ SRs, SR-3L-ttll(high-m)-ee and SR-3L-ttll(high-m)-$\mu\mu$, and are compared to the observed yields in data. The indicated uncertainties include those from the limited dataset size as well as all other systematic uncertainties, discussed in Sect. 6, before the fit to data

	SR-3L-ttll(high-m)	
Process	ee	$\mu\mu$
$t\bar{t}\,\ell^+\ell^-$	19.4 ± 1.4	27.4 ± 1.2
$t\bar{t}\,W$	19.9 ± 1.9	27.5 ± 3.5
$t\bar{t}\,H$	8.6 ± 0.8	11.9 ± 1.1
WZ	12 ± 5	20 ± 8
ZZ	1.4 ± 0.6	2.4 ± 1.0
$t\ell^+\ell^-q, tWZ$	4.2 ± 0.8	6.5 ± 1.2
F-e-ExtConv	1.2 ± 1.1	0.67 ± 0.04
F-e-IntConv	4.9 ± 1.1	6.2 ± 2.6
F-e-HF	2.1 ± 1.5	4.5 ± 0.7
F-e-LF	2.4 ± 0.7	2.0 ± 0.5
F-m-HF	5.8 ± 1.5	4.2 ± 0.5
Other (fakes)	4.4 ± 2.1	6 ± 4
Other (non-fakes)	4.6 ± 1.6	5.7 ± 1.9
Total	91 ± 7	124 ± 9
Data	89	128

Table 5 Summary of the selection criteria for the 2LSS CRs

2μ	$2e$	$e\mu$	μe
exactly 2 signal leptons			
$p_{\mathrm{T}}(\ell_1) > 27\,\mathrm{GeV}$, $p_{\mathrm{T}}(\ell_2) > 20\,\mathrm{GeV}$			
SS lepton pair			
$N_{\mathrm{jets}} \geq 3$ and $N_{b-\mathrm{tagged\,jets}} \geq 1$ at the 85% efficiency WP			
none of the leptons passes the conversion requirements			
2 muons	2 electrons $\lvert m(\ell^+\ell^-) - m_Z \rvert > 10\,\mathrm{GeV}$	$p_{\mathrm{T}}(e) > p_{\mathrm{T}}(\mu)$	$p_{\mathrm{T}}(\mu) > p_{\mathrm{T}}(e)$
CR-2LSS-$\mu\mu$	CR-2LSS-ee	CR-2LSS-$e\mu$	CR-2LSS-μe

cesses probed in this analysis means that this background can be significant.

The SRs have too few MC events to use for the fake lepton backgrounds. The default estimations, using signal leptons, are replaced by those produced with the looser preselection lepton criteria applied. The distribution with the preselection lepton requirement is then scaled to the integral of the distribution with the signal selection, with the shape of the template in $m(\ell^+\ell^-)$ agreeing very well between both of the distributions. This method significantly reduces uncertainty in the fake templates due to limited MC events.

Three regions target the HF and LF fakes: the events are required to contain exactly three leptons, two signal leptons and one lepton that satisfies the preselection lepton definition but fails the signal lepton definition, with transverse momentum greater than 27 GeV, 20 GeV and 15 GeV and the sum of charges of plus or minus one. Additionally, there have to be at least three jets, with at least one of them b-tagged at an efficiency working point of 85 %. Events are split into three regions based on requirements on the leptons. If the event contains an OSSF pair, has $E_{\mathrm{T}}^{\mathrm{miss}} < 80\,\mathrm{GeV}$ and the non-signal lepton is an electron it enters the CR-3L-Zjets-e region. If the event does not have an OSSF pair, depending on whether the non-signal lepton is an electron or muon it enters the CR-3L-$t\bar{t}$-e or CR-3L-$t\bar{t}$-μ region respectively. While the $t\bar{t}$-e/μ CRs only contain one bin, the Zjets-e CR is binned in the transverse mass of the lepton–$E_{\mathrm{T}}^{\mathrm{miss}}$ system, $m_{\mathrm{T}}(W)$. The latter binning is taken from the on-shell $t\bar{t}\,Z$ analysis [2] and is found to give a good discrimination of the LF electron fakes.

To create regions with relatively high event counts of conversion fakes and high purity a $Z(\rightarrow \mu\mu\gamma)$ CR is implemented. The events are required to contain three tight leptons, of which two are an opposite sign muon pair and one is an electron. The $E_{\mathrm{T}}^{\mathrm{miss}}$ must be smaller than 50 GeV and the event should contain no b-tagged jets at a WP of 85 %. Additionally the invariant mass of the two muons is required to be above 20 GeV but outside the Z boson peak defined as 10 GeV around the Z mass. The trileptonic invariant mass is then required to lie inside this Z mass window. Events are added to the CRs if the electron has a reconstructed conversion vertex [73]. If the conversion radius $>$ and $m(\ell^+\ell^-) < 100\,\mathrm{MeV}$ (where the mass is calculated relative to the conversion vertex) the event enters the external conversion CR, CR-$Z\gamma$-Ext. If the conversion radius < 20 mm and $m(\ell^+\ell^-) < 100\,\mathrm{MeV}$ (where the mass is calculated relative to the primary vertex) it enters the internal conversion CR, CR-$Z\gamma$-Int. Additionally to these two CRs selecting conversions, the prompt $Z\gamma$ region is added as a CR, where, similar to the SR and the other prompt background CRs, events with conversion like leptons are vetoed. This prompt region emulates a selection closer to the SR and the 2LSS CRs as it contains events that fail to satisfy the conversion rejection criteria. All three of these conversion CRs only contain one bin. As the conversion variables cannot be computed for muons, the CRs do not include conversion muons but only conversion electrons. As the physics process between internal electron and muon conversions is the same, the computed normalisation factor is applied to electrons and muons.

Finally, a data-driven charge-flip estimate is used in the 2LSS CRs. Charge-flip rates are derived for electrons in p_{T} and η bins using two $Z \rightarrow ee$ regions, one with opposite-sign electrons and one with same-sign electrons. The regions select events with exactly two signal electrons, at most one jet and no b-tagged jet. Additionally a Z peak region is defined with $71\,\mathrm{GeV} < m(e^+e^-) < 101\,\mathrm{GeV}$, where a background subtraction is performed, assuming linear backgrounds, by subtracting the event yields from two side-band regions ($61\,\mathrm{GeV} < m(e^+e^-) < 71\,\mathrm{GeV}$ and $101\,\mathrm{GeV} < m(e^+e^-) < 111\,\mathrm{GeV}$). The charge-flip rates are

then obtained by maximising a likelihood function where the charge-flip rates in each lepton p_{T} and η bin are the parameters of interest. The charge-flip estimate in the 2LSS CR are then estimated by applying these rates to a region with identical selection except with the SS switched to an OS one.

Distributions for all the CRs considered in the analysis are shown, after the fit to data, in Fig. 3.

6 Systematic uncertainties

The systematic uncertainties described in the following are separated into detector systematic uncertainties, which are related to the reconstruction and identification of physics objects in the detector, theory uncertainties related to the modelling of the different processes and uncertainties associated with the estimate of the fake-lepton background.

6.1 Detector-related uncertainties

The luminosity estimate has a relative uncertainty of 0.83%, derived following the prescriptions described in Ref. [38] and is applied to all processes determined from MC simulations.

An uncertainty related to the SFs used for MC to account for differences in pile-up distributions between MC and data is applied. This uncertainty is obtained by re-scaling the $\hat{\mu}$ value in data by $1/0.99$ and $1/1.07$, around the central SF of $1/1.03$. The uncertainty in the jet energy scale (JES) is derived combining information from test-beam data, LHC collision data and simulation [83]. The jet energy resolution (JER) is measured separately for data and MC using two in situ techniques [83]. A systematic uncertainty is defined as the quadratic difference between the jet energy resolutions for data and simulation. To determine this the energy of jets in the simulation is smeared by this residual difference, and the changes in the normalisation and shape of the final discriminant are compared with the default prediction. Uncertainties associated with the jet vertex tagging (JVT) are applied and account for the choice of MC generator and residual contamination from pile-up jets after pile-up suppression.

The effects of uncertainties in efficiencies for the heavy-flavour identification of jets by the b-tagging algorithm were evaluated. These efficiencies are measured from data and depend on the jet flavour and kinematic quantities of the jets. The SFs and their uncertainties are applied to each jet in the simulation depending on its flavour, p_{T} and η [85]. Additionally, flavour tagging extrapolation uncertainties for jets with p_{T} above the calibration range are considered.

Uncertainties associated with the electron efficiency SFs are considered for the reconstruction and trigger uncertainties (observed to be largely sub-dominant) and the electron identification and isolation SFs. The accuracy of the momentum scale and resolution of electrons in simulation is checked using reconstructed distributions of the $Z \to e^+e^-$ and $J/\psi \to e^+e^-$ masses. Small discrepancies are observed between data and simulation, and corrections for the energy scale and resolution are applied. A detailed description can be found in Ref. [73].

SFs are also applied to correct for the difference between data and simulation in the muon identification, isolation and trigger efficiency, as well as track-to-vertex association [78] and associated uncertainties in these SFs are considered. Momentum scale and resolution corrections are applied for muons in the simulation. Uncertainties in both the momentum scale and resolutions in the MS and the ID are considered and varied separately. Additional uncertainties are considered to account for the charge-dependent scale correction applied on data. A more detailed description can be found in Ref. [78].

Uncertainties are applied to the scale and resolution of the soft track component of the missing transverse energy. They are derived from the agreement between data and MC of the p_{T} balance between the hard and soft $E_{\mathrm{T}}^{\mathrm{miss}}$ components.

6.2 Modelling uncertainties

To obtain the uncertainties in $t\bar{t}\,\ell^+\ell^-$ related to missing higher-order effects, μ_{r} and μ_{f} are simultaneously varied up and down by a factor of two and compared with the nominal predictions. Uncertainties on the PDF are evaluated following the recommended `PDF4LHC` prescription [88]. The uncertainties associated with the parton showering algorithm and the underlying event model[2] are evaluated by comparing the nominal samples, generated with MadGraph5_aMC@NLO interfaced to Pythia 8, to equivalent samples interfaced to Herwig7 [89,90] instead. Uncertainties related to the modelling of initial-state radiation are obtained from the up and down `Var3c` variations of the Pythia `A14` tune in dedicated alternative samples.

Uncertainties in $t\bar{t}\,W$ due to missing higher-order QCD corrections in the modelling are considered by including simultaneous variations of μ_{r} and μ_{f} by a factor of two up and down. Matrix element and parton shower uncertainties are estimated comparing the nominal Sherpa prediction with MadGraph5_aMC@NLO interfaced with Pythia 8 using the FxFx merging prescription [91] for the QCD part and with MadGraph5_aMC@NLO+Pythia 8 for the EW part. An additional parton shower uncertainty is considered using the relative difference between Powheg+Pythia 8 and Powheg+Herwig 7 predictions. Finally a normalisation-only uncertainty in the relative yields of the EW sample within the QCD+EW $t\bar{t}W$ templates is applied by varying the EW fraction between the values of the Sherpa and the MG5_aMC@NLO prediction.

[2] In the following only, referred to as "parton shower uncertainty".

Uncertainties in the modelling of the $WZ \to \ell\ell\ell\nu$ (WZ+jets) and $ZZ \to \ell\ell\ell\ell$ (ZZ+jets) processes related to the matrix element matching scale, resummation scale and recoil scheme are estimated by using alternative "truth-level" samples. The μ_r and μ_f scale and PDF uncertainties are evaluated following the same prescription as used for the $t\bar{t}\,\ell^+\ell^-$ sample. In addition, normalisation uncertainties are applied to the different additional jet flavour components: light quarks and gluons (l), charm quarks (c) and bottom quarks (b). An uncertainty of 30% is applied to $WZ + l$ and $WZ + c$ and of 50% to the $WZ + b$ components of the WZ+jets background. Similarly, normalisation uncertainties of 10%, 30% and 50% are applied to the $ZZ + l$, $ZZ + c$ and $ZZ + b$ components of the ZZ+jets background.

A cross-section normalisation uncertainty of 14% is assigned to the $t\ell^+\ell^- q$ process, based on the dedicated ATLAS measurement presented in Ref. [92]. Uncertainties in the parton shower model, initial-state radiation, scale and PDF variations are obtained in a similar way to the $t\bar{t}\,\ell^+\ell^-$ sample.

For the tWZ background process, a flat 30 % normalisation uncertainty is added. No parton shower uncertainty is considered, but instead the difference relative to an alternative diagram removal scheme (DR2) [64] is treated as a modelling uncertainty. The DR2 scheme, additionally to the nominal DR scheme, considers the interference terms (at the level of squared amplitudes) between single- and double-resonant $t\bar{t}$ production. As with the processes described above, PDF and scale uncertainties are taken into account.

Only theory uncertainties in the normalisation of the cross-section of the $t\bar{t}\,H$ process are considered. These follow the scale and PDF uncertainties prescribed in Ref. [54].

The $t\bar{t}$ process is the dominant contribution to the fake backgrounds. While the normalisation of the fake backgrounds is obtained in the template fit, shape systematic uncertainties are considered for $t\bar{t}$ separately for each of the fake background contributions. The parton shower uncertainty is estimated by using the alternative POWHEG+HERWIG 7 sample. Additionally uncertainties in the value of h_{damp} are covered by using an alternative sample with twice the value of the default h_{damp} (set to $1.5m_t$). Finally, a sample with the POWHEG-specific parameter in PYTHIA 8 set to $p_{\text{T,hard}} = 1$ (compared with the nominal sample with $p_{\text{T,hard}} = 0$) is considered for the matrix element uncertainty.

For other minor background processes, such as HV, VVV, $t\bar{t}\,WW$ or multi-top-quark ($tt\bar{t}$) production, a common conservative overall normalisation uncertainty of 50% is applied. These background components contribute to about 2.5% of the total event yields in the signal regions. For $t\bar{t}\,t\bar{t}$, a normalisation uncertainty of $+70\%$ -15% is applied based on the measurement in Ref. [93]. Additionally, a parton shower uncertainty is obtained similarly to the $t\bar{t}\,\ell^+\ell^-$ sample.

6.3 Non-prompt background uncertainties

A normalisation uncertainty of 30 % is applied to the simulation-based charge-flip templates in the 3ℓ regions, based on the largest uncertainties seen in the data-driven estimate, and a conservative 50 % uncertainty is assigned to the fake leptons that do not fall into the categories defined in Sect. 5.1.

An uncertainty is applied to the estimate of the fake templates in the SRs, consisting of the difference between the distribution of the tight and loose selection (taking half of the difference between the event yield predicted by the tight and the loose selection in every bin and mirroring it).

Three uncertainties are considered for the data-driven charge-flip estimate: an uncertainty due to the limited event numbers of the charge-flip rate extraction samples, an uncertainty due to the choice of binning used to derived those rates and an uncertainty in the extrapolation from a Z boson-enriched region to a $t\bar{t}$-enriched region.

7 Results

Results are presented in two interpretations, one with a focus on measurement of the SM $t\bar{t}\,\ell^+\ell^-$ process in the signal region, and one using the EFT formalism to probe for signs of BSM physics. In both of these cases maximum-likelihood fits of the signal and background predictions in the signal and control regions to the event yields in data are performed. The likelihood function $\mathcal{L}(\vec{s}, \vec{\lambda}, \vec{\theta})$ is constructed as a product of Poisson probability terms over all bins considered in the measurement, and depends on the signal, $\vec{s}$, the normalisation factors for several backgrounds (see Sect. 5), $\vec{\lambda}$, and a set of nuisance parameters (NP), $\vec{\theta}$, encoding systematic uncertainties in the signal and background expectations [94,95]. Systematic uncertainties can impact the estimated signal and background rates, the migration of events between categories, and the shape of the fitted distributions. Both $\vec{s}$ and $\vec{\lambda}$ are treated as free parameters in the likelihood fit. The NPs $\vec{\theta}$ allow variations of the expectations for signal and background according to the systematic uncertainties, subject to Gaussian-shape constraints in the likelihood fit. Their fitted values represent the deviations from the nominal expectations that are needed to provide the best fit to the data. Statistical uncertainties in each bin due to the limited size of the simulated event samples are taken into account with dedicated parameters, using the Beeston–Barlow "lite" technique [96].

7.1 SM results

Measurements are reported of the SM $t\bar{t}\,\ell^+\ell^-$ signal strength, $\mu(t\bar{t}\,\ell^+\ell^-)$, inclusive in lepton flavour and split into separate electron and muon channels. The signal strength is defined as

Table 6 Results of the measurement of the SM $t\bar{t}\,\ell^+\ell^-$ signal strength and significance for the signal region with $m(\ell^+\ell^-) > m_Z + 10$ GeV. Also the expected and observed 95% confidence level (CL) upper limits on a possible BSM signal for the very high mass region with $m(\ell^+\ell^-) > 550$ GeV are shown

	$m(\ell^+\ell^-) > m_Z + 10$ GeV		$m(\ell^+\ell^-) > 550$ GeV	
	$\mu(t\bar{t}\,\ell^+\ell^-)$	Significance	Exp. 95% CL upper limit	Obs. 95% CL upper limit
$t\bar{t}\,e^+e^-$	$0.8^{+0.6}_{-0.6}$	1.4σ	25.4 ab	26.9 ab
$t\bar{t}\,\mu^+\mu^-$	$1.1^{+0.5}_{-0.5}$	2.5σ	27.5 ab	26.0 ab
$t\bar{t}\,\ell^+\ell^-$	$1.0^{+0.4}_{-0.4}$	2.9σ	30.5 ab	30.8 ab

the ratio of the $t\bar{t}\,\ell^+\ell^-$ yield in the SR measured in the data divided by the predicted yield at detector level in the same SR. These provide a direct indication of the agreement of the data with the SM expectation before moving on to consider an interpretation searching for BSM contributions. The percentage of simulated $t\bar{t}\,\ell^+\ell^-$ events passing the detector-level SR selection which have generated $m(\ell^+\ell^-) > m_Z + 10$ GeV is approximately 60%.

However, for BSM signals that contribute primarily at high mass the cross-section for the full invariant mass range, $m(\ell^+\ell^-) > m_Z + 10$ GeV, has limited use, therefore model-independent visible cross-section upper limits for a BSM contribution on top of SM $t\bar{t}\,\ell^+\ell^-$ are provided for the highest $m(\ell^+\ell^-)$ bins (> 550 GeV) at the 95% confidence level (CL) [94]. This is equivalent to fitting the highest bin in each of the signal regions shown in Fig. 4. The visible cross-section upper limit is defined by dividing the upper limit on the number of signal events in the high mass bin by the integrated luminosity.

The results are shown in Table 6. The measured signal strengths are all compatible with the SM with a combined observed (expected) $t\bar{t}\,\ell^+\ell^-$ significance of 2.9σ (2.8σ). The combined observed (expected) 95% CL cross-section upper limit for the high mass region, $m(\ell^+\ell^-) > 550$ GeV, is 30.8 ab (30.5 ab). For the $t\bar{t}\,e^+e^-$ channel the observed (expected) significance is 1.4σ (1.7σ) and the 95% CL cross-section upper limit for the high mass region is 26.9 ab (25.4 ab). For the $t\bar{t}\,\mu^+\mu^-$ channel the observed (expected) significance is 2.5σ (2.0σ) and the 95% CL cross-section upper limit for the high mass region is 26.0 ab (27.5 ab).

7.2 EFT interpretation fit

The focus of EFT interpretation of the analysis is the measurement of the WCs of the six four-fermion EFT operators outlined in Sect. 1: O_{tl}, O_{te}, O_{Qe}, O^-_{Ql} ($O^1_{Ql} - O^3_{Ql}$), O^1_{leQt} and O^3_{leQt}. These are considered in flavour-inclusive and flavour-split scenarios, the latter denoted by 11 and 22 indices ($\ell^+\ell^- = ee, \mu\mu = 11, 22$). Fits are performed individually to a single operator at a time (other WCs fixed to 0). A dedicated flavour-relative fit configuration is used to test for LFU-violating signals by testing the difference between electron and muon WCs for each operator, e.g. $\Delta(c_{tl(22)} - c_{tl(11)})$. The primary focus is on results relating to the single operator fits due to a lack of sensitivity to multi-operator fits, which is explained in more detail in Sect. 7.6.

The effect of the EFT operators on the $t\bar{t}\,\ell^+\ell^-$ process is parameterised bin by bin with a second order polynomial function parameterised by the relative change in yield from each operator due to interference with the SM at $\mathcal{O}(\Lambda^{-2})$ (linear) and pure EFT contributions (quadratic, including cross-terms where relevant) at $\mathcal{O}(\Lambda^{-4})$. The EFT contribution approximates higher order QCD effects by scaling the SM EFT prediction at LO in QCD to the SM prediction at NLO in QCD bin-by-bin. Once the EFT parameterisation is obtained, a profile-likelihood fit is performed, where the individual WCs are treated as free floating in the fit to data. Maximum-likelihood fits are performed with the signal parameterised by EFT WCs for each of the scenarios described.

The EFT contributions are only applied to the $t\bar{t}\,\ell^+\ell^-$ signal process, sensitivity to $t\ell^+\ell^-q$ was also investigated but found to be negligible and is therefore neglected. EFT contributions are considered in the on-shell $t\bar{t}\,Z$ process but these contribute very little to the overall sensitivity. This allows the overall $t\bar{t}\,\ell^+\ell^-$ normalisation, $\lambda_{t\bar{t}\,Z}$, to be controlled, primarily from the on-shell CRs, in the fit to data.

Figure 4 shows the signal regions after the fit to data for the c_{tl} WC (other WCs fixed to 0). As expected from the SM fit results, there are no significant deviations from the expected background predictions after the fit to data, the fitted normalisation factors are: $\lambda_{t\bar{t}\,Z} = 1.09 \pm 0.10$, $\lambda_{t\bar{t}\,W} = 1.18 \pm 0.11$, $\lambda_{WZ} = 0.92 \pm 0.26$, $\lambda_{\text{IntCo}} = 1.04 \pm 0.12$, $\lambda_{\text{ExtCo}} = 1.22 \pm 0.15$, $\lambda_{\text{HF}_\mu} = 1.03 \pm 0.11$, $\lambda_{\text{HF}_e} = 0.89 \pm 0.19$, $\lambda_{\text{LF}_e} = 1.84 \pm 0.82$. No significant changes in the results for the background normalisation factors are observed in the fits to other combinations of WCs. The $t\bar{t}\,W$ normalisation factor is higher than unity but compatible with measurements made previously in ATLAS in a similar phase space [97].

The data are in good agreement with the SM expectation within the quoted uncertainty which is dominated by the limited size of the data samples. For the fit to the c_{tl} WC (other

Table 7 Results of the fit to data for each WC fitted individually considering $\mathcal{O}(\Lambda^{-4})$ effects. The best fit value, 68% and 95% confidence intervals for the asymptotic assumption (Asymp. CI) and the coverage calculated from pseudodata (Pseud. CI) are shown

	$\mathcal{O}(\Lambda^{-4})$[TeV^{-2}]				
	Best fit	68% Asymp. CI	68% Pseud. CI	95% Asymp. CI	95% Pseud. CI
c_{tl}	−0.44	[−1.10, 1.24]	[−1.17, 1.31]	[−1.65, 1.80]	[−1.71, 1.86]
c_{te}	−0.45	[−1.05, 1.18]	[−1.21, 1.41]	[−1.57, 1.79]	[−1.64, 1.96]
c_{Qe}	−0.54	[−1.23, 1.19]	[−1.32, 1.32]	[−1.82, 1.83]	[−1.87, 1.88]
c_{Ql}^{-}	0.69	[−0.98, 1.41]	[−1.15, 1.74]	[−1.57, 2.03]	[−1.66, 2.33]
c_{leQt}^{1}	−0.61	[−1.51, 1.50]	[−1.55, 1.54]	[−2.27, 2.27]	[−2.32, 2.33]
c_{leQt}^{3}	−0.12	[−0.26, 0.26]	[−0.27, 0.27]	[−0.37, 0.37]	[−0.38, 0.38]

Table 8 Results of the fit to data for each WC fitted individually considering only $\mathcal{O}(\Lambda^{-2})$ effects. The best fit value and 68% and 95% confidence intervals from the asymptotic assumption (Asymp.) are shown

	$\mathcal{O}(\Lambda^{-2})$[TeV^{-2}]		
	Best fit value	68% Asymp. CI	95% Asymp. CI
c_{tl}	−1.21	[−8.23, 4.22]	[−11.83, 8.62]
c_{te}	−1.42	[−4.45, 1.09]	[−7.94, 3.10]
c_{Qe}	−11.65	[−25.75, 0.98]	[−40.97, 11.53]
c_{Ql}^{-}	−0.16	[−2.66, 1.91]	[−5.58, 3.67]

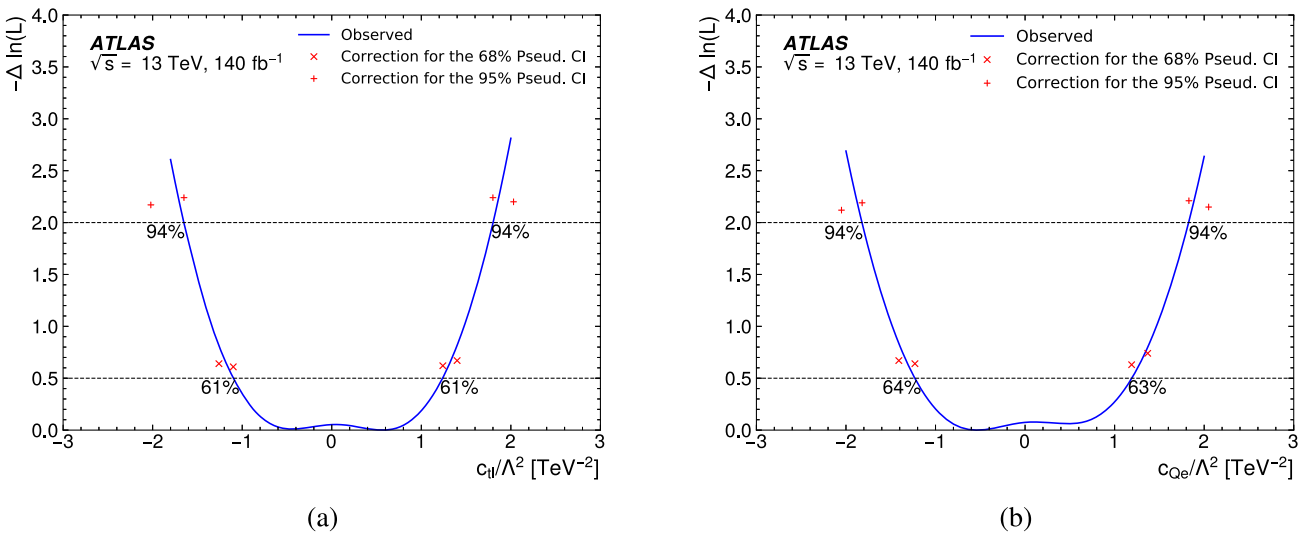

Fig. 5 Scans of the fitted negative log-likelihood value as a function of the WC value for **a** c_{tl} and **b** c_{Qe}. The solid line shows the standard profile likelihood ratio approach, the cross and plus markers show the values of the 68% and 95% coverage, respectively, calculated from the fits to pseudodata (Pseud.)

WCs fixed to 0) the statistical uncertainty due to limited data set size is $^{+1.63}_{-0.60}$ TeV^{-2} compared with the total systematic uncertainty of $^{+0.41}_{-0.28}$ TeV^{-2}. The largest systematic uncertainties are due to the SM $t\bar{t}\,\ell^+\ell^-$ and $t\bar{t}\,W$ modelling, and the limited size of MC samples in some of the high $m(\ell^+\ell^-)$ bins.

The EFT WC values are fitted and further confirm compatibility with the SM as reported in the following.

7.3 EFT flavour-inclusive fit results

The results for the various flavour-inclusive fit configurations described above are shown in Tables 7 and 8 for cases where all EFT effects are considered, $\mathcal{O}(\Lambda^{-4})$, and where only SM interference effects of the EFT operators are considered, $\mathcal{O}(\Lambda^{-2})$, respectively. In the latter case the O_{leQt}^{1} and O_{leQt}^{3} operators are not included as they have no equivalent SM interaction so there is no interference with the SM and sensitivity only arises from the pure EFT contribution.

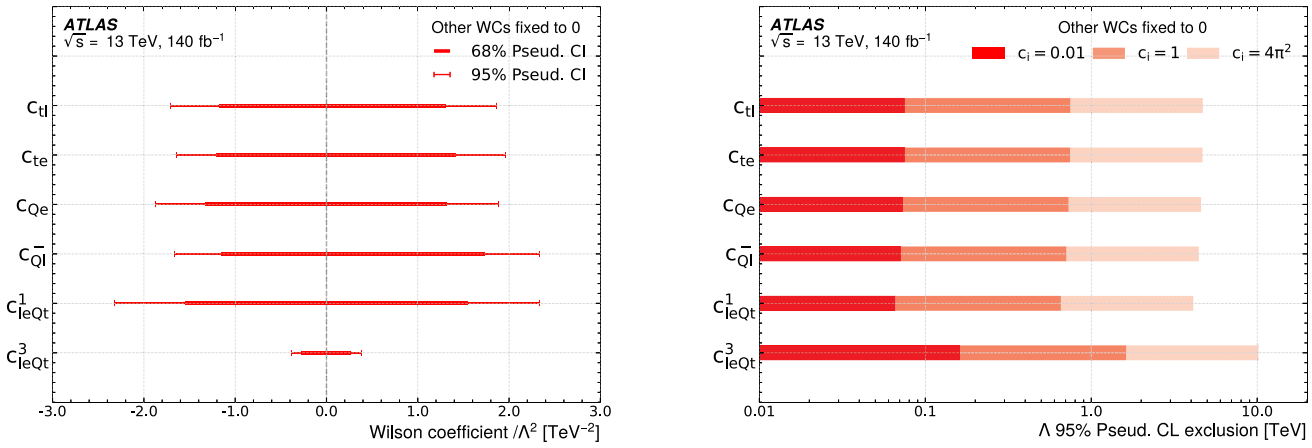

(a) (b)

Fig. 6 Confidence intervals on the WCs for a fit to data with only one WC constrained at a time for **a** the flavour-inclusive WCs and **b** the corresponding 95% exclusion limits on new physics scale Λ for different assumptions on the value of the (dimensionless) coupling. The results have the coverage calculated from pseudodata (Pseud.)

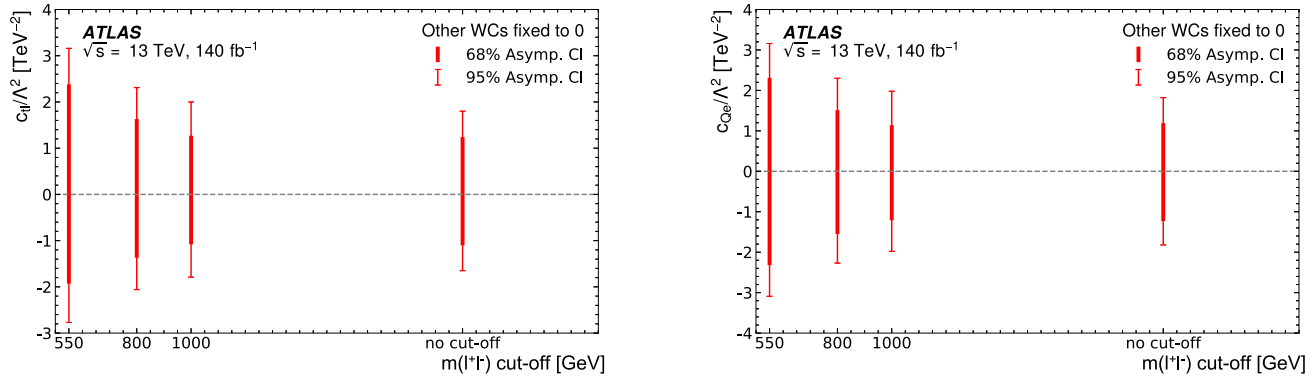

(a) (b)

Fig. 7 The confidence intervals for **a** c_{tl} and **b** c_{Qe} from fits to data for different values of the $m(\ell^+\ell^-)$ upper cut-off. The results use the asymptotic assumption to calculate the intervals (Asymp.)

Table 7 shows the best fit values, 68% and 95% confidence intervals (CIs) from the fit to data including $\mathcal{O}(\Lambda^{-4})$ EFT contributions. All the fitted WC values are compatible with the SM. The dominant uncertainty in all cases is due to the limited data size. Constraints on the O^3_{leQt} operator are tighter than for other operators, this is expected due to the definition of this operator. These limits improve upon previous constraints on these operators from the CMS Collaboration [15].

In the case of EFT paramerisations where the (quadratic) pure-EFT $\mathcal{O}(\Lambda^{-4})$ terms are dominant a breakdown of a key axiom of Wilks' theorem [98] can occur, the profile-likelihood ratio (PLR) may not follow the expected χ^2-distribution [99]. This can lead to coverage in the test statistic different to what is expected in the asymptotic case. The true coverage can be determined with toy pseudodata and adjusting where to read off the CI accordingly. Therefore, additionally to the non-coverage adjusted results (Asymp. CI), results are also given where the 68% and 95% CIs are coverage-adjusted (Pseud. CI) for the fits to data where only a single WC at a time is a free parameter in the fit. This adjustment is calculated by generating toy pseudodata and taking the value of the 68% and 95% percentiles of the fitted pseudodata test statistics. Scans of the fitted negative log-likelihood value as a function of the WC value are shown in Fig. 5 for c_{tl} and c_{Qe}. The solid line shows the negative log-likelihood as a function of the WC, the crosses and plusses show the values of the 68% and 95% coverage calculated from the fits to pseudodata, compared with the coverage value in the asymptotic assumption of a profile likelihood ratio, $-\Delta \ln L = 0.5$ and $-\Delta \ln L = 1.96$. The confidence intervals calculated with the coverage from pseudodata are quoted by interpolating between the markers and giving the intersection with the likelihood scan. The percentage value written in text is

Table 9 Fit results for the considered EFT flavour specific WCs. Results are shown for the 68% and 96% confidence intervals for the asymptotic assumption (Asymp.) and the coverage calculated from pseudodata (Pseud.). In all cases only one EFT operator is considered at a time but both of the corresponding flavour-dependent WCs are constrained at the same time

	$\mathcal{O}(\Lambda^{-4})[\text{TeV}^{-2}]$				
	Best fit	68% Asymp. CI	68% Pseud. CI	95% Asymp. CI	95% Pseud. CI
$c_{tl(11)}$	0.22	$[-1.10, 1.24]$	$[-1.20, 1.36]$	$[-2.23, 2.37]$	$[-2.31, 2.52]$
$c_{tl(22)}$	−0.81	$[-1.57, 1.79]$	$[-1.64, 1.85]$	$[-2.25, 2.49]$	$[-2.28, 2.51]$
$c_{te(11)}$	−0.24	$[-1.19, 1.21]$	$[-1.44, 1.55]$	$[-2.32, 2.47]$	$[-2.48, 3.10]$
$c_{te(22)}$	−0.67	$[-1.40, 1.79]$	$[-1.56, 2.07]$	$[-2.06, 2.52]$	$[-2.09, 2.66]$
$c_{Qe(11)}$	−0.24	$[-1.28, 1.22]$	$[-1.40, 1.31]$	$[-2.52, 2.45]$	$[-2.61, 2.58]$
$c_{Qe(22)}$	−0.89	$[-1.72, 1.77]$	$[-1.76, 1.84]$	$[-2.46, 2.53]$	$[-2.48, 2.55]$
$c^{-}_{Ql(11)}$	0.48	$[-1.00, 1.49]$	$[-1.30, 2.09]$	$[-2.16, 2.81]$	$[-2.30, 3.43]$
$c^{-}_{Ql(22)}$	−0.66	$[-1.46, 1.99]$	$[-1.65, 2.44]$	$[-2.17, 2.78]$	$[-2.45, 3.10]$
$c^{1}_{leQt(11)}$	−0.22	$[-1.57, 1.58]$	$[-1.67, 1.70]$	$[-3.13, 3.13]$	$[-3.12, 3.12]$
$c^{1}_{leQt(22)}$	−1.08	$[-2.21, 2.20]$	$[-2.27, 2.26]$	$[-3.22, 3.22]$	$[-3.21, 3.21]$
$c^{3}_{leQt(11)}$	0.0	$[-0.26, 0.26]$	$[-0.28, 0.27]$	$[-0.50, 0.50]$	$[-0.50, 0.50]$
$c^{3}_{leQt(22)}$	−0.20	$[-0.35, 0.35]$	$[-0.36, 0.35]$	$[-0.48, 0.48]$	$[-0.48, 0.48]$

the actual coverage value at the WC value corresponding to the nominal $-\Delta \ln L = 0.5$ and $-\Delta \ln L = 1.96$ points. The $\mathcal{O}(\Lambda^{-4})$ CIs calculated from pseudodata and the corresponding 95% confidence level limits on the new physics scale, Λ, are also summarised in Fig. 6.

Table 8 shows results of the fit to data considering only $\mathcal{O}(\Lambda^{-2})$ EFT–SM interference contributions. As expected given that no significant deviation from the expectation is observed in the data, the fitted WC values are compatible with the SM. There is only limited sensitivity to this contribution alone, as the energy growth that gives the best sensitivity at high mass comes primarily from $\mathcal{O}(\Lambda^{-4})$ contributions.

It is important to consider the range of EFT validity for measurements which are sensitive to the pure EFT contribution. As suggested by the LHC EFT Working Group [100] clipping can be applied by removing events above a particular $m(\ell^+\ell^-)$ value. Figure 7 shows the results for the c_{tl} and c_{Qe} WCs as a function of different values of the high $m(\ell^+\ell^-)$ cut-off used in the analysis. The clipping values are chosen to be 550 GeV, 800 GeV and 1 TeV. It can be seen that the WC contraints degrade, as expected, when lower cut-offs are applied but that they are rather stable for 1 TeV and above. This gives confidence that the nominal result without clipping can be trusted and does not suffer from issues related to the region of validity of the EFT model. Therefore, the default EFT results are obtained without applying any $m(\ell^+\ell^-)$ cut-off.

7.4 EFT flavour-separated fit results

Table 9 shows the results of the flavour-separated EFT WC fits to data. Due to the limited sensitivity of the $\mathcal{O}(\Lambda^{-2})$ contribution alone results are considered only with full EFT $\mathcal{O}(\Lambda^{-4})$ effects taken into account. The sensitivity is diluted relative to the equivalent flavour-inclusive results, as expected due to the additional degrees of freedom in the fit and reduction in number of sensitive bins per WC, but significant constraining power still remains due to the good lepton flavour identification efficiency of ATLAS. Again, all WCs are compatible with the SM, as expected from the good agreement between data and expectation for each flavour-split signal region. These results are also summarised in Fig. 8.

7.5 EFT lepton flavour universality violation sensitive fits

Flavour-relative fits to data are also performed in the configuration targetting LFU-violation in the EFT effects. This is captured by the difference between the flavour-split WCs for different operators, O_X, defined as $\Delta(c_{[X](22)} - c_{[X](11)})$, that are probed to search for EFT effects that apply preferentially on either electron or muon couplings to the top quark. In these fits the difference between flavours is a free parameter but apply relative to a single-flavour reference WC. A convention is chosen to make the electron flavour WC, $c_{[X](11)}$, the reference, so this is additionally a free parameter in the fit. Table 10 shows the results of the fits to data, in the case $\mathcal{O}(\Lambda^{-4})$ terms are considered and only single operators, O_X, have WCs included in the fit at a time (other WCs fixed to 0). These results are also summarised in Fig. 8.

There is potential for systematic uncertainties to cancel out in the $\Delta(c_{[X](22)} - c_{[X](11)})$, but this analysis is now limited by the available Run 2 data sample size, so it is observed that the sensitivity to the flavour-split WC difference is lower than that of the individual flavour-specific WCs. Nonetheless,

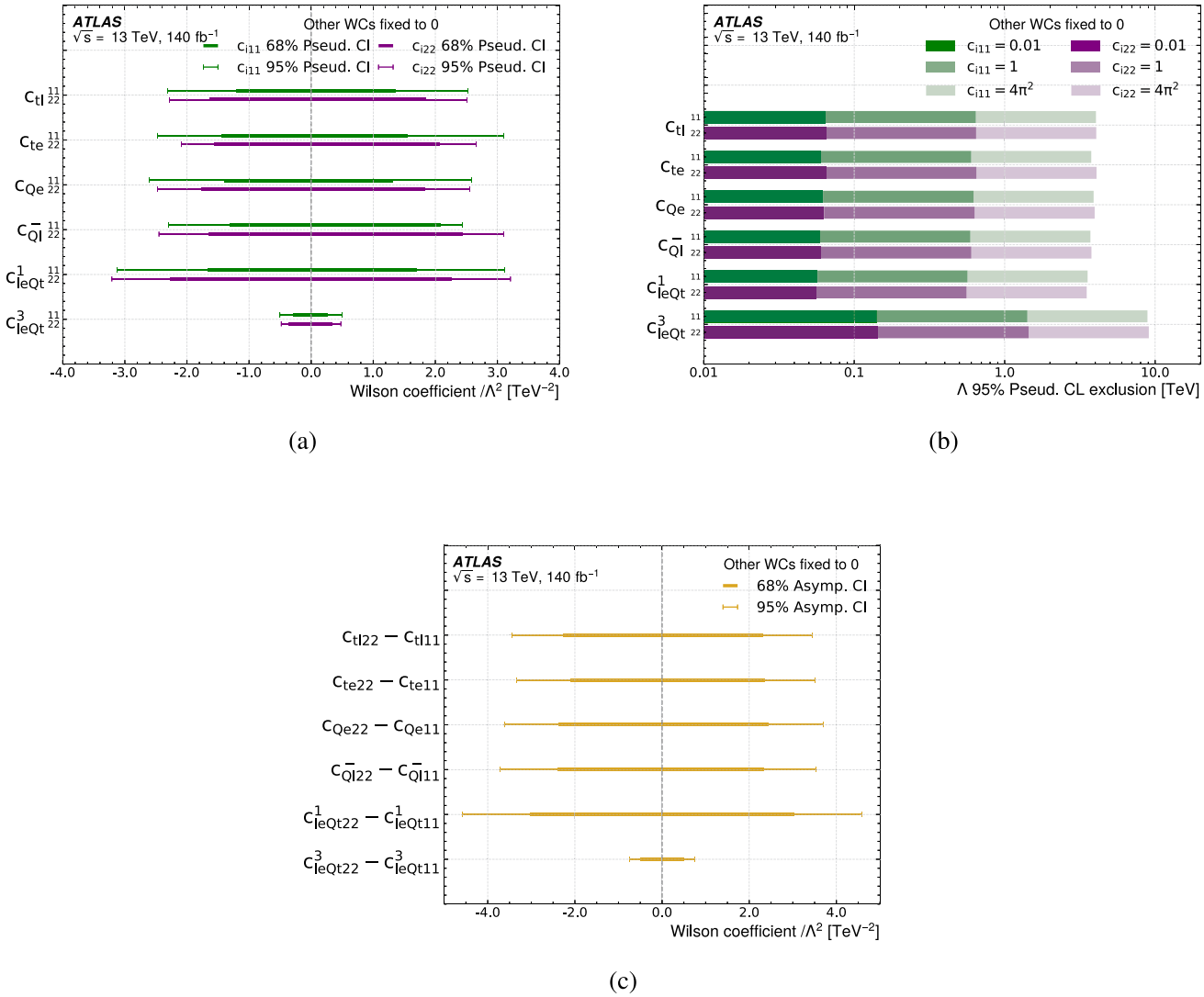

Fig. 8 Confidence intervals on the WCs for a fit to data with only one WC constrained at a time for **a** the flavour-dependent WCs and **b** the corresponding 95% exclusion limits on new physics scale Λ for different assumptions on the value of the (dimensionless) coupling. Both of these results account for the coverage calculated from pseudodata (Pseud.). In addition **c** limits on the difference between flavour dependent WCs per operator are shown. These results use the asymptotic assumption to calculate the intervals (Asymp.)

this marks the first search for LFU-violation for EFT effects using this final state and cancellation of systematic uncertainties is observed which will become valuable with a larger data sample size. For example, systematic uncertainties in backgrounds common to both $t\bar{t}\,e^+e^-$ and $t\bar{t}\,\mu^+\mu^-$ SRs, such as the $t\bar{t}\,W$ and fake lepton backgrounds, are reduced while uncertainties relating specifically one lepton flavour, such as those in the electron isolation SFs, become of higher relative importance.

As with the other results, all fitted WC values are in good agreement with the SM, both for the flavour-split results and for the different WCs between flavours. In most cases the central value of the fitted $\Delta(c_{[X](22)} - c_{[X](11)})$ value corresponds to the calculation based on the results in Table 9, however for c_{tl} and $c^1_{leQt(11)}$ this is not the case. This is due to the double-minimum structure as can be seen in Fig. 5a, where in this case an alternative minimum is preferred. Overall, the confidence intervals are the more meaningful quantities when interpreting the flavour-relative results.

7.6 Discussion of multi-operator EFT fit sensitivity

Despite there being differences in behaviour as a function of $m(\ell^+\ell^-)$ for the different EFT operators of interest it is challenging to simultaneously constrain all six operators of interest. This is expected given that sensitivity comes from only a limited number of high-mass bins. The behaviour of the multi-operator fits is non-trivial as correlations are hidden in the case that the WC values are close to zero, as happens when calculating expected sensitivity with Asimov fits.

Table 10 Results of the fit to data of the difference between the flavour-specific WCs. The results use the asymptotic assumption to calculate the intervals (Asymp. CI)

	$\mathcal{O}(\Lambda^{-4})[\text{TeV}^{-2}]$		
	Best fit	68% Asymp. CI	95% Asymp. CI
$c_{tl(22)} - c_{tl(11)}$	0.79	$[-2.28, 2.32]$	$[-3.44, 3.45]$
$c_{te(22)} - c_{te(11)}$	−0.43	$[-2.10, 2.36]$	$[-3.34, 3.51]$
$c_{Qe(22)} - c_{Qe(11)}$	−0.66	$[-2.39, 2.43]$	$[-3.62, 3.71]$
$c^{-}_{Ql(22)} - c^{-}_{Ql(11)}$	−1.14	$[-2.38, 2.37]$	$[-3.72, 3.54]$
$c^{1}_{leQt(22)} - c^{1}_{leQt(11)}$	−1.32	$[-3.03, 3.03]$	$[-4.58, 4.58]$
$c^{3}_{leQt(22)} - c^{3}_{leQt(11)}$	−0.20	$[-0.50, 0.50]$	$[-0.75, 0.75]$

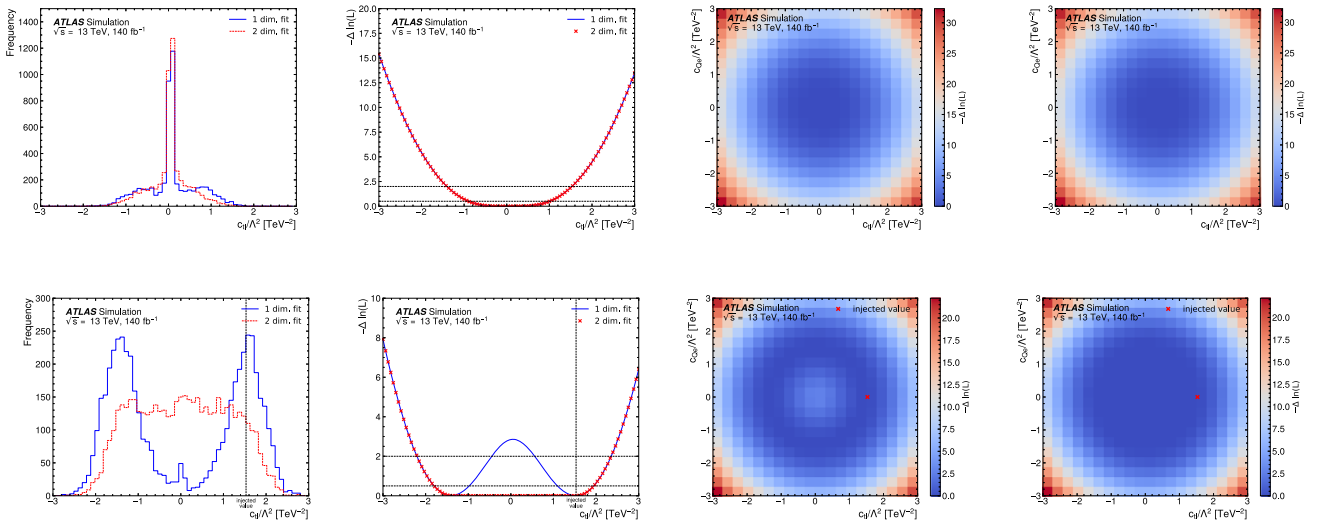

(a) (b) (c) (d)

Fig. 9 Studies on the sensitivity to multiple WCs at a time. Results are shown for fits considering only the statistical uncertainties for the SM expectation, for (top) all WCs= 0, and (bottom) for an injected value of $c_{tl} = 1.53$, close to the 95% confidence interval limit. The distributions considered in each case are **a** the fitted pseudodata, **b** the 1D likelihood scans, **c** the 2D likelihood scan for a 2D fit and **d** the 2D likelihood scan for a 3D fit

Therefore, many tests are performed with and without EFT signal injection to show how the expected sensitivity can decrease when a signal is present and the fit is exposed to the possible correlations. Figure 9 demonstrates the lack of an ability to probe all operators at once by showing results in two scenarios, one without any signal injection i.e. all WCs with a nominal value of zero (Fig. 9 top), and another where a signal is injected with $c_{tl} = 1.53$, chosen as it is close to the 95% confidence interval limit (Fig. 9 bottom). These results are derived with only statistical uncertainties considered in the fits to the pseudodata as this is the dominant uncertainty component and the inclusion of full systematic uncertainties is very computationally demanding. The distributions considered in each case are the fitted pseudodata (a), 1D likelihood scans (b), 2D likelihood scan for a 2D fit (c) and 2D likelihood scan for a 3D fit (d). These results show that although it can seem that there is minimal correlation between WCs in a multi-operator Asimov fit with no signal injection, this is misleading. There cannot be anticorrelations between WCs with large quadratic component to accommodate low observed signal, as changes to the WCs can only increase the signal yield, not decrease it. However, if a sizeable signal were to be observed then the correlation is much more strongly manifested as intermediate values of the WCs between zero and the injected value can be absorbed by smaller non-zero values of multiple WCs. This is illustrated in 1D in Fig. 9 (b-bottom) and in 2D for Fig. 9 (d-bottom). It is these results that motivate not including multi-operator fits in the results even though there is sensitivity when the observed EFT signal is small.

8 Conclusion

This paper presents a search for new physics in the $t\bar{t}\,\ell^{+}\ell^{-}$ final state. This process is highly interesting as it provides a

probe of the $t\bar{t}\,\ell^+\ell^-$ interaction vertex, which offers unique sensitivity to four-fermion EFT operators. To exploit this sensitivity the measurement is focused on the region of high invariant mass of $\ell^+\ell^-$ pair that has not previously been probed directly by ATLAS. Data from proton–proton collisions corresponding to an integrated luminosity of 140 fb^{-1} at $\sqrt{s} = 13$ TeV are used.

The three-lepton final state is targeted due to the high $t\bar{t}\,\ell^+\ell^-$ purity. Important backgrounds arise through the $t\bar{t}\,W$ process and fake leptons from $t\bar{t}$ events, these are controlled using dedicated control regions.

Profile likelihood fits to the data are used for several interpretations. This includes measurement of the signal strength of SM $t\bar{t}\,\ell^+\ell^-$ for $m(\ell^+\ell^-) > m_Z + 10$ GeV, computation of cross-section upper limits for a BSM signature in the region of $m(\ell^+\ell^-) > 550$ GeV, and extraction of EFT coefficients in various combinations. These include flavour-inclusive and, for the first time, flavour-split results, with configurations that test for lepton flavour universality-violating signals.

The best-fit values are compatible with the SM and limits on the relevant EFT WCs are set. These limits improve upon previous constraints on these operators from the CMS Collaboration [15].

The search for lepton flavour universality-violating EFT effects is still limited by the available Run 2 statistical precision, but this result demonstrates that cancellation of systematic uncertainties is possible and with more data this method could provide higher-precision tests of the SM. Again, no deviations from the SM or signs of lepton flavour universality violation are observed.

Acknowledgements We thank CERN for the very successful operation of the LHC and its injectors, as well as the support staff at CERN and at our institutions worldwide without whom ATLAS could not be operated efficiently. The crucial computing support from all WLCG partners is acknowledged gratefully, in particular from CERN, the ATLAS Tier-1 facilities at TRIUMF/SFU (Canada), NDGF (Denmark, Norway, Sweden), CC-IN2P3 (France), KIT/GridKA (Germany), INFN-CNAF (Italy), NL-T1 (Netherlands), PIC (Spain), RAL (UK) and BNL (USA), the Tier-2 facilities worldwide and large non-WLCG resource providers. Major contributors of computing resources are listed in Ref. [101]. We gratefully acknowledge the support of ANPCyT, Argentina; YerPhI, Armenia; ARC, Australia; BMWFW and FWF, Austria; ANAS, Azerbaijan; CNPq and FAPESP, Brazil; NSERC, NRC and CFI, Canada; CERN; ANID, Chile; CAS, MOST and NSFC, China; Minciencias, Colombia; MEYS CR, Czech Republic; DNRF and DNSRC, Denmark; IN2P3-CNRS and CEA-DRF/IRFU, France; SRNSFG, Georgia; BMFTR, HGF and MPG, Germany; GSRI, Greece; RGC and Hong Kong SAR, China; ICHEP and Academy of Sciences and Humanities, Israel; INFN, Italy; MEXT and JSPS, Japan; CNRST, Morocco; NWO, Netherlands; RCN, Norway; MNiSW, Poland; FCT, Portugal; MNE/IFA, Romania; MSTDI, Serbia; MSSR, Slovakia; ARIS and MVZI, Slovenia; DSI/NRF, South Africa; MICIU/AEI, Spain; SRC and Wallenberg Foundation, Sweden; SERI, SNSF and Cantons of Bern and Geneva, Switzerland; NSTC, Taipei; TENMAK, Türkiye; STFC/UKRI, United Kingdom; DOE and NSF, United States of America. Individual groups and members have received support from BCKDF, CANARIE, CRC and DRAC, Canada; CERN-CZ, FORTE and PRIMUS, Czech Republic; COST, ERC, ERDF, Horizon 2020, ICSC-NextGenerationEU and Marie Skłodowska-Curie Actions, European Union; Investissements d'Avenir Labex, Investissements d'Avenir Idex and ANR, France; DFG and AvH Foundation, Germany; Herakleitos, Thales and Aristeia programmes co-financed by EU-ESF and the Greek NSRF, Greece; BSF-NSF and MINERVA, Israel; NCN and NAWA, Poland; La Caixa Banking Foundation, CERCA Programme Generalitat de Catalunya and PROMETEO and GenT Programmes Generalitat Valenciana, Spain; Göran Gustafssons Stiftelse, Sweden; The Royal Society and Leverhulme Trust, United Kingdom. In addition, individual members wish to acknowledge support from Armenia: Yerevan Physics Institute (FAPERJ); CERN: European Organization for Nuclear Research (CERN DOCT); Chile: Agencia Nacional de Investigación y Desarrollo (FONDECYT 1230812, FONDECYT 1240864, FONDECYT 3240661); China: Chinese Ministry of Science and Technology (MOST-2023YFA1605700, MOST-2023YFA1609300), National Natural Science Foundation of China (NSFC – 12175119, NSFC 12275265); Czech Republic: Czech Science Foundation (GACR – 24-11373S), Ministry of Education Youth and Sports (ERC-CZ-LL2327, FORTE CZ.02.01.01/00/22_008/0004632), PRIMUS Research Programme (PRIMUS/21/SCI/017); EU: H2020 European Research Council (ERC - 101002463); European Union: European Research Council (BARD No. 101116429, ERC – 948254, ERC 101089007), European Regional Development Fund (SMASH COFUND 101081355, SLO ERDF), Horizon 2020 Framework Programme (MUCCA – CHIST-ERA-19-XAI-00), European Union, Future Artificial Intelligence Research (FAIR-NextGenerationEU PE000000 13), Horizon 2020 (EuroHPC – EHPC-DEV-2024D11-051), Italian Center for High Performance Computing, Big Data and Quantum Computing (ICSC, NextGenerationEU); France: Agence Nationale de la Recherche (ANR-21-CE31-0022, ANR-22-EDIR-0002); Germany: Baden-Württemberg Stiftung (BW Stiftung-Postdoc Eliteprogramme), Deutsche Forschungsgemeinschaft (DFG – 469666862, DFG – CR 312/5-2); China: Research Grants Council (GRF); Italy: Istituto Nazionale di Fisica Nucleare (ICSC, NextGenerationEU), Ministero dell'Università e della Ricerca (NextGenEU 153D23001490006 M4C2.1.1, NextGenEU I53D23000820006 M4C2.1.1, NextGenEU I53D23001490006 M4C2.1.1); Japan: Japan Society for the Promotion of Science (JSPS KAKENHI JP22H01227, JSPS KAKENHI JP22H04944, JSPS KAKENHI JP22KK0227, JSPS KAKENHI JP23KK0245, JSPS KAKENHI JP24K23939); Norway: Research Council of Norway (RCN-314472); Poland: Ministry of Science and Higher Education (IDUB AGH, POB8, D4 no 9722), Polish National Science Centre (NCN 2021/42/E/ST2/00350, NCN OPUS 2023/51/B/ST2/02507, NCN OPUS nr 2022/47/B/ST2/03059, NCN UMO-2019/34/E/ST2/00393, UMO-2022/47/O/ST2/00148, UMO-2023/49/B/ST2/04085, UMO-2023/51/B/ST2/00920, UMO-2024/53/N/ST2/00869); Portugal: Foundation for Science and Technology (FCT); Spain: Generalitat Valenciana (Artemisa, FEDER, IDIFEDER/2018/048), Ministry of Science and Innovation (MCIN & NextGenEU PCI2022-135018-2, MICIN & FEDER PID2021-125273NB, RYC2019-028510-I, RYC2020-030254-I, RYC2021-031273-I, RYC2022-038164-I); Sweden: Carl Trygger Foundation (Carl Trygger Foundation CTS 22:2312), Swedish Research Council (Swedish Research Council 2023-04654, VR 2021-03651, VR 2022-03845, VR 2022-04683, VR 2023-03403, VR 2024-05451), Knut and Alice Wallenberg Foundation (KAW 2018.0458, KAW 2022.0358, KAW 2023.0366); Switzerland: Swiss National Science Foundation (SNSF – PCEFP2_194658); United Kingdom: Leverhulme Trust (Leverhulme Trust RPG-2020-004), Royal Society (NIF-R1-231091); United States of America: U.S. Department of Energy (ECA DE-AC02-76SF00515), Neubauer Family Foundation.

Data Availability Statement Data cannot be made available for reasons disclosed in the data availability statement.

Code Availability Statement Code/software cannot be made available for reasons disclosed in the code availability statement.

Funded by SCOAP[3].

References

1. L. Evans, P. Bryant, L.H.C. Machine, JINST **3**, S08001 (2008). https://doi.org/10.1088/1748-0221/3/08/S08001
2. ATLAS Collaboration, Inclusive and differential cross-section measurements of $t\bar{t}$ production in pp collisions at $\sqrt{s} = 13$ TeV with the ATLAS detector, including EFT and spin-correlation interpretations. JHEP **07**, 163 (2024). https://doi.org/10.1007/JHEP07(2024)163. arXiv:2312.04450 [hep-ex]
3. CMS Collaboration, Probing effective field theory operators in the associated production of top quarks with a Z boson in multilepton final states at $\sqrt{s} = 13$ TeV. JHEP **12**, 083 (2021). https://doi.org/10.1007/JHEP12(2021)083. arXiv:2107.13896 [hep-ex]
4. CMS Collaboration, Measurements of inclusive and differential cross sections for top quark production in association with a Z boson in proton-proton collisions at $\sqrt{s} = 13$ TeV. JHEP **02**, 177 (2025). https://doi.org/10.1007/JHEP02(2025)177. arXiv:2410.23475 [hep-ex]
5. J.A. Aguilar-Saavedra, Identifying top partners at LHC. JHEP **11**, 030 (2009). https://doi.org/10.1088/1126-6708/2009/11/030. arXiv:0907.3155 [hep-ph]
6. J.A. Aguilar-Saavedra, R. Benbrik, S. Heinemeyer, M. Pérez-Victoria, Handbook of vectorlike quarks: mixing and single production. Phys. Rev. D **88**, 094010 (2013). https://doi.org/10.1103/PhysRevD.88.094010. arXiv:1306.0572 [hep-ph]
7. M. Perelstein, Little Higgs models and their phenomenology. Prog. Part. Nucl. Phys. **58**, 247 (2007). https://doi.org/10.1016/j.ppnp.2006.04.001. arXiv:hep-ph/9512128
8. R.S. Chivukula, S.B. Selipsky, E.H. Simmons, Nonoblique effects in the Zbb vertex from extended technicolor dynamics. Phys. Rev. Lett. **69**, 575 (1992). https://doi.org/10.1103/PhysRevLett.69.575. arXiv:hep-ph/9204214
9. R.S. Chivukula, E.H. Simmons, J. Terning, A heavy top quark and the Zbb vertex in non-commuting extended technicolor. Phys. Lett. B **331**, 383 (1994). https://doi.org/10.1016/0370-2693(94)91068-5. arXiv:hep-ph/9404209
10. K. Hagiwara, N. Kitazawa, Extended technicolor contribution to the Zbb vertex. Phys. Rev. D **52**, 5374 (1995). https://doi.org/10.1103/PhysRevD.52.5374. arXiv:hep-ph/9504332
11. U. Mahanta, Noncommuting ETC corrections to the $Zt\bar{t}$ vertex. Phys. Rev. D **55**, 5848 (1997). https://doi.org/10.1103/PhysRevD.55.5848. arXiv:hep-ph/9611289
12. U. Mahanta, Probing noncommuting extended technicolor effects by $e^+e^- \to t\bar{t}$ at the Next Linear Collider. Phys. Rev. D **56**, 402 (1997). https://doi.org/10.1103/PhysRevD.56.402
13. O.B. Bylund, F. Maltoni, I. Tsinikos, E. Vryonidou, C. Zhang, Probing top quark neutral couplings in the Standard Model Effective Field Theory at NLO in QCD. JHEP **05**, 052 (2016). https://doi.org/10.1007/JHEP05(2016)052. arXiv:1601.08193 [hep-ph]
14. Y. Afik, S. Bar-Shalom, K. Pal, A. Soni, J. Wudka, Multi-lepton probes of new physics and lepton-universality in top-quark interactions. Nucl. Phys. B **980**, 115849 (2022). https://doi.org/10.1016/j.nuclphysb.2022.115849. arXiv:2111.13711 [hep-ph]
15. CMS Collaboration, Search for physics beyond the standard model in top quark production with additional leptons in the context of effective field theory. JHEP **12**, 068 (2023). https://doi.org/10.1007/JHEP12(2023)068. arXiv:2307.15761 [hep-ex]
16. BaBar Collaboration, Evidence for an excess of $\bar{B} \to D^{(*)}\tau^-\bar{\nu}_\tau$ decays. Phys. Rev. Lett. **109**, 101802 (2012). https://doi.org/10.1103/PhysRevLett.109.101802. arXiv:1205.5442 [hep-ex]
17. BaBar Collaboration, Measurement of an excess of $\bar{B} \to D^{(*)}\tau^-\bar{\nu}_\tau$ decays and implications for charged Higgs bosons. Phys. Rev. D **88**, 072012 (2013). https://doi.org/10.1103/PhysRevD.88.072012. arXiv:1303.0571 [hep-ex]
18. Belle Collaboration, Measurement of the branching ratio of $\bar{B} \to D^{(*)}\tau^-\bar{\nu}_\tau$ relative to $B \to D^{(*)}l^-\bar{\nu}_l$ decays with hadronic tagging at Belle. Phys. Rev. D **92**, 072014 (2015). https://doi.org/10.1103/PhysRevD.92.072014. arXiv:1507.03233 [hep-ex]
19. Belle Collaboration, Measurement of the τ lepton polarization and $R(D^*)$ in the decay $\bar{B} \to D^*\tau^-\bar{\nu}_\tau$. Phys. Rev. Lett. **118**, 211801 (2017). https://doi.org/10.1103/PhysRevLett.118.211801. arXiv:1612.00529 [hep-ex]
20. Belle Collaboration, Measurement of the τ lepton polarization and $R(D^*)$ in the decay $\bar{B} \to D^*\tau^-\bar{\nu}_\tau$ with one-prong hadronic τ decays at Belle. Phys. Rev. D **97**, 012004 (2018). https://doi.org/10.1103/PhysRevD.97.012004. arXiv:1709.00129 [hep-ex]
21. Belle Collaboration, Measurement of $\mathcal{R}(D)$ and $\mathcal{R}(D^*)$ with a semileptonic tagging method. Phys. Rev. Lett. **124**, 161803 (2020). https://doi.org/10.1103/PhysRevLett.124.161803. arXiv:1910.05864 [hep-ex]
22. LHCb Collaboration, Measurement of the ratios of branching fractions $R(D^*)$ and $R(D^0)$. Phys. Rev. Lett. **131**, 111802 (2023). https://doi.org/10.1103/PhysRevLett.131.111802. arXiv:2302.02886 [hep-ex]
23. LHCb Collaboration, Test of lepton flavor universality using $B^0 \to D^{*-}\tau^+\nu_\tau$ decays with hadronic τ channels. Phys. Rev. D **108**, 012018 (2023). https://doi.org/10.1103/PhysRevD.108.012018. arXiv:2305.01463 [hep-ex]
24. S. Biflmann, C. Grunwald, G. Hiller, K. Kröninger, Top and Beauty synergies in SMEFT-fits at present and future colliders. JHEP **06**, 010 (2021). https://doi.org/10.1007/JHEP06(2021)010. arXiv:2012.10456 [hep-ph]
25. J. Fuentes-Martin, A. Greljo, J.M. Camalich, J.D. Ruiz-Alvarez, Charm physics confronts high-p_T lepton tails. JHEP **11**, 080 (2020). https://doi.org/10.1007/JHEP11(2020)080. arXiv:2003.12421 [hep-ph]
26. C. Grunwald, G. Hiller, K. Kröninger, L. Nollen, More synergies from beauty, top Z and Drell–Yan measurements in SMEFT. JHEP **11**, 110 (2023). https://doi.org/10.1007/JHEP11(2023)110. arXiv:2304.12837 [hep-ph]
27. R. Bartocci, A. Bickötter, T. Hurth, A global analysis of the SMEFT under the minimal MFV assumption. JHEP **05**, 074 (2024). https://doi.org/10.1007/JHEP05(2024)074. arXiv:2311.04963 [hep-ph]
28. L. Allwicher, C. Cornella, G. Isidori, B.A. Stefanek, New physics in the third generation. A comprehensive SMEFT analysis and future prospects. JHEP **03**, 049 (2024). https://doi.org/10.1007/JHEP03(2024)049. arXiv:2311.00920 [hep-ph]
29. O. Atkinson, C. Englert, M. Kirk, G. Tetlalmatzi-Xolocotzi, Collider-flavour complementarity from the bottom to the top.

Eur. Phys. J. C **85**, 258 (2025). https://doi.org/10.1140/epjc/s10052-024-13739. arXiv:2411.00940 [hep-ph]
30. I. Brivio, SMEFTsim 3.0—a practical guide. JHEP **04**, 073 (2021). https://doi.org/10.1007/JHEP04(2021)073. arXiv:2012.11343 [hep-ph]
31. ATLAS Collaboration, The ATLAS experiment at the CERN large hadron collider. JINST **3**, S08003 (2008). https://doi.org/10.1088/1748-0221/3/08/S08003
32. ATLAS Collaboration, ATLAS Inner Detector B-Layer: Technical Design Report, ATLAS-TDR-19: CERN-LHCC-2010-013 (2010). https://cds.cern.ch/record/1291633 [Addendum: ATLAS-TDR-19-ADD-1: CERN-LHCC-2012-009 (2012)]. https://cds.cern.ch/record/1451888
33. B. Abbott et al., Production and integration of the ATLAS Innerdelable B-Layer. JINST **13**, T05008 (2018). https://doi.org/10.1088/1748-0221/13/05/T05008. arXiv:1803.00844 [physics.ins-det]
34. G. Avoni et al., The new LUCID-2 detector for luminosity measurement and monitoring in ATLAS. JINST **13**, P07017 (2018). https://doi.org/10.1088/1748-0221/13/07/P07017
35. ATLAS Collaboration, Performance of the ATLAS trigger system in 2015, Eur. Phys. J. C **77**, 317 (2017). https://doi.org/10.1140/epjc/s10052-017-4852-3. arXiv:1611.09661 [hep-ex]
36. ATLAS Collaboration, Software and computing for Run 3 of the ATLAS experiment at the LHC. Eur. Phys. J. C **85**, 234 (2025). https://doi.org/10.1140/epjc/s10052-024-13701-w. arXiv:2404.06335 [hep-ex]
37. ATLAS Collaboration, ATLAS data quality operations and performance for 2015-2018 data-taking. JINST **15**, P04003 (2020). https://doi.org/10.1088/1748-0221/15/04/P04003. arXiv:1911.04632 [physics.ins-det]
38. ATLAS Collaboration, Luminosity determination in pp collisions at $\sqrt{s} = 13$ TeV using the ATLAS detector at the LHC. Eur. Phys. J. C **83**, 982 (2023). https://doi.org/10.1140/epjc/s10052-023-11747-w. arXiv:2212.09579 [hep-ex]
39. ATLAS Collaboration, Performance of electron and photon triggers in ATLAS during LHC Run 2. Eur. Phys. J. C **80**, 47 (2020). https://doi.org/10.1140/epjc/s10052-019-7500-2. arXiv:1909.09761 [hep-ex]
40. ATLAS Collaboration, Performance of the ATLAS muon triggers in Run 2. JINST **15**, P09015 (2020). https://doi.org/10.1088/1748-0221/15/09/p09015. arXiv:2004.13447 [physics.ins-det]
41. ATLAS Collaboration, The ATLAS inner detector trigger performance in pp collisions at 13 TeV during LHC Run 2. Eur. Phys. J. C **82**, 206 (2022). https://doi.org/10.1140/epjc/s10052-021-09920-0. arXiv:2107.02485 [hep-ex]
42. ATLAS Collaboration, The ATLAS simulation infrastructure. Eur. Phys. J. C **70**, 823 (2010). https://doi.org/10.1140/epjc/s10052-010-1429-9. arXiv:1005.4568 [physics.ins-det]
43. S. Agostinelli et al., GEANT4—a simulation toolkit. Nucl. Instrum. Meth. A **506**, 250 (2003). https://doi.org/10.1016/S0168-9002(03)01368-8
44. ATLAS Collaboration, The new Fast Calorimeter Simulation in ATLAS, ATL-SOFT-PUB-2018-002 (2018). https://cds.cern.ch/record/2630434
45. T. Sjostrand, S. Mrenna, P. Skands, A brief introduction to PYTHIA 8.1. Comput. Phys. Commun. **178**, 852 (2008). https://doi.org/10.1016/j.cpc.2008.01.036. arXiv:0710.3820 [hep-ph]
46. ATLAS Collaboration, Further ATLAS tunes of PYTHIA 6 and Pythia 8, ATL-PHYS-PUB-2011-014 (2011). https://cds.cern.ch/record/1400677
47. J. Alwall et al., The automated computation of tree-level and next-to-leading order differential cross sections, and their matching to parton shower simulations. JHEP **07**, 079 (2014). https://doi.org/10.1007/JHEP07(2014)079. arXiv:1405.0301 [hep-ph]
48. NNPDF Collaboration, R.D. Ball et al., Parton distributions for the LHC run II. JHEP **04**, 040 (2015). https://doi.org/10.1007/JHEP04(2015)040. arXiv:1410.8849 [hep-ph]
49. S. Frixione, E. Laenen, P. Motylinski, B.R. Webber, Angular correlations of lepton pairs from vector boson and top quark decays in Monte Carlo simulations. JHEP **04**, 081 (2007). https://doi.org/10.1088/1126-6708/2007/04/081. arXiv:hep-ph/0702198
50. P. Artoisenet, R. Frederikx, O. Mattelaer, R. Rietkerk, Automatic spin-entangled decays of heavy resonances in Monte Carlo simulations. JHEP **03**, 015 (2013). https://doi.org/10.1007/JHEP03(2013)015. arXiv:1212.3460 [hep-ph]
51. T. Sjöstrand et al., An introduction to PYTHIA 8.2. Comput. Phys. Commun. **191**, 159 (2015). https://doi.org/10.1016/j.cpc.2015.01.024. arXiv:1410.3012 [hep-ph]
52. ATLAS Collaboration, ATLAS Pythia 8 tunes to 7 TeV data, ATL-PHYS-PUB-2014-021 (2014). https://cds.cern.ch/record/1966419
53. D.J. Lange, The EvtGen particle decay simulation package. Nucl. Instrum. Meth. A **462**, 152 (2001). https://doi.org/10.1016/S0168-9002(01)00089-4
54. D. de Florian et al., Handbook of LHC Higgs Cross Sections: 4. Deciphering the Nature of the Higgs Sector (2017). https://doi.org/10.23731/CYRM-2017-002. arXiv:1610.07922 [hep-ph]
55. ATLAS Collaboration, Modelling of the $t\bar{t}H$ and $t\bar{t}V$ (V=W, Z) processes for $\sqrt{s} = 13$ TeV ATLAS analyses, ATL-PHYS-PUB-2016-005 (2016). https://cds.cern.ch/record/2129826
56. E. Bothmann et al., Event generation with SHERPA 2.2. SciPost Phys. **7**, 034 (2019). https://doi.org/10.21468/SciPostPhys.7.3.034. arXiv:1905.09127 [hep-ph]
57. T. Gleisberg et al., Event generation with SHERPA 1.1. JHEP **02**, 007 (2009). https://doi.org/10.1088/1126-6708/2009/02/007. arXiv:0811.4622 [hep-ph]
58. S. Höche, F. Krauss, M. Schönherr, F. Siegert, A critical appraisal of NLO+PS matching methods. JHEP **09**, 049 (2012). https://doi.org/10.1007/JHEP09(2012)049. arXiv:1111.1220 [hep-ph]
59. S. Höche, F. Krauss, M. Schönherr, F. Siegert, QCD matrix elements + parton showers. The NLO case. JHEP **04**, 027 (2013). https://doi.org/10.1007/JHEP04(2013)027. arXiv:1207.5030 [hep-ph]
60. S. Catani, F. Krauss, B.R. Webber, R. Kuhn, QCD matrix elements + parton showers. JHEP **11**, 063 (2001). https://doi.org/10.1088/1126-6708/2001/11/063. arXiv:hep-ph/0109231
61. S. Höche, F. Krauss, S. Schumann, F. Siegert, QCD matrix elements and truncated showers. JHEP **05**, 053 (2009). https://doi.org/10.1088/1126-6708/2009/05/053. arXiv:0903.1219 [hep-ph]
62. NNPDF Collaboration, R.D. Ball et al., Parton distributions from high-precision collider data. Eur. Phys. J. C **77**, 663 (2017). https://doi.org/10.1140/epjc/s10052-017-5199-5. arXiv:1706.00428 [hep-ph]
63. R. Frederikx, I. Tsinikos, On improving NLO merging for $t\bar{t}W$ production. JHEP **11**, 029 (2021). https://doi.org/10.1007/JHEP11(2021)029. arXiv:2108.07826 [hep-ph]
64. F. Demartin, B. Maier, F. Maltoni, K. Mawatari, M. Zaro, tWh associated production at the LHC. Eur. Phys. J. C **77**, 34 (2017). https://doi.org/10.1140/epjc/s10052-017-4601-7. arXiv:1607.05862 [hep-ph]
65. S. Alioli, P. Nason, C. Oleari, E. Re, A general framework for implementing NLO calculations in shower Monte Carlo programs: the POWHEG BOX. JHEP **06**, 043 (2010). https://doi.org/10.1007/JHEP06(2010)043. arXiv:1002.2581 [hep-ph]
66. T. Gleisberg, S. Höche, Comix, a new matrix element generator. JHEP **12**, 039 (2008). https://doi.org/10.1088/1126-6708/2008/12/039. arXiv:0808.3674 [hep-ph]
67. S. Schumann, F. Krauss, A parton shower algorithm based on Catani–Seymour dipole factorisation. JHEP **03**, 038

(2008). https://doi.org/10.1088/1126-6708/2008/03/038. arXiv:0709.1027 [hep-ph]
68. F. Cascioli, P. Maierhöfer, S. Pozzorini, Scattering amplitudes with open loops. Phys. Rev. Lett. **108**, 111601 (2012). https://doi.org/10.1103/PhysRevLett.108.111601. arXiv:1111.5206 [hep-ph]
69. A. Denner, S. Dittmaier, L. Hofer, Collier: a fortran-based complex one-loop library in extended regularizations. Comput. Phys. Commun. **212**, 220 (2017). https://doi.org/10.1016/j.cpc.2016.10.013. arXiv:1604.06792 [hep-ph]
70. F. Buccioni et al., OpenLoops 2. Eur. Phys. J. C **79**, 866 (2019). https://doi.org/10.1140/epjc/s10052-019-7306-2. arXiv:1907.13071 [hep-ph]
71. I. Brivio et al., Electroweak input parameters (2021). arXiv:2111.12515 [hep-ph]
72. O. Mattelaer, On the maximal use of Monte Carlo samples: re-weighting events at NLO accuracy. Eur. Phys. J. C **76**, 674 (2016). https://doi.org/10.1140/epjc/s10052-016-4533-7. arXiv:1607.00763 [hep-ph]
73. ATLAS Collaboration, Electron and photon performance measurements with the ATLAS detector using the 2015-2017 LHC proton-proton collision data. JINST **14**, P12006 (2019). https://doi.org/10.1088/1748-0221/14/12/P12006. arXiv:1908.00005 [hep-ex]
74. ATLAS Collaboration, Electron and photon energy calibration with the ATLAS detector using LHC Run 2 data. JINST **19**, P02009 (2024). https://doi.org/10.1088/1748-0221/19/02/P02009. arXiv:2309.05471 [hep-ex]
75. ATLAS Collaboration, Electron and photon efficiencies in LHC Run 2 with the ATLAS experiment. JHEP **05**, 162 (2024). https://doi.org/10.1007/JHEP05(2024)162. arXiv:2308.13362 [hep-ex]
76. ATLAS Collaboration, Evidence for the associated production of the Higgs boson and a top quark pair with the ATLAS detector. Phys. Rev. D **97**, 072003 (2018). https://doi.org/10.1103/PhysRevD.97.072003. arXiv:1712.08891 [hep-ex]
77. ATLAS Collaboration, Studies of the muon momentum calibration and performance of the ATLAS detector with pp collisions at $\sqrt{s} = 13$ TeV. Eur. Phys. J. C **83**, 686 (2023). https://doi.org/10.1140/epjc/s10052-023-11584-x. arXiv:2212.07338 [hep-ex]
78. ATLAS Collaboration, Muon reconstruction and identification efficiency in ATLAS using the full Run 2 pp collision data set at $\sqrt{s} = 13$ TeV. Eur. Phys. J. C **81**, 578 (2021). https://doi.org/10.1140/epjc/s10052-021-09233-2. arXiv:2012.00578 [hep-ex]
79. M. Cacciari, G.P. Salam, G. Soyez, The anti-k_t jet clustering algorithm. JHEP **04**, 063 (2008). https://doi.org/10.1088/1126-6708/2008/04/063. arXiv:0802.1189 [hep-ph]
80. M. Cacciari, G.P. Salam, G. Soyez, FastJet user manual. Eur. Phys. J. C **72**, 1896 (2012). https://doi.org/10.1140/epjc/s10052-012-1896-2. arXiv:1111.6097 [hep-ph]
81. ATLAS Collaboration, Properties of jets and inputs to jet reconstruction and calibration with the ATLAS detector using proton-proton collisions at $\sqrt{s} = 13$ TeV, ATL-PHYS-PUB-2015-036 (2015). https://cds.cern.ch/record/2044564
82. ATLAS Collaboration, Jet reconstruction and performance using particle flow with the ATLAS detector. Eur. Phys. J. C **77**, 466 (2017). https://doi.org/10.1140/epjc/s10052-017-5031-2. arXiv:1703.10485 [hep-ex]
83. ATLAS Collaboration, Jet energy scale and resolution measured in proton-proton collisions at $\sqrt{s} = 13$ TeV with the ATLAS detector. Eur. Phys. J. C **81**, 689 (2021). https://doi.org/10.1140/epjc/s10052-021-09402-3. arXiv:2007.02645 [hep-ex]
84. ATLAS Collaboration, Tagging and suppression of pileup jets with the ATLAS detector, ATLAS-CONF-2014-018 (2014). https://cds.cern.ch/record/1700870
85. ATLAS Collaboration, ATLAS b-jet identification performance and efficiency measurement with $t\bar{t}$ events in pp collisions at $\sqrt{s} = 13$ TeV. Eur. Phys. J. C **79**, 970 (2019). https://doi.org/10.1140/epjc/s10052-019-7450-8. arXiv:1907.05120 [hep-ex]
86. ATLAS Collaboration, The performance of missing transverse momentum reconstruction and its significance with the ATLAS detector using 140 fb^{-1} of $\sqrt{s} = 13$ TeV pp collisions. Eur. Phys. J. C **85**, 606 (2025). https://doi.org/10.1140/epjc/s10052-025-14062-8. arXiv:2402.05858 [hep-ex]
87. M. Cacciari, G.P. Salam, G. Soyez, The catchment area of jets. JHEP **04**, 005 (2008). https://doi.org/10.1088/1126-6708/2008/04/005. arXiv:0802.1188 [hep-ph]
88. J. Butterworth et al., PDF4LHC recommendations for LHC Run II. J. Phys. G **43**, 023001 (2016). https://doi.org/10.1088/0954-3899/43/2/023001. arXiv:1510.03865 [hep-ph]
89. M. Bähr et al., Herwig++ physics and manual. Eur. Phys. J. C **58**, 639 (2008). https://doi.org/10.1140/epjc/s10052-008-0798-9. arXiv:0803.0883 [hep-ph]
90. J. Bellm et al., Herwig 7.0/Herwig++ 3.0 release note. Eur. Phys. J. C **76**, 196 (2016). https://doi.org/10.1140/epjc/s10052-016-4018-8. arXiv:1512.01178 [hep-ph]
91. R. Frederikx, S. Frixione, Merging meets matching in MC@NLO. JHEP **12**, 061 (2012). https://doi.org/10.1007/JHEP12(2012)061. arXiv:1209.6215 [hep-ph]
92. ATLAS Collaboration, Observation of the associated production of a top quark and a Z boson in pp collisions at $\sqrt{s} = 13$ TeV with the ATLAS detector. JHEP **07**, 124 (2020). https://doi.org/10.1007/JHEP07(2020)124. arXiv:2002.07546 [hep-ex]
93. ATLAS Collaboration, Observation of four-top-quark production in the multilepton final state with the ATLAS detector. Eur. Phys. J. C **83**, 496 (2023). https://doi.org/10.1140/epjc/s10052-023-11573-0. arXiv:2303.15061 [hep-ex] [Erratum: Eur. Phys. J. C **84**, 156 (2024)]
94. G. Cowan, K. Cranmer, E. Gross, O. Vitells, Asymptotic formulae for likelihood-based tests of new physics. Eur. Phys. J. C **71**, 1554 (2011). https://doi.org/10.1140/epjc/s10052-011-1554-0. arXiv:1007.1727 [physics.data-an] [Erratum: Eur. Phys. J. C **73**, 2501 (2013), https://doi.org/10.1140/epjc/s10052-013-2501-z]
95. ROOT Collaboration, HistFactory: a tool for creating statistical models for use with RooFit and RooStats, CERN-OPEN-2012-016 (2012). https://doi.org/10.17181/CERN-OPEN-2012-016
96. R. Barlow, C. Beeston, Fitting using finite Monte Carlo samples. Comput. Phys. Commun. **77**, 219 (1993). https://doi.org/10.1016/0010-4655(93)90005-W
97. ATLAS Collaboration, Measurement of the total and differential cross-sections of $t\bar{t}W$ production in pp collisions at $\sqrt{s} = 13$ TeV with the ATLAS detector. JHEP **05**, 131 (2024). https://doi.org/10.1007/JHEP05(2024)131. arXiv:2401.05299 [hep-ex]
98. S.S. Wilks, The large-sample distribution of the likelihood ratio for testing composite hypotheses. Ann. Math. Stat. **9**, 60 (1938). https://doi.org/10.1214/aoms/1177732360
99. F. Urs Bernlochner, D.C. Fry, S. Burns Menary, E. Persson, Cover your bases: asymptotic distributions of the profile likelihood ratio when constraining effective field theories in high-energy physics. SciPost Phys. Core **6**, 013 (2023). https://doi.org/10.21468/SciPostPhysCore.6.1.013. arXiv:2207.01350 [physics.data-an]
100. I. Brivio et al., Truncation, validity, uncertainties (2022). https://arxiv.org/abs/2201.04974. arXiv:2201.04974 [hep-ph]
101. ATLAS Collaboration, ATLAS computing acknowledgements, ATL-SOFT-PUB-2025-001 (2025). https://cds.cern.ch/record/2922210

The ATLAS Collaboration[★]

G. Aad[104], E. Aakvaag[17], B. Abbott[123], S. Abdelhameed[119a], K. Abeling[55], N. J. Abicht[49], S. H. Abidi[30], M. Aboelela[45], A. Aboulhorma[36e], H. Abramowicz[157], Y. Abulaiti[120], B. S. Acharya[69a,69b,n], A. Ackermann[63a], C. Adam Bourdarios[4], L. Adamczyk[86a], S. V. Addepalli[149], M. J. Addison[103], J. Adelman[118], A. Adiguzel[22c], T. Adye[137], A. A. Affolder[139], Y. Afik[40], M. N. Agaras[13], A. Aggarwal[102], C. Agheorghiesei[28c], F. Ahmadov[39,ae], S. Ahuja[97], X. Ai[143b], G. Aielli[76a,76b], A. Aikot[169], M. Ait Tamlihat[36e], B. Aitbenchikh[36a], M. Akbiyik[102], T. P. A. Åkesson[100], A. V. Akimov[151], D. Akiyama[174], N. N. Akolkar[25], S. Aktas[22a], G. L. Alberghi[24b], J. Albert[171], P. Albicocco[53], G. L. Albouy[60], S. Alderweireldt[52], Z. L. Alegria[124], M. Aleksa[37], I. N. Aleksandrov[39], C. Alexa[28b], T. Alexopoulos[10], F. Alfonsi[24b], M. Algren[56], M. Alhroob[173], B. Ali[135], H. M. J. Ali[93,x], S. Ali[32], S. W. Alibocus[94], M. Aliev[34c], G. Alimonti[71a], W. Alkakhi[55], C. Allaire[66], B. M. M. Allbrooke[152], J. S. Allen[103], J. F. Allen[52], P. P. Allport[21], A. Aloisio[72a,72b], F. Alonso[92], C. Alpigiani[142], Z. M. K. Alsolami[93], A. Alvarez Fernandez[102], M. Alves Cardoso[56], M. G. Alviggi[72a,72b], M. Aly[103], Y. Amaral Coutinho[83b], A. Ambler[106], C. Amelung[37], M. Amerl[103], C. G. Ames[111], T. Amezza[130], D. Amidei[108], B. Amini[54], K. Amirie[161], A. Amirkhanov[39], S. P. Amor Dos Santos[133a], K. R. Amos[169], D. Amperiadou[158], S. An[84], C. Anastopoulos[145], T. Andeen[11], J. K. Anders[94], A. C. Anderson[59], A. Andreazza[71a,71b], S. Angelidakis[9], A. Angerami[42], A. V. Anisenkov[39], A. Annovi[74a], C. Antel[56], E. Antipov[151], M. Antonelli[53], F. Anulli[75a], M. Aoki[84], T. Aoki[159], M. A. Aparo[152], L. Aperio Bella[48], M. Apicella[31], C. Appelt[157], A. Apyan[27], S. J. Arbiol Val[87], C. Arcangeletti[53], A. T. H. Arce[51], J-F. Arguin[110], S. Argyropoulos[158], J.-H. Arling[48], O. Arnaez[4], H. Arnold[151], G. Artoni[75a,75b], H. Asada[113], K. Asai[121], S. Asai[159], S. Asatryan[179], N. A. Asbah[37], R. A. Ashby Pickering[173], A. M. Aslam[97], K. Assamagan[30], R. Astalos[29a], K. S. V. Astrand[100], S. Atashi[165], R. J. Atkin[34a], H. Atmani[36f], P. A. Atmasiddha[131], K. Augsten[135], A. D. Auriol[41], V. A. Austrup[103], G. Avolio[37], K. Axiotis[56], G. Azuelos[110,ai], D. Babal[29b], H. Bachacou[138], K. Bachas[158,r], A. Bachiu[35], E. Bachmann[50], M. J. Backes[63a], A. Badea[40], T. M. Baer[108], P. Bagnaia[75a,75b], M. Bahmani[19], D. Bahner[54], K. Bai[126], J. T. Baines[137], L. Baines[96], O. K. Baker[178], E. Bakos[16], D. Bakshi Gupta[8], L. E. Balabram Filho[83b], V. Balakrishnan[123], R. Balasubramanian[4], E. M. Baldin[38], P. Balek[86a], E. Ballabene[24b,24a], F. Balli[138], L. M. Baltes[63a], W. K. Balunas[33], J. Balz[102], I. Bamwidhi[119b], E. Banas[87], M. Bandieramonte[132], A. Bandyopadhyay[25], S. Bansal[25], L. Barak[157], M. Barakat[48], E. L. Barberio[107], D. Barberis[18b], M. Barbero[104], M. Z. Barel[117], T. Barillari[112], M-S. Barisits[37], T. Barklow[149], P. Baron[136], D. A. Baron Moreno[103], A. Baroncelli[62], A. J. Barr[129], J. D. Barr[98], F. Barreiro[101], J. Barreiro Guimarães da Costa[14], M. G. Barros Teixeira[133a], S. Barsov[38], F. Bartels[63a], R. Bartoldus[149], A. E. Barton[93], P. Bartos[29a], A. Basan[102], M. Baselga[49], S. Bashiri[87], A. Bassalat[66,b], M. J. Basso[162a], S. Bataju[45], R. Bate[170], R. L. Bates[59], S. Batlamous[101], M. Battaglia[139], D. Battulga[19], M. Bauce[75a,75b], M. Bauer[79], P. Bauer[25], L. T. Bayer[48], L. T. Bazzano Hurrell[31], J. B. Beacham[112], T. Beau[130], J. Y. Beaucamp[92], P. H. Beauchemin[164], P. Bechtle[25], H. P. Beck[20,q], K. Becker[173], A. J. Beddall[82], V. A. Bednyakov[39], C. P. Bee[151], L. J. Beemster[16], M. Begalli[83d], M. Begel[30], J. K. Behr[48], J. F. Beirer[37], F. Beisiegel[25], M. Belfkir[119b], G. Bella[157], L. Bellagamba[24b], A. Bellerive[35], C. D. Bellgraph[68], P. Bellos[21], K. Beloborodov[38], D. Benchekroun[36a], F. Bendebba[36a], Y. Benhammou[157], K. C. Benkendorfer[61], L. Beresford[48], M. Beretta[53], E. Bergeaas Kuutmann[167], N. Berger[4], B. Bergmann[135], J. Beringer[18a], G. Bernardi[5], C. Bernius[149], F. U. Bernlochner[25], F. Bernon[37], A. Berrocal Guardia[13], T. Berry[97], P. Berta[136], A. Berthold[50], A. Berti[133a], R. Bertrand[104], S. Bethke[112], A. Betti[75a,75b], A. J. Bevan[96], L. Bezio[56], N. K. Bhalla[54], S. Bharthuar[112], S. Bhatta[151], P. Bhattarai[149], Z. M. Bhatti[120], K. D. Bhide[54], V. S. Bhopatkar[124], R. M. Bianchi[132], G. Bianco[24b,24a], O. Biebel[111], M. Biglietti[77a], C. S. Billingsley[45], Y. Bimgdi[36f], M. Bindi[55], A. Bingham[177], A. Bingul[22b], C. Bini[75a,75b], G. A. Bird[33], M. Birman[175], M. Biros[136], S. Biryukov[152], T. Bisanz[49], E. Bisceglie[24b,24a], J. P. Biswal[137], D. Biswas[147], I. Bloch[48], A. Blue[59], U. Blumenschein[96], J. Blumenthal[102], V. S. Bobrovnikov[39], M. Boehler[54], B. Boehm[172], D. Bogavac[13], A. G. Bogdanchikov[38], L. S. Boggia[130], V. Boisvert[97], P. Bokan[37], T. Bold[86a], M. Bomben[5], M. Bona[96], M. Boonekamp[138], A. G. Borbély[59], I. S. Bordulev[38], G. Borissov[93], D. Bortoletto[129], D. Boscherini[24b], M. Bosman[13], K. Bouaouda[36a], N. Bouchhar[169], L. Boudet[4], J. Boudreau[132], E. V. Bouhova-Thacker[93], D. Boumediene[41], R. Bouquet[57b,57a], A. Boveia[122], J. Boyd[37], D. Boye[30], I. R. Boyko[39], L. Bozianu[56], J. Bracinik[21], N. Brahimi[4], G. Brandt[177], O. Brandt[33], B. Brau[105], J. E. Brau[126], R. Brener[175], L. Brenner[117], R. Brenner[167], S. Bressler[175], G. Brianti[78a,78b],

D. Britton[59], D. Britzger[112], I. Brock[25], R. Brock[109], G. Brooijmans[42], A. J. Brooks[68], E. M. Brooks[162b], E. Brost[30], L. M. Brown[171,162a], L. E. Bruce[61], T. L. Bruckler[129], P. A. Bruckman de Renstrom[87], B. Brüers[48], A. Bruni[24b], G. Bruni[24b], D. Brunner[47a,47b], M. Bruschi[24b], N. Bruscino[75a,75b], T. Buanes[17], Q. Buat[142], D. Buchin[112], A. G. Buckley[59], O. Bulekov[82], B. A. Bullard[149], S. Burdin[94], C. D. Burgard[49], A. M. Burger[91], B. Burghgrave[8], O. Burlayenko[54], J. Burleson[168], J. C. Burzynski[148], E. L. Busch[42], V. Büscher[102], P. J. Bussey[59], J. M. Butler[26], C. M. Buttar[59], J. M. Butterworth[98], W. Buttinger[137], C. J. Buxo Vazquez[109], A. R. Buzykaev[39], S. Cabrera Urbán[169], L. Cadamuro[66], D. Caforio[58], H. Cai[132], Y. Cai[24b,114c,24a], Y. Cai[114a], V. M. M. Cairo[37], O. Cakir[3a], N. Calace[37], P. Calafiura[18a], G. Calderini[130], P. Calfayan[35], G. Callea[59], L. P. Caloba[83b], D. Calvet[41], S. Calvet[41], R. Camacho Toro[130], S. Camarda[37], D. Camarero Munoz[27], P. Camarri[76a,76b], C. Camincher[171], M. Campanelli[98], A. Camplani[43], V. Canale[72a,72b], A. C. Canbay[3a], E. Canonero[97], J. Cantero[169], Y. Cao[168], F. Capocasa[27], M. Capua[44b,44a], A. Carbone[71a,71b], R. Cardarelli[76a], J. C. J. Cardenas[8], M. P. Cardiff[27], G. Carducci[44b,44a], T. Carli[37], G. Carlino[72a], J. I. Carlotto[13], B. T. Carlson[132,s], E. M. Carlson[171], J. Carmignani[94], L. Carminati[71a,71b], A. Carnelli[4], M. Carnesale[37], S. Caron[116], E. Carquin[140f], I. B. Carr[107], S. Carrá[73a,73b], G. Carratta[24b,24a], A. M. Carroll[126], M. P. Casado[13,i], M. Caspar[48], F. L. Castillo[4], L. Castillo Garcia[13], V. Castillo Gimenez[169], N. F. Castro[133a,133e], A. Catinaccio[37], J. R. Catmore[128], T. Cavaliere[4], V. Cavaliere[30], L. J. Caviedes Betancourt[23b], E. Celebi[82], S. Cella[37], V. Cepaitis[56], K. Cerny[125], A. S. Cerqueira[83a], A. Cerri[74a,74b,al], L. Cerrito[76a,76b], F. Cerutti[18a], B. Cervato[71a,71b], A. Cervelli[24b], G. Cesarini[53], S. A. Cetin[82], P. M. Chabrillat[130], S. Chakraborty[173], J. Chan[18a], W. Y. Chan[159], J. D. Chapman[33], E. Chapon[138], B. Chargeishvili[155b], D. G. Charlton[21], C. Chauhan[136], Y. Che[114a], S. Chekanov[6], S. V. Chekulaev[162a], G. A. Chelkov[39,a], B. Chen[157], B. Chen[171], H. Chen[114a], H. Chen[30], J. Chen[144a], J. Chen[148], M. Chen[129], S. Chen[89], S. J. Chen[114a], X. Chen[144a], X. Chen[15,ah], Z. Chen[62], C. L. Cheng[176], H. C. Cheng[64a], S. Cheong[149], A. Cheplakov[39], E. Cherepanova[117], R. Cherkaoui El Moursli[36e], E. Cheu[7], K. Cheung[65], L. Chevalier[138], V. Chiarella[53], G. Chiarelli[74a], G. Chiodini[70a], A. S. Chisholm[21], A. Chitan[28b], M. Chitishvili[169], M. V. Chizhov[39,t], K. Choi[11], Y. Chou[142], E. Y. S. Chow[116], K. L. Chu[175], M. C. Chu[64a], X. Chu[14,114c], Z. Chubinidze[53], J. Chudoba[134], J. J. Chwastowski[87], D. Cieri[112], K. M. Ciesla[86a], V. Cindro[95], A. Ciocio[18a], F. Cirotto[72a,72b], Z. H. Citron[175], M. Citterio[71a], D. A. Ciubotaru[28b], A. Clark[56], P. J. Clark[52], N. Clarke Hall[98], C. Clarry[161], S. E. Clawson[48], C. Clement[47a,47b], Y. Coadou[104], M. Cobal[69a,69c], A. Coccaro[57b], R. F. Coelho Barrue[133a], R. Coelho Lopes De Sa[105], S. Coelli[71a], L. S. Colangeli[161], B. Cole[42], P. Collado Soto[101], J. Collot[60], R. Coluccia[70a,70b], P. Conde Muiño[133a,133g], M. P. Connell[34c], S. H. Connell[34c], E. I. Conroy[129], M. Contreras Cossio[11], F. Conventi[72a,aj], H. G. Cooke[21], A. M. Cooper-Sarkar[129], L. Corazzina[75a,75b], F. A. Corchia[24b,24a], A. Cordeiro Oudot Choi[142], L. D. Corpe[41], M. Corradi[75a,75b], F. Corriveau[106,ac], A. Cortes-Gonzalez[159], M. J. Costa[169], F. Costanza[4], D. Costanzo[145], B. M. Cote[122], J. Couthures[4], G. Cowan[97], K. Cranmer[176], L. Cremer[49], D. Cremonini[24b,24a], S. Crépé-Renaudin[60], F. Crescioli[130], T. Cresta[73a,73b], M. Cristinziani[147], M. Cristoforetti[78a,78b], V. Croft[117], J. E. Crosby[124], G. Crosetti[44b,44a], A. Cueto[101], H. Cui[98], Z. Cui[7], W. R. Cunningham[59], F. Curcio[169], J. R. Curran[52], M. J. Da Cunha Sargedas De Sousa[57b,57a], J. V. Da Fonseca Pinto[83b], C. Da Via[103], W. Dabrowski[86a], T. Dado[37], S. Dahbi[154], T. Dai[108], D. Dal Santo[20], C. Dallapiccola[105], M. Dam[43], G. D'amen[30], V. D'Amico[111], J. Damp[102], J. R. Dandoy[35], D. Dannheim[37], G. D'anniballe[74a,74b], M. Danninger[148], V. Dao[151], G. Darbo[57b], S. J. Das[30], F. Dattola[48], S. D'Auria[71a,71b], A. D'Avanzo[72a,72b], T. Davidek[136], J. Davidson[173], I. Dawson[96], K. De[8], C. De Almeida Rossi[161], R. De Asmundis[72a], N. De Biase[48], S. De Castro[24b,24a], N. De Groot[116], P. de Jong[117], H. De la Torre[118], A. De Maria[114a], A. De Salvo[75a], U. De Sanctis[76a,76b], F. De Santis[70a,70b], A. De Santo[152], J. B. De Vivie De Regie[60], J. Debevc[95], D. V. Dedovich[39], J. Degens[94], A. M. Deiana[45], J. Del Peso[101], L. Delagrange[130], F. Deliot[138], C. M. Delitzsch[49], M. Della Pietra[72a,72b], D. Della Volpe[56], A. Dell'Acqua[37], L. Dell'Asta[71a,71b], M. Delmastro[4], C. C. Delogu[102], P. A. Delsart[60], S. Demers[178], M. Demichev[39], S. P. Denisov[38], H. Denizli[22a,m], L. D'Eramo[41], D. Derendarz[87], F. Derue[130], P. Dervan[94,*], K. Desch[25], F. A. Di Bello[57b,57a], A. Di Ciaccio[76a,76b], L. Di Ciaccio[4], A. Di Domenico[75a,75b], C. Di Donato[72a,72b], A. Di Girolamo[37], G. Di Gregorio[37], A. Di Luca[78a,78b], B. Di Micco[77a,77b], R. Di Nardo[77a,77b], K. F. Di Petrillo[40], M. Diamantopoulou[35], F. A. Dias[117], M. A. Diaz[140a,140b], A. R. Didenko[39], M. Didenko[169], S. D. Diefenbacher[18a], E. B. Diehl[108], S. Díez Cornell[48], C. Diez Pardos[147], C. Dimitriadi[150], A. Dimitrievska[21], A. Dimri[151], J. Dingfelder[25], T. Dingley[129], I-M. Dinu[28b], S. J. Dittmeier[63b], F. Dittus[37], M. Divisek[136], B. Dixit[94], F. Djama[104], T. Djobava[155b], C. Doglioni[103,100],

A. Dohnalova[29a], Z. Dolezal[136], K. Domijan[86a], K. M. Dona[40], M. Donadelli[83d], B. Dong[109], J. Donini[41], A. D'Onofrio[72a,72b], M. D'Onofrio[94], J. Dopke[137], A. Doria[72a], N. Dos Santos Fernandes[133a], P. Dougan[103], M. T. Dova[92], A. T. Doyle[59], M. A. Draguet[129], M. P. Drescher[55], E. Dreyer[175], I. Drivas-koulouris[10], M. Drnevich[120], M. Drozdova[56], D. Du[62], T. A. du Pree[117], Z. Duan[114a], F. Dubinin[39], M. Dubovsky[29a], E. Duchovni[175], G. Duckeck[111], P. K. Duckett[98], O. A. Ducu[28b], D. Duda[52], A. Dudarev[37], E. R. Duden[27], M. D'uffizi[103], L. Duflot[66], M. Dührssen[37], I. Duminica[28g], A. E. Dumitriu[28b], M. Dunford[63a], S. Dungs[49], K. Dunne[47a,47b], A. Duperrin[104], H. Duran Yildiz[3a], M. Düren[58], A. Durglishvili[155b], D. Duvnjak[35], B. L. Dwyer[118], G. I. Dyckes[18a], M. Dyndal[86a], B. S. Dziedzic[37], Z. O. Earnshaw[152], G. H. Eberwein[129], B. Eckerova[29a], S. Eggebrecht[55], E. Egidio Purcino De Souza[83e], G. Eigen[17], K. Einsweiler[18a], T. Ekelof[167], P. A. Ekman[100], S. El Farkh[36b], Y. El Ghazali[62], H. El Jarrari[37], A. El Moussaouy[36a], V. Ellajosyula[167], M. Ellert[167], F. Ellinghaus[177], N. Ellis[37], J. Elmsheuser[30], M. Elsawy[119a], M. Elsing[37], D. Emeliyanov[137], Y. Enari[84], I. Ene[18a], S. Epari[110], D. Ernani Martins Neto[87], F. Ernst[37], M. Errenst[177], M. Escalier[66], C. Escobar[169], E. Etzion[157], G. Evans[133a,133b], H. Evans[68], L. S. Evans[97], A. Ezhilov[38], S. Ezzarqtouni[36a], F. Fabbri[24b,24a], L. Fabbri[24b,24a], G. Facini[98], V. Fadeyev[139], R. M. Fakhrutdinov[38], D. Fakoudis[102], S. Falciano[75a], L. F. Falda Ulhoa Coelho[133a], F. Fallavollita[112], G. Falsetti[44b,44a], J. Faltova[136], C. Fan[168], K. Y. Fan[64b], Y. Fan[14], Y. Fang[14,114c], M. Fanti[71a,71b], M. Faraj[69a,69b], Z. Farazpay[99], A. Farbin[8], A. Farilla[77a], T. Farooque[109], J. N. Farr[178], S. M. Farrington[137,52], F. Fassi[36e], D. Fassouliotis[9], L. Fayard[66], P. Federic[136], P. Federicova[134], O. L. Fedin[38,a], M. Feickert[176], L. Feligioni[104], D. E. Fellers[18a], C. Feng[143a], Z. Feng[117], M. J. Fenton[165], L. Ferencz[48], B. Fernandez Barbadillo[93], P. Fernandez Martinez[67], M. J. V. Fernoux[104], J. Ferrando[93], A. Ferrari[167], P. Ferrari[117,116], R. Ferrari[73a], D. Ferrere[56], C. Ferretti[108], M. P. Fewell[1], D. Fiacco[75a,75b], F. Fiedler[102], P. Fiedler[135], S. Filimonov[39], M. S. Filip[28b,u], A. Filipčič[95], E. K. Filmer[162a], F. Filthaut[116], M. C. N. Fiolhais[133a,133c,c], L. Fiorini[169], W. C. Fisher[109], T. Fitschen[103], P. M. Fitzhugh[138], I. Fleck[147], P. Fleischmann[108], T. Flick[177], M. Flores[34d,ag], L. R. Flores Castillo[64a], L. Flores Sanz De Acedo[37], F. M. Follega[78a,78b], N. Fomin[33], J. H. Foo[161], A. Formica[138], A. C. Forti[103], E. Fortin[37], A. W. Fortman[18a], L. Foster[18a], L. Fountas[9,j], D. Fournier[66], H. Fox[93], P. Francavilla[74a,74b], S. Francescato[61], S. Franchellucci[56], M. Franchini[24b,24a], S. Franchino[63a], D. Francis[37], L. Franco[116], V. Franco Lima[37], L. Franconi[48], M. Franklin[61], G. Frattari[27], Y. Y. Frid[157], J. Friend[59], N. Fritzsche[37], A. Froch[56], D. Froidevaux[37], J. A. Frost[129], Y. Fu[109], S. Fuenzalida Garrido[140f], M. Fujimoto[104], K. Y. Fung[64a], E. Furtado De Simas Filho[83e], M. Furukawa[159], J. Fuster[169], A. Gaa[55], A. Gabrielli[24b,24a], A. Gabrielli[161], P. Gadow[37], G. Gagliardi[57b,57a], L. G. Gagnon[18a], S. Gaid[88b], S. Galantzan[157], J. Gallagher[1], E. J. Gallas[129], A. L. Gallen[167], B. J. Gallop[137], K. K. Gan[122], S. Ganguly[159], Y. Gao[52], A. Garabaglu[142], F. M. Garay Walls[140a,140b], C. García[169], A. Garcia Alonso[117], A. G. Garcia Caffaro[178], J. E. García Navarro[169], M. Garcia-Sciveres[18a], G. L. Gardner[131], R. W. Gardner[40], N. Garelli[164], R. B. Garg[149], J. M. Gargan[52], C. A. Garner[161], C. M. Garvey[34a], V. K. Gassmann[164], G. Gaudio[73a], V. Gautam[13], P. Gauzzi[75a,75b], J. Gavranovic[95], I. L. Gavrilenko[133a], A. Gavrilyuk[38], C. Gay[170], G. Gaycken[126], E. N. Gazis[10], A. Gekow[122], C. Gemme[57b], M. H. Genest[60], A. D. Gentry[115], S. George[97], T. Geralis[46], A. A. Gerwin[123], P. Gessinger-Befurt[37], M. E. Geyik[177], M. Ghani[173], K. Ghorbanian[96], A. Ghosal[147], A. Ghosh[165], A. Ghosh[7], B. Giacobbe[24b], S. Giagu[75a,75b], T. Giani[117], A. Giannini[62], S. M. Gibson[97], M. Gignac[139], D. T. Gil[86b], A. K. Gilbert[86a], B. J. Gilbert[42], D. Gillberg[35], G. Gilles[117], D. M. Gingrich[2,ai], M. P. Giordani[69a,69c], P. F. Giraud[138], G. Giugliarelli[69a,69c], D. Giugni[71a], F. Giuli[76a,76b], I. Gkialas[9,j], L. K. Gladilin[38], C. Glasman[101], M. Glazewska[20], R. M. Gleason[165], G. Glemža[48], M. Glisic[126], I. Gnesi[44b], Y. Go[30], M. Goblirsch-Kolb[37], B. Gocke[49], D. Godin[110], B. Gokturk[22a], S. Goldfarb[107], T. Golling[56], M. G. D. Gololo[34c], D. Golubkov[38], J. P. Gombas[109], A. Gomes[133a,133b], G. Gomes Da Silva[147], A. J. Gomez Delegido[169], R. Gonçalo[133a], L. Gonella[21], A. Gongadze[155c], F. Gonnella[21], J. L. Gonski[149], R. Y. González Andana[52], S. González de la Hoz[169], M. V. Gonzalez Rodrigues[48], R. Gonzalez Suarez[167], S. Gonzalez-Sevilla[56], L. Goossens[37], B. Gorini[37], E. Gorini[70a,70b], A. Gorišek[95], T. C. Gosart[131], A. T. Goshaw[51], M. I. Gostkin[39], S. Goswami[124], C. A. Gottardo[37], S. A. Gotz[111], M. Gouighri[36b], A. G. Goussiou[142], N. Govender[34c], R. P. Grabarczyk[129], I. Grabowska-Bold[86a], K. Graham[35], E. Gramstad[128], S. Grancagnolo[70a,70b], C. M. Grant[1], P. M. Gravila[28f], F. G. Gravili[70a,70b], H. M. Gray[18a], M. Greco[112], M. J. Green[1], C. Grefe[25], A. S. Grefsrud[17], I. M. Gregor[48], K. T. Greif[165], P. Grenier[149], S. G. Grewe[112], A. A. Grillo[139], K. Grimm[32], S. Grinstein[13,y], J.-F. Grivaz[66], E. Gross[175], J. Grosse-Knetter[55], L. Guan[108], G. Guerrieri[37], R. Guevara[128], R. Gugel[102], J. A. M. Guhit[108], A. Guida[19], E. Guilloton[173], S. Guindon[37], F. Guo[14,114c], J. Guo[144a], L. Guo[48], L. Guo[114b,w],

Y. Guo[108], A. Gupta[49], R. Gupta[132], S. Gupta[27], S. Gurbuz[25], S. S. Gurdasani[48], G. Gustavino[75a,75b], P. Gutierrez[123], L. F. Gutierrez Zagazeta[131], M. Gutsche[50], C. Gutschow[98], C. Gwenlan[129], C. B. Gwilliam[94], E. S. Haaland[128], A. Haas[120], M. Habedank[59], C. Haber[18a], H. K. Hadavand[8], A. Haddad[41], A. Hadef[50], A. I. Hagan[93], J. J. Hahn[147], E. H. Haines[98], M. Haleem[172], J. Haley[124], G. D. Hallewell[104], L. Halser[20], K. Hamano[171], M. Hamer[25], S. E. D. Hammoud[66], E. J. Hampshire[97], J. Han[143a], L. Han[114a], L. Han[62], S. Han[18a], K. Hanagaki[84], M. Hance[139], D. A. Hangal[42], H. Hanif[148], M. D. Hank[131], J. B. Hansen[43], P. H. Hansen[43], D. Harada[56], T. Harenberg[177], S. Harkusha[179], M. L. Harris[105], Y. T. Harris[25], J. Harrison[13], N. M. Harrison[122], P. F. Harrison[173], M. L. E. Hart[98], N. M. Hartman[112], N. M. Hartmann[111], R. Z. Hasan[97,137], Y. Hasegawa[146], F. Haslbeck[129], S. Hassan[17], R. Hauser[109], M. Haviernik[136], C. M. Hawkes[21], R. J. Hawkings[37], Y. Hayashi[159], D. Hayden[109], C. Hayes[108], R. L. Hayes[117], C. P. Hays[129], J. M. Hays[96], H. S. Hayward[94], M. He[14,114c], Y. He[48], Y. He[98], N. B. Heatley[96], V. Hedberg[100], C. Heidegger[54], K. K. Heidegger[54], J. Heilman[35], S. Heim[48], T. Heim[18a], J. G. Heinlein[131], J. J. Heinrich[126], L. Heinrich[112], J. Hejbal[134], M. Helbig[50], A. Held[176], S. Hellesund[17], C. M. Helling[170], S. Hellman[47a,47b], A. M. Henriques Correia[37], H. Herde[100], Y. Hernández Jiménez[151], L. M. Herrmann[25], T. Herrmann[50], G. Herten[54], R. Hertenberger[111], L. Hervas[37], M. E. Hesping[102], N. P. Hessey[162a], J. Hessler[112], M. Hidaoui[36b], N. Hidic[136], E. Hill[161], T. S. Hillersoy[17], S. J. Hillier[21], J. R. Hinds[109], F. Hinterkeuser[25], M. Hirose[127], S. Hirose[163], D. Hirschbuehl[177], T. G. Hitchings[103], B. Hiti[95], J. Hobbs[151], R. Hobincu[28e], N. Hod[175], A. M. Hodges[168], M. C. Hodgkinson[145], B. H. Hodkinson[129], A. Hoecker[37], D. D. Hofer[108], J. Hofer[169], M. Holzbock[37], L. B. A. H. Hommels[33], V. Homsak[129], B. P. Honan[103], J. J. Hong[68], T. M. Hong[132], B. H. Hooberman[168], W. H. Hopkins[6], M. C. Hoppesch[168], Y. Horii[113], M. E. Horstmann[112], S. Hou[154], M. R. Housenga[168], A. S. Howard[95], J. Howarth[59], J. Hoya[6], M. Hrabovsky[125], T. Hryn'ova[4], P. J. Hsu[65], S.-C. Hsu[142], T. Hsu[66], M. Hu[18a], Q. Hu[62], S. Huang[33], X. Huang[14,114c], Y. Huang[136], Y. Huang[114b], Y. Huang[102], Y. Huang[14], Z. Huang[66], Z. Hubacek[135], M. Huebner[25], F. Huegging[25], T. B. Huffman[129], M. Hufnagel Maranha De Faria[83a], C. A. Hugli[48], M. Huhtinen[37], S. K. Huiberts[17], R. Hulsken[106], C. E. Hultquist[18a], N. Huseynov[12,g], J. Huston[109], J. Huth[61], R. Hyneman[7], G. Iacobucci[56], G. Iakovidis[30], L. Iconomidou-Fayard[66], J. P. Iddon[37], P. Iengo[72a,72b], R. Iguchi[159], Y. Iiyama[159], T. Iizawa[159], Y. Ikegami[84], D. Iliadis[158], N. Ilic[161], H. Imam[36a], G. Inacio Goncalves[83d], S. A. Infante Cabanas[140c], T. Ingebretsen Carlson[47a,47b], J. M. Inglis[96], G. Introzzi[73a,73b], M. Iodice[77a], V. Ippolito[75a,75b], R. K. Irwin[94], M. Ishino[159], W. Islam[176], C. Issever[19], S. Istin[22a,an], K. Itabashi[84], H. Ito[174], R. Iuppa[78a,78b], A. Ivina[175], V. Izzo[72a], P. Jacka[134], P. Jackson[1], P. Jain[48], K. Jakobs[54], T. Jakoubek[175], J. Jamieson[59], W. Jang[159], S. Jankovych[136], M. Javurkova[105], P. Jawahar[103], L. Jeanty[126], J. Jejelava[155a,af], P. Jenni[54,f], C. E. Jessiman[35], C. Jia[143a], H. Jia[170], J. Jia[151], X. Jia[14,114c], Z. Jia[114a], C. Jiang[52], Q. Jiang[64b], S. Jiggins[48], M. Jimenez Ortega[169], J. Jimenez Pena[13], S. Jin[114a], A. Jinaru[28b], O. Jinnouchi[141], P. Johansson[145], K. A. Johns[7], J. W. Johnson[139], F. A. Jolly[48], D. M. Jones[152], E. Jones[48], K. S. Jones[8], P. Jones[33], R. W. L. Jones[93], T. J. Jones[94], H. L. Joos[55,37], R. Joshi[122], J. Jovicevic[16], X. Ju[18a], J. J. Junggeburth[37], T. Junkermann[63a], A. Juste Rozas[13,y], M. K. Juzek[87], S. Kabana[140e], A. Kaczmarska[87], M. Kado[112], H. Kagan[122], M. Kagan[149], A. Kahn[131], C. Kahra[102], T. Kaji[159], E. Kajomovitz[156], N. Kakati[175], N. Kakoty[13], I. Kalaitzidou[54], S. Kandel[8], N. J. Kang[139], D. Kar[34g], K. Karava[129], E. Karentzos[25], O. Karkout[117], S. N. Karpov[39], Z. M. Karpova[39], V. Kartvelishvili[93], A. N. Karyukhin[38], E. Kasimi[158], J. Katzy[48], S. Kaur[35], K. Kawade[146], M. P. Kawale[123], C. Kawamoto[89], T. Kawamoto[62], E. F. Kay[37], F. I. Kaya[164], S. Kazakos[109], V. F. Kazanin[38], J. M. Keaveney[34a], R. Keeler[171], G. V. Kehris[61], J. S. Keller[35], J. J. Kempster[152], O. Kepka[134], J. Kerr[162b], B. P. Kerridge[137], B. P. Kerševan[95], L. Keszeghova[29a], R. A. Khan[132], A. Khanov[124], A. G. Kharlamov[38], T. Kharlamova[38], E. E. Khoda[142], M. Kholodenko[133a], T. J. Khoo[19], G. Khoriauli[172], Y. Khoulaki[36a], J. Khubua[155b,*], Y. A. R. Khwaira[130], B. Kibirige[34g], D. Kim[6], D. W. Kim[47a,47b], Y. K. Kim[40], N. Kimura[98], M. K. Kingston[55], A. Kirchhoff[55], C. Kirfel[25], F. Kirfel[25], J. Kirk[137], A. E. Kiryunin[112], S. Kita[163], O. Kivernyk[25], M. Klassen[164], C. Klein[35], L. Klein[172], M. H. Klein[45], S. B. Klein[56], U. Klein[94], A. Klimentov[30], T. Klioutchnikova[37], P. Kluit[117], S. Kluth[112], E. Kneringer[79], T. M. Knight[161], A. Knue[49], M. Kobel[50], D. Kobylianskii[175], S. F. Koch[129], M. Kocian[149], P. Kodyš[136], D. M. Koeck[126], T. Koffas[35], O. Kolay[50], I. Koletsou[4], T. Komarek[87], K. Köneke[55], A. X. Y. Kong[1], T. Kono[121], N. Konstantinidis[98], P. Kontaxakis[56], B. Konya[100], R. Kopeliansky[42], S. Koperny[86a], K. Korcyl[87], K. Kordas[158,d], A. Korn[98], S. Korn[55], I. Korolkov[13], N. Korotkova[38], B. Kortman[117], O. Kortner[112], S. Kortner[112], W. H. Kostecka[118], M. Kostov[29a], V. V. Kostyukhin[147],

A. Kotsokechagia[37], A. Kotwal[51], A. Koulouris[37], A. Kourkoumeli-Charalampidi[73a,73b], C. Kourkoumelis[9], E. Kourlitis[112], O. Kovanda[126], R. Kowalewski[171], W. Kozanecki[126], A. S. Kozhin[38], V. A. Kramarenko[38], G. Kramberger[95], P. Kramer[25], M. W. Krasny[130], A. Krasznahorkay[105], A. C. Kraus[118], J. W. Kraus[177], J. A. Kremer[48], N. B. Krengel[147], T. Kresse[50], L. Kretschmann[177], J. Kretzschmar[94], K. Kreul[19], P. Krieger[161], K. Krizka[21], K. Kroeninger[49], H. Kroha[112], J. Kroll[134], J. Kroll[131], K. S. Krowpman[109], U. Kruchonak[39], H. Krüger[25], N. Krumnack[81], M. C. Kruse[51], O. Kuchinskaia[39], S. Kuday[3a], S. Kuehn[37], R. Kuesters[54], T. Kuhl[48], V. Kukhtin[39], Y. Kulchitsky[39], S. Kuleshov[140d,140b], J. Kull[1], M. Kumar[34g], N. Kumari[48], P. Kumari[162b], A. Kupco[134], T. Kupfer[49], A. Kupich[38], O. Kuprash[54], H. Kurashige[85], L. L. Kurchaninov[162a], O. Kurdysh[4], Y. A. Kurochkin[38], A. Kurova[38], M. Kuze[141], A. K. Kvam[105], J. Kvita[125], N. G. Kyriacou[108], C. Lacasta[169], F. Lacava[75a,75b], H. Lacker[19], D. Lacour[130], N. N. Lad[98], E. Ladygin[39], A. Lafarge[41], B. Laforge[130], T. Lagouri[178], F. Z. Lahbabi[36a], S. Lai[55], J. E. Lambert[171], S. Lammers[68], W. Lampl[7], C. Lampoudis[158,d], G. Lamprinoudis[102], A. N. Lancaster[118], E. Lançon[30], U. Landgraf[54], M. P. J. Landon[96], V. S. Lang[54], O. K. B. Langrekken[128], A. J. Lankford[165], F. Lanni[37], K. Lantzsch[25], A. Lanza[73a], M. Lanzac Berrocal[169], J. F. Laporte[138], T. Lari[71a], D. Larsen[17], L. Larson[11], F. Lasagni Manghi[24b], M. Lassnig[37], S. D. Lawlor[145], R. Lazaridou[173], M. Lazzaroni[71a,71b], H. D. M. Le[109], E. M. Le Boulicaut[178], L. T. Le Pottier[18a], B. Leban[24b,24a], F. Ledroit-Guillon[60], T. F. Lee[162b], L. L. Leeuw[34c], M. Lefebvre[171], C. Leggett[18a], G. Lehmann Miotto[37], M. Leigh[56], W. A. Leight[105], W. Leinonen[116], A. Leisos[158,v], M. A. L. Leite[83c], C. E. Leitgeb[19], R. Leitner[136], K. J. C. Leney[45], T. Lenz[25], S. Leone[74a], C. Leonidopoulos[52], A. Leopold[150], J. H. Lepage Bourbonnais[35], R. Les[109], C. G. Lester[33], M. Levchenko[38], J. Levêque[4], L. J. Levinson[175], G. Levrini[24b,24a], M. P. Lewicki[87], C. Lewis[142], D. J. Lewis[4], L. Lewitt[145], A. Li[30], B. Li[143a], C. Li[108], C-Q. Li[112], H. Li[143a], H. Li[103], H. Li[15], H. Li[62], H. Li[143a], J. Li[144a], K. Li[14], L. Li[144a], R. Li[178], S. Li[14,114c], S. Li[144b,144a], T. Li[5], X. Li[106], Z. Li[159], Z. Li[14,114c], Z. Li[62], S. Liang[14,114c], Z. Liang[14], M. Liberatore[138], B. Liberti[76a], K. Lie[64c], J. Lieber Marin[83e], H. Lien[68], H. Lin[108], S. F. Lin[151], L. Linden[111], R. E. Lindley[7], J. H. Lindon[37], J. Ling[61], E. Lipeles[131], A. Lipniacka[17], A. Lister[170], J. D. Little[68], B. Liu[14], B. X. Liu[114b], D. Liu[144b,144a], D. Liu[139], E. H. L. Liu[21], J. K. K. Liu[120], K. Liu[144b], K. Liu[144b,144a], M. Liu[62], M. Y. Liu[62], P. Liu[14], Q. Liu[144b,142,144a], X. Liu[62], X. Liu[143a], Y. Liu[114b,114c], Y. L. Liu[143a], Y. W. Liu[62], Z. Liu[66,l], S. L. Lloyd[96], E. M. Lobodzinska[48], P. Loch[7], E. Lodhi[161], T. Lohse[19], K. Lohwasser[145], E. Loiacono[48], J. D. Lomas[21], J. D. Long[42], I. Longarini[165], R. Longo[168], A. Lopez Solis[13], N. A. Lopez-canelas[7], N. Lorenzo Martinez[4], A. M. Lory[111], M. Losada[119a], G. Löschcke Centeno[152], X. Lou[47a,47b], X. Lou[14,114c], A. Lounis[66], P. A. Love[93], M. Lu[66], S. Lu[131], Y. J. Lu[154], H. J. Lubatti[142], C. Luci[75a,75b], F. L. Lucio Alves[114a], F. Luehring[68], B. S. Lunday[131], O. Lundberg[150], J. Lunde[37], N. A. Luongo[6], M. S. Lutz[37], A. B. Lux[26], D. Lynn[30], R. Lysak[134], V. Lysenko[135], E. Lytken[100], V. Lyubushkin[39], T. Lyubushkina[39], M. M. Lyukova[151], M. F. Mohd Soberi[52], H. Ma[30], K. Ma[62], L. L. Ma[143a], W. Ma[62], Y. Ma[124], J. C. MacDonald[102], P. C. Machado De Abreu Farias[83e], R. Madar[41], T. Madula[98], J. Maeda[85], T. Maeno[30], P. T. Mafa[34c,k], H. Maguire[145], V. Maiboroda[66], A. Maio[133a,133b,133d], K. Maj[86a], O. Majersky[48], S. Majewski[126], R. Makhmanazarov[38], N. Makovec[66], V. Maksimovic[16], B. Malaescu[130], J. Malamant[128], Pa. Malecki[87], V. P. Maleev[38], F. Malek[60,p], M. Mali[95], D. Malito[97], U. Mallik[80,*], A. Maloizel[5], S. Maltezos[10], A. Malvezzi Lopes[83d], S. Malyukov[39], J. Mamuzic[13], G. Mancini[53], M. N. Mancini[27], G. Manco[73a,73b], J. P. Mandalia[96], S. S. Mandarry[152], I. Mandić[95], L. Manhaes de Andrade Filho[83a], I. M. Maniatis[175], J. Manjarres Ramos[91], D. C. Mankad[175], A. Mann[111], T. Manoussos[37], M. N. Mantinan[40], S. Manzoni[37], L. Mao[144a], X. Mapekula[34c], A. Marantis[158], R. R. Marcelo Gregorio[96], G. Marchiori[5], M. Marcisovsky[134], C. Marcon[71a], E. Maricic[16], M. Marinescu[48], S. Marium[48], M. Marjanovic[123], A. Markhoos[54], M. Markovitch[66], M. K. Maroun[105], G. T. Marsden[103], E. J. Marshall[93], Z. Marshall[18a], S. Marti-Garcia[169], J. Martin[98], T. A. Martin[137], V. J. Martin[52], B. Martin dit Latour[17], L. Martinelli[75a,75b], M. Martinez[13,y], P. Martinez Agullo[169], V. I. Martinez Outschoorn[105], P. Martinez Suarez[13], S. Martin-Haugh[137], G. Martinovicova[136], V. S. Martoiu[28b], A. C. Martyniuk[98], A. Marzin[37], D. Mascione[78a,78b], L. Masetti[102], J. Masik[103], A. L. Maslennikov[39], S. L. Mason[42], P. Massarotti[72a,72b], P. Mastrandrea[74a,74b], A. Mastroberardino[44b,44a], T. Masubuchi[127], T. T. Mathew[126], J. Matousek[136], D. M. Mattern[49], J. Maurer[28b], T. Maurin[59], A. J. Maury[66], B. Maček[95], C. Mavungu Tsava[104], D. A. Maximov[38], A. E. May[103], E. Mayer[41], R. Mazini[34g], I. Maznas[118], S. M. Mazza[139], E. Mazzeo[37], J. P. Mc Gowan[171], S. P. Mc Kee[108], C. A. Mc Lean[6], C. C. McCracken[170], E. F. McDonald[107], A. E. McDougall[117], L. F. Mcelhinney[93], J. A. Mcfayden[152], R. P. McGovern[131],

R. P. Mckenzie[34g], T. C. Mclachlan[48], D. J. Mclaughlin[98], S. J. McMahon[137], C. M. Mcpartland[94], R. A. McPherson[171,ac], S. Mehlhase[111], A. Mehta[94], D. Melini[169], B. R. Mellado Garcia[34g], A. H. Melo[55], F. Meloni[48], A. M. Mendes Jacques Da Costa[103], L. Meng[93], S. Menke[112], M. Mentink[37], E. Meoni[44b,44a], G. Mercado[118], S. Merianos[158], C. Merlassino[69a,69c], C. Meroni[71a,71b], J. Metcalfe[6], A. S. Mete[6], E. Meuser[102], C. Meyer[68], J-P. Meyer[138], Y. Miao[114a], R. P. Middleton[137], M. Mihovilovic[66], L. Mijović[52], G. Mikenberg[175], M. Mikestikova[134], M. Mikuž[95], H. Mildner[102], A. Milic[37], D. W. Miller[40], E. H. Miller[149], L. S. Miller[35], A. Milov[175], D. A. Milstead[47a,47b], T. Min[114a], A. A. Minaenko[38], I. A. Minashvili[155b], A. I. Mincer[120], B. Mindur[86a], M. Mineev[39], Y. Mino[89], L. M. Mir[13], M. Miralles Lopez[59], M. Mironova[18a], M. C. Missio[116], A. Mitra[173], V. A. Mitsou[169], Y. Mitsumori[113], O. Miu[161], P. S. Miyagawa[96], T. Mkrtchyan[63a], M. Mlinarevic[98], T. Mlinarevic[98], M. Mlynarikova[37], S. Mobius[20], M. H. Mohamed Farook[115], S. Mohapatra[42], S. Mohiuddin[124], G. Mokgatitswane[34g], L. Moleri[175], U. Molinatti[129], L. G. Mollier[20], B. Mondal[134], S. Mondal[135], K. Mönig[48], E. Monnier[104], L. Monsonis Romero[169], J. Montejo Berlingen[13], A. Montella[47a,47b], M. Montella[122], F. Montereali[77a,77b], F. Monticelli[92], S. Monzani[69a,69c], A. Morancho Tarda[43], N. Morange[66], A. L. Moreira De Carvalho[48], M. Moreno Llácer[169], C. Moreno Martinez[56], J. M. Moreno Perez[23b], P. Morettini[57b], S. Morgenstern[37], M. Morii[61], M. Morinaga[159], M. Moritsu[90], F. Morodei[75a,75b], P. Moschovakos[37], B. Moser[54], M. Mosidze[155b], T. Moskalets[45], P. Moskvitina[116], J. Moss[32], P. Moszkowicz[86a], A. Moussa[36d], Y. Moyal[175], H. Moyano Gomez[13], E. J. W. Moyse[105], O. Mtintsilana[34g], S. Muanza[104], M. Mucha[25], J. Mueller[132], R. Müller[37], G. A. Mullier[167], A. J. Mullin[33], J. J. Mullin[51], A. C. Mullins[45], A. E. Mulski[61], D. P. Mungo[161], D. Munoz Perez[169], F. J. Munoz Sanchez[103], W. J. Murray[173,137], M. Muškinja[95], C. Mwewa[48], A. G. Myagkov[38,a], A. J. Myers[8], G. Myers[108], M. Myska[135], B. P. Nachman[18a], K. Nagai[129], K. Nagano[84], R. Nagasaka[159], J. L. Nagle[30,ak], E. Nagy[104], A. M. Nairz[37], Y. Nakahama[84], K. Nakamura[84], K. Nakkalil[5], A. Nandi[63b], H. Nanjo[127], E. A. Narayanan[45], Y. Narukawa[159], I. Naryshkin[38], L. Nasella[71a,71b], S. Nasri[119b], C. Nass[25], G. Navarro[23a], J. Navarro-Gonzalez[169], A. Nayaz[19], P. Y. Nechaeva[38], S. Nechaeva[24b,24a], F. Nechansky[134], L. Nedic[129], T. J. Neep[21], A. Negri[73a,73b], M. Negrini[24b], C. Nellist[117], C. Nelson[106], K. Nelson[108], S. Nemecek[134], M. Nessi[37,h], M. S. Neubauer[168], J. Newell[94], P. R. Newman[21], Y. W. Y. Ng[168], B. Ngair[119a], H. D. N. Nguyen[110], J. D. Nichols[123], R. B. Nickerson[129], R. Nicolaidou[138], J. Nielsen[139], M. Niemeyer[55], J. Niermann[37], N. Nikiforou[37], V. Nikolaenko[38,a], I. Nikolic-Audit[130], P. Nilsson[30], I. Ninca[48], G. Ninio[157], A. Nisati[75a], N. Nishu[2], R. Nisius[112], N. Nitika[69a,69c], J-E. Nitschke[50], E. K. Nkadimeng[34b], T. Nobe[159], T. Nommensen[153], M. B. Norfolk[145], B. J. Norman[35], M. Noury[36a], J. Novak[95], T. Novak[95], R. Novotny[135], L. Nozka[125], K. Ntekas[165], N. M. J. Nunes De Moura Junior[83b], J. Ocariz[130], A. Ochi[85], I. Ochoa[133a], S. Oerdek[48,z], J. T. Offermann[40], A. Ogrodnik[136], A. Oh[103], C. C. Ohm[150], H. Oide[84], M. L. Ojeda[37], Y. Okumura[159], L. F. Oleiro Seabra[133a], I. Oleksiyuk[56], G. Oliveira Correa[13], D. Oliveira Damazio[30], J. L. Oliver[165], Ö. O. Öncel[54], A. P. O'Neill[20], A. Onofre[133a,133e,e], P. U. E. Onyisi[11], M. J. Oreglia[40], D. Orestano[77a,77b], R. Orlandini[77a,77b], R. S. Orr[161], L. M. Osojnak[131], Y. Osumi[113], G. Otero y Garzon[31], H. Otono[90], G. J. Ottino[18a], M. Ouchrif[36d], F. Ould-Saada[128], T. Ovsiannikova[142], M. Owen[59], R. E. Owen[137], V. E. Ozcan[22a], F. Ozturk[87], N. Ozturk[8], S. Ozturk[82], H. A. Pacey[129], K. Pachal[162a], A. Pacheco Pages[13], C. Padilla Aranda[13], G. Padovano[75a,75b], S. Pagan Griso[18a], G. Palacino[68], A. Palazzo[70a,70b], J. Pampel[25], J. Pan[178], T. Pan[64a], D. K. Panchal[11], C. E. Pandini[60], J. G. Panduro Vazquez[137], H. D. Pandya[1], H. Pang[138], P. Pani[48], G. Panizzo[69a,69c], L. Panwar[130], L. Paolozzi[56], S. Parajuli[168], A. Paramonov[6], C. Paraskevopoulos[53], D. Paredes Hernandez[64b], A. Pareti[73a,73b], K. R. Park[42], T. H. Park[112], F. Parodi[57b,57a], J. A. Parsons[42], U. Parzefall[54], B. Pascual Dias[41], L. Pascual Dominguez[101], E. Pasqualucci[75a], S. Passaggio[57b], F. Pastore[97], P. Patel[87], U. M. Patel[51], J. R. Pater[103], T. Pauly[37], F. Pauwels[136], C. I. Pazos[164], M. Pedersen[128], R. Pedro[133a], S. V. Peleganchuk[38], O. Penc[37], E. A. Pender[52], S. Peng[15], G. D. Penn[178], K. E. Penski[111], M. Penzin[38], B. S. Peralva[83d], A. P. Pereira Peixoto[142], L. Pereira Sanchez[149], D. V. Perepelitsa[30,ak], G. Perera[105], E. Perez Codina[37], M. Perganti[10], H. Pernegger[37], S. Perrella[75a,75b], O. Perrin[41], K. Peters[48], R. F. Y. Peters[103], B. A. Petersen[37], T. C. Petersen[43], E. Petit[104], V. Petousis[135], A. R. Petri[71a,71b], C. Petridou[158,d], T. Petru[136], A. Petrukhin[147], M. Pettee[18a], A. Petukhov[82], K. Petukhova[37], R. Pezoa[140f], L. Pezzotti[24b,24a], G. Pezzullo[178], L. Pfaffenbichler[37], A. J. Pfleger[37], T. M. Pham[176], T. Pham[107], P. W. Phillips[137], G. Piacquadio[151], E. Pianori[18a], F. Piazza[126], R. Piegaia[31], D. Pietreanu[28b], A. D. Pilkington[103], M. Pinamonti[69a,69c], J. L. Pinfold[2], B. C. Pinheiro Pereira[133a], J. Pinol Bel[13], A. E. Pinto Pinoargote[130], L. Pintucci[69a,69c], K. M. Piper[152],

A. Pirttikoski[56], D. A. Pizzi[35], L. Pizzimento[64b], A. Plebani[33], M.-A. Pleier[30], V. Pleskot[136], E. Plotnikova[39], G. Poddar[96], R. Poettgen[100], L. Poggioli[130], S. Polacek[136], G. Polesello[73a], A. Poley[148], A. Polini[24b], C. S. Pollard[173], Z. B. Pollock[122], E. Pompa Pacchi[123], N. I. Pond[98], D. Ponomarenko[68], L. Pontecorvo[37], S. Popa[28a], G. A. Popeneciu[28d], A. Poreba[37], D. M. Portillo Quintero[162a], S. Pospisil[135], M. A. Postill[145], P. Postolache[28c], K. Potamianos[173], P. A. Potepa[86a], I. N. Potrap[39], C. J. Potter[33], H. Potti[153], J. Poveda[169], M. E. Pozo Astigarraga[37], R. Pozzi[37], A. Prades Ibanez[76a,76b], J. Pretel[171], D. Price[103], M. Primavera[70a], L. Primomo[69a,69c], M. A. Principe Martin[101], R. Privara[125], T. Procter[86b], M. L. Proffitt[142], N. Proklova[131], K. Prokofiev[64c], G. Proto[112], J. Proudfoot[6], M. Przybycien[86a], W. W. Przygoda[86b], A. Psallidas[46], J. E. Puddefoot[145], D. Pudzha[53], D. Pyatiizbyantseva[116], J. Qian[108], R. Qian[109], D. Qichen[103], Y. Qin[13], T. Qiu[52], A. Quadt[55], M. Queitsch-Maitland[103], G. Quetant[56], R. P. Quinn[170], G. Rabanal Bolanos[61], D. Rafanoharana[112], F. Raffaeli[76a,76b], F. Ragusa[71a,71b], J. L. Rainbolt[40], J. A. Raine[56], S. Rajagopalan[30], E. Ramakoti[39], L. Rambelli[57b,57a], I. A. Ramirez-Berend[35], K. Ran[48,114c], D. S. Rankin[131], N. P. Rapheeha[34g], H. Rasheed[28b], D. F. Rassloff[63a], A. Rastogi[18a], S. Rave[102], S. Ravera[57b,57a], B. Ravina[37], I. Ravinovich[175], M. Raymond[37], A. L. Read[128], N. P. Readioff[145], D. M. Rebuzzi[73a,73b], A. S. Reed[112], K. Reeves[27], J. A. Reidelsturz[177], D. Reikher[126], A. Rej[49], C. Rembser[37], H. Ren[62], M. Renda[28b], F. Renner[48], A. G. Rennie[59], A. L. Rescia[48], S. Resconi[71a], M. Ressegotti[57b,57a], S. Rettie[37], W. F. Rettie[35], E. Reynolds[18a], O. L. Rezanova[39], P. Reznicek[136], H. Riani[36d], N. Ribaric[51], E. Ricci[78a,78b], R. Richter[112], S. Richter[47a,47b], E. Richter-Was[86b], M. Ridel[130], S. Ridouani[36d], P. Rieck[120], P. Riedler[37], E. M. Riefel[47a,47b], J. O. Rieger[117], M. Rijssenbeek[151], M. Rimoldi[37], L. Rinaldi[24b,24a], P. Rincke[167,55], G. Ripellino[167], I. Riu[13], J. C. Rivera Vergara[171], F. Rizatdinova[124], E. Rizvi[96], B. R. Roberts[18a], S. S. Roberts[139], D. Robinson[33], M. Robles Manzano[102], A. Robson[59], A. Rocchi[76a,76b], C. Roda[74a,74b], S. Rodriguez Bosca[37], Y. Rodriguez Garcia[23a], A. M. Rodríguez Vera[118], S. Roe[37], J. T. Roemer[37], O. Røhne[128], R. A. Rojas[37], C. P. A. Roland[130], A. Romaniouk[79], E. Romano[73a,73b], M. Romano[24b], A. C. Romero Hernandez[168], N. Rompotis[94], L. Roos[130], S. Rosati[75a], B. J. Rosser[40], E. Rossi[129], E. Rossi[72a,72b], L. P. Rossi[61], L. Rossini[54], R. Rosten[122], M. Rotaru[28b], B. Rottler[54], D. Rousseau[66], D. Rousso[48], S. Roy-Garand[161], A. Rozanov[104], Z. M. A. Rozario[59], Y. Rozen[156], A. Rubio Jimenez[169], V. H. Ruelas Rivera[19], T. A. Ruggeri[1], A. Ruggiero[129], A. Ruiz-Martinez[169], A. Rummler[37], Z. Rurikova[54], N. A. Rusakovich[39], H. L. Russell[171], G. Russo[75a,75b], J. P. Rutherfoord[7], S. Rutherford Colmenares[33], M. Rybar[136], P. Rybczynski[86a], A. Ryzhov[45], J. A. Sabater Iglesias[56], H.F-W. Sadrozinski[139], F. Safai Tehrani[75a], S. Saha[1], M. Sahinsoy[82], B. Sahoo[175], A. Saibel[169], B. T. Saifuddin[123], M. Saimpert[138], G. T. Saito[83c], M. Saito[159], T. Saito[159], A. Sala[71a,71b], A. Salnikov[149], J. Salt[169], A. Salvador Salas[157], F. Salvatore[152], A. Salzburger[37], D. Sammel[54], E. Sampson[93], D. Sampsonidis[158,d], D. Sampsonidou[126], J. Sánchez[169], V. Sanchez Sebastian[169], H. Sandaker[128], C. O. Sander[48], J. A. Sandesara[176], M. Sandhoff[177], C. Sandoval[23b], L. Sanfilippo[63a], D. P. C. Sankey[137], T. Sano[89], A. Sansoni[53], L. Santi[37], C. Santoni[41], H. Santos[133a,133b], A. Santra[175], E. Sanzani[24b,24a], K. A. Saoucha[88b], J. G. Saraiva[133a,133d], J. Sardain[7], O. Sasaki[84], K. Sato[163], C. Sauer[37], E. Sauvan[4], P. Savard[161,ai], R. Sawada[159], C. Sawyer[137], L. Sawyer[99], C. Sbarra[24b], A. Sbrizzi[24b,24a], T. Scanlon[98], J. Schaarschmidt[142], U. Schäfer[102], A. C. Schaffer[66,45], D. Schaile[111], R. D. Schamberger[151], C. Scharf[19], M. M. Schefer[20], V. A. Schegelsky[38], D. Scheirich[136], M. Schernau[140c], C. Scheulen[56], C. Schiavi[57b,57a], M. Schioppa[44b,44a], B. Schlag[149], S. Schlenker[37], J. Schmeing[177], E. Schmidt[112], M. A. Schmidt[177], K. Schmieden[102], C. Schmitt[102], N. Schmitt[102], S. Schmitt[48], L. Schoeffel[138], A. Schoening[63b], P. G. Scholer[35], E. Schopf[147], M. Schott[25], S. Schramm[56], T. Schroer[56], H-C. Schultz-Coulon[63a], M. Schumacher[54], B. A. Schumm[139], Ph. Schune[138], H. R. Schwartz[139], A. Schwartzman[149], T. A. Schwarz[108], Ph. Schwemling[138], R. Schwienhorst[109], F. G. Sciacca[20], A. Sciandra[30], G. Sciolla[27], F. Scuri[74a], C. D. Sebastiani[37], K. Sedlaczek[118], S. C. Seidel[115], A. Seiden[139], B. D. Seidlitz[42], C. Seitz[48], J. M. Seixas[83b], G. Sekhniaidze[72a], L. Selem[60], N. Semprini-Cesari[24b,24a], A. Semushin[179], D. Sengupta[56], V. Senthilkumar[169], L. Serin[66], M. Sessa[72a,72b], H. Severini[123], F. Sforza[57b,57a], A. Sfyrla[56], Q. Sha[14], E. Shabalina[55], H. Shaddix[118], A. H. Shah[33], R. Shaheen[150], J. D. Shahinian[131], M. Shamim[37], L. Y. Shan[14], M. Shapiro[18a], A. Sharma[37], A. S. Sharma[170], P. Sharma[30], P. B. Shatalov[38], K. Shaw[152], S. M. Shaw[103], Q. Shen[14], D. J. Sheppard[148], P. Sherwood[98], L. Shi[98], X. Shi[14], S. Shimizu[84], C. O. Shimmin[178], I. P. J. Shipsey[129,*], S. Shirabe[90], M. Shiyakova[39,aa], M. J. Shochet[40], D. R. Shope[128], B. Shrestha[123], S. Shrestha[122,am], I. Shreyber[39], M. J. Shroff[171], P. Sicho[134], A. M. Sickles[168], E. Sideras Haddad[34g,166], A. C. Sidley[117], A. Sidoti[24b], F. Siegert[50], Dj. Sijacki[16], F. Sili[92], J. M. Silva[52], I. Silva Ferreira[83b],

M. V. Silva Oliveira[30], S. B. Silverstein[47a], S. Simion[66], R. Simoniello[37], E. L. Simpson[103], H. Simpson[152], L. R. Simpson[6], S. Simsek[82], S. Sindhu[55], P. Sinervo[161], S. N. Singh[27], S. Singh[30], S. Sinha[48], S. Sinha[103], M. Sioli[24b,24a], K. Sioulas[9], I. Siral[37], E. Sitnikova[48], J. Sjölin[47a,47b], A. Skaf[55], E. Skorda[21], P. Skubic[123], M. Slawinska[87], I. Slazyk[17], I. Sliusar[128], V. Smakhtin[175], B. H. Smart[137], S. Yu. Smirnov[140b], Y. Smirnov[82], L. N. Smirnova[38,a], O. Smirnova[100], A. C. Smith[42], D. R. Smith[165], J. L. Smith[103], M. B. Smith[35], R. Smith[149], H. Smitmanns[102], M. Smizanska[93], K. Smolek[135], P. Smolyanskiy[135], A. A. Snesarev[39], H. L. Snoek[117], S. Snyder[30], R. Sobie[171,ac], A. Soffer[157], C. A. Solans Sanchez[37], E. Yu. Soldatov[39], U. Soldevila[169], A. A. Solodkov[34g], S. Solomon[27], A. Soloshenko[39], K. Solovieva[54], O. V. Solovyanov[41], P. Sommer[50], A. Sonay[13], A. Sopczak[135], A. L. Sopio[52], F. Sopkova[29b], J. D. Sorenson[115], I. R. Sotarriva Alvarez[141], V. Sothilingam[63a], O. J. Soto Sandoval[140c,140b], S. Sottocornola[68], R. Soualah[88a], Z. Soumaimi[36e], D. South[48], N. Soybelman[175], S. Spagnolo[70a,70b], M. Spalla[112], D. Sperlich[54], B. Spisso[72a,72b], D. P. Spiteri[59], L. Splendori[104], M. Spousta[136], E. J. Staats[35], R. Stamen[63a], E. Stanecka[87], W. Stanek-Maslouska[48], M. V. Stange[50], B. Stanislaus[18a], M. M. Stanitzki[48], B. Stapf[48], E. A. Starchenko[38], G. H. Stark[139], J. Stark[91], P. Staroba[134], P. Starovoitov[88b], R. Staszewski[87], G. Stavropoulos[46], A. Stefl[37], P. Steinberg[30], B. Stelzer[148,162a], H. J. Stelzer[132], O. Stelzer[162a], H. Stenzel[58], T. J. Stevenson[152], G. A. Stewart[37], J. R. Stewart[124], M. C. Stockton[37], G. Stoicea[28b], M. Stolarski[133a], S. Stonjek[112], A. Straessner[50], J. Strandberg[150], S. Strandberg[47a,47b], M. Stratmann[177], M. Strauss[123], T. Strebler[104], P. Strizenec[29b], R. Ströhmer[172], D. M. Strom[126], R. Stroynowski[45], A. Strubig[47a,47b], S. A. Stucci[30], B. Stugu[17], J. Stupak[123], N. A. Styles[48], D. Su[149], S. Su[62], X. Su[62], D. Suchy[29a], K. Sugizaki[131], V. V. Sulin[38], M. J. Sullivan[94], D. M. S. Sultan[129], L. Sultanaliyeva[38], S. Sultansoy[3b], S. Sun[176], W. Sun[14], O. Sunneborn Gudnadottir[167], N. Sur[100], M. R. Sutton[152], H. Suzuki[163], M. Svatos[134], P. N. Swallow[33], M. Swiatlowski[162a], T. Swirski[172], I. Sykora[29a], M. Sykora[136], T. Sykora[136], D. Ta[102], K. Tackmann[48,z], A. Taffard[165], R. Tafirout[162a], Y. Takubo[84], M. Talby[104], A. A. Talyshev[38], K. C. Tam[64b], N. M. Tamir[157], A. Tanaka[159], J. Tanaka[159], R. Tanaka[66], M. Tanasini[151], Z. Tao[170], S. Tapia Araya[140f], S. Tapprogge[102], A. Tarek Abouelfadl Mohamed[109], S. Tarem[156], K. Tariq[14], G. Tarna[28b], G. F. Tartarelli[71a], M. J. Tartarin[91], P. Tas[136], M. Tasevsky[134], E. Tassi[44b,44a], A. C. Tate[168], G. Tateno[159], Y. Tayalati[36e,ab], G. N. Taylor[107], W. Taylor[162b], A. S. Tegetmeier[91], P. Teixeira-Dias[97], J. J. Teoh[161], K. Terashi[159], J. Terron[101], S. Terzo[13], M. Testa[53], R. J. Teuscher[161,ac], A. Thaler[79], O. Theiner[56], T. Theveneaux-Pelzer[104], D. W. Thomas[97], J. P. Thomas[21], E. A. Thompson[18a], P. D. Thompson[21], E. Thomson[131], R. E. Thornberry[45], C. Tian[62], Y. Tian[56], V. Tikhomirov[82], Yu. A. Tikhonov[39], S. Timoshenko[38], D. Timoshyn[136], E. X. L. Ting[1], P. Tipton[178], A. Tishelman-Charny[30], K. Todome[141], S. Todorova-Nova[136], S. Todt[50], L. Toffolin[69a,69c], M. Togawa[84], J. Tojo[90], S. Tokár[29a], O. Toldaiev[68], G. Tolkachev[104], M. Tomoto[84,113], L. Tompkins[149,o], E. Torrence[126], H. Torres[91], E. Torró Pastor[169], M. Toscani[31], C. Tosciri[40], M. Tost[11], D. R. Tovey[145], T. Trefzger[172], P. M. Tricarico[13], A. Tricoli[30], I. M. Trigger[162a], S. Trincaz-Duvoid[130], D. A. Trischuk[27], A. Tropina[39], L. Truong[34c], M. Trzebinski[87], A. Trzupek[87], F. Tsai[151], M. Tsai[108], A. Tsiamis[158], P. V. Tsiareshka[39], S. Tsigaridas[162a], A. Tsirigotis[158,v], V. Tsiskaridze[161], E. G. Tskhadadze[155a], M. Tsopoulou[158], Y. Tsujikawa[89], I. I. Tsukerman[38], V. Tsulaia[18a], S. Tsuno[84], K. Tsuri[121], D. Tsybychev[151], Y. Tu[64b], A. Tudorache[28b], V. Tudorache[28b], S. Turchikhin[57b,57a], I. Turk Cakir[3a], R. Turra[71a], T. Turtuvshin[39,ad], P. M. Tuts[42], S. Tzamarias[158,d], E. Tzovara[102], Y. Uematsu[84], F. Ukegawa[163], P. A. Ulloa Poblete[140c,140b], E. N. Umaka[30], G. Unal[37], A. Undrus[30], G. Unel[165], J. Urban[29b], P. Urrejola[140a], G. Usai[8], R. Ushioda[160], M. Usman[110], F. Ustuner[52], Z. Uysal[82], V. Vacek[135], B. Vachon[106], T. Vafeiadis[37], A. Vaitkus[98], C. Valderanis[111], E. Valdes Santurio[47a,47b], M. Valente[37], S. Valentinetti[24b,24a], A. Valero[169], E. Valiente Moreno[169], A. Vallier[91], J. A. Valls Ferrer[169], D. R. Van Arneman[117], T. R. Van Daalen[142], A. Van Der Graaf[49], H. Z. Van Der Schyf[34g], P. Van Gemmeren[6], M. Van Rijnbach[37], S. Van Stroud[98], I. Van Vulpen[117], P. Vana[136], M. Vanadia[76a,76b], U. M. Vande Voorde[150], W. Vandelli[37], E. R. Vandewall[124], D. Vannicola[157], L. Vannoli[53], R. Vari[75a], M. Varma[178], E. W. Varnes[7], C. Varni[18b], D. Varouchas[66], L. Varriale[169], K. E. Varvell[153], M. E. Vasile[28b], L. Vaslin[84], M. D. Vassilev[149], A. Vasyukov[39], L. M. Vaughan[124], R. Vavricka[136], T. Vazquez Schroeder[13], J. Veatch[32], V. Vecchio[103], M. J. Veen[105], I. Veliscek[30], I. Velkovska[95], L. M. Veloce[161], F. Veloso[133a,133c], S. Veneziano[75a], A. Ventura[70a,70b], S. Ventura Gonzalez[138], A. Verbytskyi[112], M. Verducci[74a,74b], C. Vergis[96], M. Verissimo De Araujo[83b], W. Verkerke[117], J. C. Vermeulen[117], C. Vernieri[149], M. Vessella[165], M. C. Vetterli[148,ai], A. Vgenopoulos[102], N. Viaux Maira[140f], T. Vickey[145], O. E. Vickey Boeriu[145], G. H. A. Viehhauser[129], L. Vigani[63b], M. Vigl[112], M. Villa[24b,24a], M. Villaplana Perez[169], E. M. Villhauer[40],

E. Vilucchi[53], M. Vincent[169], M. G. Vincter[35], A. Visibile[117], C. Vittori[37], I. Vivarelli[24b,24a], E. Voevodina[112], F. Vogel[111], J. C. Voigt[50], P. Vokac[135], Yu. Volkotrub[86b], E. Von Toerne[25], B. Vormwald[37], K. Vorobev[51], M. Vos[169], K. Voss[147], M. Vozak[37], L. Vozdecky[123], N. Vranjes[16], M. Vranjes Milosavljevic[16], M. Vreeswijk[117], N. K. Vu[144b,144a], R. Vuillermet[37], O. Vujinovic[102], I. Vukotic[40], I. K. Vyas[35], J. F. Wack[33], S. Wada[163], C. Wagner[149], J. M. Wagner[18a], W. Wagner[177], S. Wahdan[177], H. Wahlberg[92], C. H. Waits[123], J. Walder[137], R. Walker[111], K. Walkingshaw Pass[59], W. Walkowiak[147], A. Wall[131], E. J. Wallin[100], T. Wamorkar[18a], A. Wang[62], A. Z. Wang[139], C. Wang[102], C. Wang[11], H. Wang[18a], J. Wang[64c], P. Wang[103], P. Wang[98], R. Wang[61], R. Wang[6], S. M. Wang[154], S. Wang[14], T. Wang[62], T. Wang[62], W. T. Wang[80], W. Wang[14], X. Wang[168], X. Wang[144a], X. Wang[48], Y. Wang[114a], Y. Wang[62], Z. Wang[108], Z. Wang[144b], Z. Wang[108], C. Wanotayaroj[84], A. Warburton[106], A. L. Warnerbring[147], N. Warrack[59], S. Waterhouse[97], A. T. Watson[21], H. Watson[52], M. F. Watson[21], E. Watton[59], G. Watts[142], B. M. Waugh[98], J. M. Webb[54], C. Weber[30], H. A. Weber[19], M. S. Weber[20], S. M. Weber[63a], C. Wei[62], Y. Wei[54], A. R. Weidberg[129], E. J. Weik[120], J. Weingarten[49], C. Weiser[54], C. J. Wells[48], T. Wenaus[30], B. Wendland[49], T. Wengler[37], N. S. Wenke[112], N. Wermes[25], M. Wessels[63a], A. M. Wharton[93], A. S. White[61], A. White[8], M. J. White[1], D. Whiteson[165], L. Wickremasinghe[127], W. Wiedenmann[176], M. Wielers[137], R. Wierda[150], C. Wiglesworth[43], H. G. Wilkens[37], J. J. H. Wilkinson[33], D. M. Williams[42], H. H. Williams[131], S. Williams[33], S. Willocq[105], B. J. Wilson[103], D. J. Wilson[103], P. J. Windischhofer[40], F. I. Winkel[31], F. Winklmeier[126], B. T. Winter[54], M. Wittgen[149], M. Wobisch[99], T. Wojtkowski[60], Z. Wolffs[117], J. Wollrath[37], M. W. Wolter[87], H. Wolters[133a,133c], M. C. Wong[139], E. L. Woodward[42], S. D. Worm[48], B. K. Wosiek[87], K. W. Woźniak[87], S. Wozniewski[55], K. Wraight[59], C. Wu[161], C. Wu[21], J. Wu[159], M. Wu[114b], M. Wu[116], S. L. Wu[176], S. Wu[14], X. Wu[62], Y. Wu[62], Z. Wu[4], J. Wuerzinger[112], T. R. Wyatt[103], B. M. Wynne[52], S. Xella[43], L. Xia[114a], M. Xia[15], M. Xie[62], A. Xiong[126], J. Xiong[18a], D. Xu[14], H. Xu[62], L. Xu[62], R. Xu[131], T. Xu[108], Y. Xu[142], Z. Xu[52], Z. Xu[114a], B. Yabsley[153], S. Yacoob[34a], Y. Yamaguchi[84], E. Yamashita[159], H. Yamauchi[163], T. Yamazaki[18a], Y. Yamazaki[85], S. Yan[59], Z. Yan[105], H. J. Yang[144a,144b], H. T. Yang[62], S. Yang[62], T. Yang[64c], X. Yang[37], X. Yang[14], Y. Yang[159], Y. Yang[62], W-M. Yao[18a], C. L. Yardley[152], J. Ye[14], S. Ye[30], X. Ye[62], Y. Yeh[98], I. Yeletskikh[39], B. Yeo[18b], M. R. Yexley[98], T. P. Yildirim[129], P. Yin[42], K. Yorita[174], C. J. S. Young[37], C. Young[149], N. D. Young[126], Y. Yu[62], J. Yuan[14,114c], M. Yuan[108], R. Yuan[144b,144a], L. Yue[98], M. Zaazoua[62], B. Zabinski[87], I. Zahir[36a], A. Zaio[57b,57a], Z. K. Zak[87], T. Zakareishvili[169], S. Zambito[56], J. A. Zamora Saa[140d], J. Zang[159], R. Zanzottera[71a,71b], O. Zaplatilek[135], C. Zeitnitz[177], H. Zeng[14], J. C. Zeng[168], D. T. Zenger Jr[27], O. Zenin[38], T. Ženiš[29a], S. Zenz[96], D. Zerwas[66], M. Zhai[14,114c], D. F. Zhang[145], G. Zhang[14], J. Zhang[143a], J. Zhang[6], K. Zhang[14,114c], L. Zhang[62], L. Zhang[114a], P. Zhang[14,114c], R. Zhang[114a], S. Zhang[91], T. Zhang[159], Y. Zhang[142], Y. Zhang[98], Y. Zhang[62], Y. Zhang[114a], Z. Zhang[143a], Z. Zhang[66], H. Zhao[142], T. Zhao[143a], Y. Zhao[35], Z. Zhao[62], Z. Zhao[62], A. Zhemchugov[39], J. Zheng[114a], K. Zheng[168], X. Zheng[62], Z. Zheng[149], D. Zhong[168], B. Zhou[108], H. Zhou[7], N. Zhou[144a], Y. Zhou[15], Y. Zhou[114a], Y. Zhou[7], C. G. Zhu[143a], J. Zhu[108], X. Zhu[144b], Y. Zhu[144a], Y. Zhu[62], X. Zhuang[14], K. Zhukov[68], N. I. Zimine[39], J. Zinsser[63b], M. Ziolkowski[147], L. Živković[16], A. Zoccoli[24b,24a], K. Zoch[61], A. Zografos[37], T. G. Zorbas[145], O. Zormpa[46], L. Zwalinski[37]

[1] Department of Physics, University of Adelaide, Adelaide, Australia
[2] Department of Physics, University of Alberta, Edmonton, AB, Canada
[3] [(a)]Department of Physics, Ankara University, Ankara, Türkiye; [(b)]Division of Physics, TOBB University of Economics and Technology, Ankara, Türkiye
[4] LAPP, Université Savoie Mont Blanc, CNRS/IN2P3, Annecy, France
[5] APC, Université Paris Cité, CNRS/IN2P3, Paris, France
[6] High Energy Physics Division, Argonne National Laboratory, Argonne, IL, USA
[7] Department of Physics, University of Arizona, Tucson, AZ, USA
[8] Department of Physics, University of Texas at Arlington, Arlington, TX, USA
[9] Physics Department, National and Kapodistrian University of Athens, Athens, Greece
[10] Physics Department, National Technical University of Athens, Zografou, Greece
[11] Department of Physics, University of Texas at Austin, Austin, TX, USA
[12] Institute of Physics, Azerbaijan Academy of Sciences, Baku, Azerbaijan
[13] Institut de Física d'Altes Energies (IFAE), Barcelona Institute of Science and Technology, Barcelona, Spain

[14] Institute of High Energy Physics, Chinese Academy of Sciences, Beijing, China
[15] Physics Department, Tsinghua University, Beijing, China
[16] Institute of Physics, University of Belgrade, Belgrade, Serbia
[17] Department for Physics and Technology, University of Bergen, Bergen, Norway
[18] [(a)]Physics Division, Lawrence Berkeley National Laboratory, Berkeley, CA, USA; [(b)]University of California, Berkeley, CA, USA
[19] Institut für Physik, Humboldt Universität zu Berlin, Berlin, Germany
[20] Albert Einstein Center for Fundamental Physics and Laboratory for High Energy Physics, University of Bern, Bern, Switzerland
[21] School of Physics and Astronomy, University of Birmingham, Birmingham, UK
[22] [(a)]Department of Physics, Bogazici University, Istanbul, Türkiye; [(b)]Department of Physics Engineering, Gaziantep University, Gaziantep, Türkiye; [(c)]Department of Physics, Istanbul University, Istanbul, Türkiye
[23] [(a)]Facultad de Ciencias y Centro de Investigaciónes, Universidad Antonio Nariño, Bogotá, Colombia; [(b)]Departamento de Física, Universidad Nacional de Colombia, Bogotá, Colombia
[24] [(a)]Dipartimento di Fisica e Astronomia A. Righi, Università di Bologna, Bologna, Italy; [(b)]INFN Sezione di Bologna, Bologna, Italy
[25] Physikalisches Institut, Universität Bonn, Bonn, Germany
[26] Department of Physics, Boston University, Boston, MA, USA
[27] Department of Physics, Brandeis University, Waltham, MA, USA
[28] [(a)]Transilvania University of Brasov, Brasov, Romania; [(b)]Horia Hulubei National Institute of Physics and Nuclear Engineering, Bucharest, Romania; [(c)]Department of Physics, Alexandru Ioan Cuza University of Iasi, Iasi, Romania; [(d)]National Institute for Research and Development of Isotopic and Molecular Technologies, Physics Department, Cluj-Napoca, Romania; [(e)]National University of Science and Technology Politechnica, Bucharest, Romania; [(f)]West University in Timisoara, Timisoara, Romania; [(g)]Faculty of Physics, University of Bucharest, Bucharest, Romania
[29] [(a)]Faculty of Mathematics, Physics and Informatics, Comenius University, Bratislava, Slovakia; [(b)]Department of Subnuclear Physics, Institute of Experimental Physics of the Slovak Academy of Sciences, Kosice, Slovak Republic
[30] Physics Department, Brookhaven National Laboratory, Upton, NY, USA
[31] Universidad de Buenos Aires, Facultad de Ciencias Exactas y Naturales, Departamento de Física, y CONICET, Instituto de Física de Buenos Aires (IFIBA), Buenos Aires, Argentina
[32] California State University, Long Beach, CA, USA
[33] Cavendish Laboratory, University of Cambridge, Cambridge, UK
[34] [(a)]Department of Physics, University of Cape Town, Cape Town, South Africa; [(b)]iThemba Labs, Western Cape, South Africa; [(c)]Department of Mechanical Engineering Science, University of Johannesburg, Johannesburg, South Africa; [(d)]National Institute of Physics, University of the Philippines, Diliman, Philippines; [(e)]Department of Physics, University of South Africa, Pretoria, South Africa; [(f)]University of Zululand, KwaDlangezwa, South Africa; [(g)]School of Physics, University of the Witwatersrand, Johannesburg, South Africa
[35] Department of Physics, Carleton University, Ottawa, ON, Canada
[36] [(a)]Faculté des Sciences Ain Chock, Université Hassan II de Casablanca, Casablanca, Morocco; [(b)]Faculté des Sciences, Université Ibn-Tofail, Kénitra, Morocco; [(c)]Faculté des Sciences Semlalia, Université Cadi Ayyad, LPHEA-Marrakech, Morocco; [(d)]LPMR, Faculté des Sciences, Université Mohamed Premier, Oujda, Morocco; [(e)]Faculté des sciences, Université Mohammed V, Rabat, Morocco; [(f)]Institute of Applied Physics, Mohammed VI Polytechnic University, Ben Guerir, Morocco
[37] CERN, Geneva, Switzerland
[38] Affiliated with an Institute Formerly Covered by a Cooperation Agreement with CERN, Geneva, Switzerland
[39] Affiliated with an International Laboratory Covered by a Cooperation Agreement with CERN, Geneva, Switzerland
[40] Enrico Fermi Institute, University of Chicago, Chicago, IL, USA
[41] LPC, Université Clermont Auvergne, CNRS/IN2P3, Clermont-Ferrand, France
[42] Nevis Laboratory, Columbia University, Irvington, NY, USA
[43] Niels Bohr Institute, University of Copenhagen, Copenhagen, Denmark
[44] [(a)]Dipartimento di Fisica, Università della Calabria, Rende, Italy; [(b)]INFN Gruppo Collegato di Cosenza, Laboratori Nazionali di Frascati, Frascati, Italy
[45] Physics Department, Southern Methodist University, Dallas, TX, USA

[46] National Centre for Scientific Research "Demokritos", Agia Paraskevi, Greece
[47] [(a)]Department of Physics, Stockholm University, Stockholm, Sweden; [(b)]Oskar Klein Centre, Stockholm, Sweden
[48] Deutsches Elektronen-Synchrotron DESY, Hamburg and Zeuthen, Germany
[49] Fakultät Physik , Technische Universität Dortmund, Dortmund, Germany
[50] Institut für Kern- und Teilchenphysik, Technische Universität Dresden, Dresden, Germany
[51] Department of Physics, Duke University, Durham, NC, USA
[52] SUPA-School of Physics and Astronomy, University of Edinburgh, Edinburgh, UK
[53] INFN e Laboratori Nazionali di Frascati, Frascati, Italy
[54] Physikalisches Institut, Albert-Ludwigs-Universität Freiburg, Freiburg, Germany
[55] II. Physikalisches Institut, Georg-August-Universität Göttingen, Göttingen, Germany
[56] Département de Physique Nucléaire et Corpusculaire, Université de Genève, Geneva, Switzerland
[57] [(a)]Dipartimento di Fisica, Università di Genova, Genova, Italy; [(b)]INFN Sezione di Genova, Genova, Italy
[58] II. Physikalisches Institut, Justus-Liebig-Universität Giessen, Giessen, Germany
[59] SUPA-School of Physics and Astronomy, University of Glasgow, Glasgow, UK
[60] LPSC, Université Grenoble Alpes, CNRS/IN2P3, Grenoble INP, Grenoble, France
[61] Laboratory for Particle Physics and Cosmology, Harvard University, Cambridge, MA, USA
[62] Department of Modern Physics and State Key Laboratory of Particle Detection and Electronics, University of Science and Technology of China, Hefei, China
[63] [(a)]Kirchhoff-Institut für Physik, Ruprecht-Karls-Universität Heidelberg, Heidelberg, Germany; [(b)]Physikalisches Institut, Ruprecht-Karls-Universität Heidelberg, Heidelberg, Germany
[64] [(a)]Department of Physics, Chinese University of Hong Kong, Shatin, N.T., Hong Kong, China; [(b)]Department of Physics, University of Hong Kong, Hong Kong, China; [(c)]Department of Physics and Institute for Advanced Study, Hong Kong University of Science and Technology, Clear Water Bay, Kowloon, Hong Kong, China
[65] Department of Physics, National Tsing Hua University, Hsinchu, Taiwan
[66] IJCLab, Université Paris-Saclay, CNRS/IN2P3, 91405 Orsay, France
[67] Centro Nacional de Microelectrónica (IMB-CNM-CSIC), Barcelona, Spain
[68] Department of Physics, Indiana University, Bloomington, IN, USA
[69] [(a)]INFN Gruppo Collegato di Udine, Sezione di Trieste, Udine, Italy; [(b)]ICTP, Trieste, Italy; [(c)]Dipartimento Politecnico di Ingegneria e Architettura, Università di Udine, Udine, Italy
[70] [(a)]INFN Sezione di Lecce, Lecce, Italy; [(b)]Dipartimento di Matematica e Fisica, Università del Salento, Lecce, Italy
[71] [(a)]INFN Sezione di Milano, Milan, Italy; [(b)]Dipartimento di Fisica, Università di Milano, Milan, Italy
[72] [(a)]INFN Sezione di Napoli, Naples, Italy; [(b)]Dipartimento di Fisica, Università di Napoli, Naples, Italy
[73] [(a)]INFN Sezione di Pavia, Pavia, Italy; [(b)]Dipartimento di Fisica, Università di Pavia, Pavia, Italy
[74] [(a)]INFN Sezione di Pisa, Pisa, Italy; [(b)]Dipartimento di Fisica E. Fermi, Università di Pisa, Pisa, Italy
[75] [(a)]INFN Sezione di Roma, Rome, Italy; [(b)]Dipartimento di Fisica, Sapienza Università di Roma, Rome, Italy
[76] [(a)]INFN Sezione di Roma Tor Vergata, Rome, Italy; [(b)]Dipartimento di Fisica, Università di Roma Tor Vergata, Rome, Italy
[77] [(a)]INFN Sezione di Roma Tre, Rome, Italy; [(b)]Dipartimento di Matematica e Fisica, Università Roma Tre, Rome, Italy
[78] [(a)]INFN-TIFPA, Povo, Italy; [(b)]Università degli Studi di Trento, Trento, Italy
[79] Department of Astro and Particle Physics, Universität Innsbruck, Innsbruck, Austria
[80] University of Iowa, Iowa City, IA, USA
[81] Department of Physics and Astronomy, Iowa State University, Ames, IA, USA
[82] Istinye University, Sariyer, Istanbul, Türkiye
[83] [(a)]Departamento de Engenharia Elétrica, Universidade Federal de Juiz de Fora (UFJF), Juiz de Fora, Brazil; [(b)]Universidade Federal do Rio De Janeiro COPPE/EE/IF, Rio de Janeiro, Brazil; [(c)]Instituto de Física, Universidade de São Paulo, São Paulo, Brazil; [(d)]Rio de Janeiro State University, Rio de Janeiro, Brazil; [(e)]Federal University of Bahia, Bahia, Brazil
[84] KEK, High Energy Accelerator Research Organization, Tsukuba, Japan
[85] Graduate School of Science, Kobe University, Kobe, Japan
[86] [(a)]Faculty of Physics and Applied Computer Science, AGH University of Krakow, Krakow, Poland; [(b)]Marian Smoluchowski Institute of Physics, Jagiellonian University, Krakow, Poland
[87] Institute of Nuclear Physics Polish Academy of Sciences, Krakow, Poland

[88] [(a)]Khalifa University of Science and Technology, Abu Dhabi, United Arab Emirates; [(b)]University of Sharjah, Sharjah, United Arab Emirates
[89] Faculty of Science, Kyoto University, Kyoto, Japan
[90] Research Center for Advanced Particle Physics and Department of Physics, Kyushu University, Fukuoka , Japan
[91] L2IT, Université de Toulouse, CNRS/IN2P3, UPS, Toulouse, France
[92] Instituto de Física La Plata, Universidad Nacional de La Plata and CONICET, La Plata, Argentina
[93] Physics Department, Lancaster University, Lancaster, UK
[94] Oliver Lodge Laboratory, University of Liverpool, Liverpool, UK
[95] Department of Experimental Particle Physics, Jožef Stefan Institute and Department of Physics, University of Ljubljana, Ljubljana, Slovenia
[96] Department of Physics and Astronomy, Queen Mary University of London, London, UK
[97] Department of Physics, Royal Holloway University of London, Egham, UK
[98] Department of Physics and Astronomy, University College London, London, UK
[99] Louisiana Tech University, Ruston, LA, USA
[100] Fysiska institutionen, Lunds universitet, Lund, Sweden
[101] Departamento de Física Teorica C-15 and CIAFF, Universidad Autónoma de Madrid, Madrid, Spain
[102] Institut für Physik, Universität Mainz, Mainz, Germany
[103] School of Physics and Astronomy, University of Manchester, Manchester, UK
[104] CPPM, Aix-Marseille Université, CNRS/IN2P3, Marseille, France
[105] Department of Physics, University of Massachusetts, Amherst, MA, USA
[106] Department of Physics, McGill University, Montreal, QC, Canada
[107] School of Physics, University of Melbourne, Victoria, Australia
[108] Department of Physics, University of Michigan, Ann Arbor, MI, USA
[109] Department of Physics and Astronomy, Michigan State University, East Lansing, MI, USA
[110] Group of Particle Physics, University of Montreal, Montreal, QC, Canada
[111] Fakultät für Physik, Ludwig-Maximilians-Universität München, Munich, Germany
[112] Max-Planck-Institut für Physik (Werner-Heisenberg-Institut), Munich, Germany
[113] Graduate School of Science and Kobayashi-Maskawa Institute, Nagoya University, Nagoya, Japan
[114] [(a)]Department of Physics, Nanjing University, Nanjing, China; [(b)]School of Science, Shenzhen Campus of Sun Yat-sen University, Shenzhen, China; [(c)]University of Chinese Academy of Science (UCAS), Beijing, China
[115] Department of Physics and Astronomy, University of New Mexico, Albuquerque, NM, USA
[116] Institute for Mathematics, Astrophysics and Particle Physics, Radboud University/Nikhef, Nijmegen, The Netherlands
[117] Nikhef National Institute for Subatomic Physics and University of Amsterdam, Amsterdam, The Netherlands
[118] Department of Physics, Northern Illinois University, DeKalb, IL, USA
[119] [(a)]New York University Abu Dhabi, Abu Dhabi, United Arab Emirates; [(b)]United Arab Emirates University, Al Ain, United Arab Emirates
[120] Department of Physics, New York University, New York, NY, USA
[121] Ochanomizu University, Otsuka, Bunkyo-ku, Tokyo, Japan
[122] Ohio State University, Columbus, OH, USA
[123] Homer L. Dodge Department of Physics and Astronomy, University of Oklahoma, Norman, OK, USA
[124] Department of Physics, Oklahoma State University, Stillwater, OK, USA
[125] Palacký University, Joint Laboratory of Optics, Olomouc, Czech Republic
[126] Institute for Fundamental Science, University of Oregon, Eugene, OR, USA
[127] Graduate School of Science, University of Osaka, Osaka, Japan
[128] Department of Physics, University of Oslo, Oslo, Norway
[129] Department of Physics, Oxford University, Oxford, UK
[130] LPNHE, Sorbonne Université, Université Paris Cité, CNRS/IN2P3, Paris, France
[131] Department of Physics, University of Pennsylvania, Philadelphia, PA, USA
[132] Department of Physics and Astronomy, University of Pittsburgh, Pittsburgh, PA, USA
[133] [(a)]Laboratório de Instrumentação e Física Experimental de Partículas - LIP, Lisbon, Portugal; [(b)]Departamento de Física, Faculdade de Ciências, Universidade de Lisboa, Lisbon, Portugal; [(c)]Departamento de Física, Universidade de Coimbra, Coimbra, Portugal; [(d)]Centro de Física Nuclear da Universidade de Lisboa, Lisbon, Portugal; [(e)]Departamento de Física, Escola de Ciências, Universidade do Minho, Braga, Portugal; [(f)]Departamento de Física Teórica y del Cosmos,

Universidad de Granada, Granada, Spain; [g]Departamento de Física, Instituto Superior Técnico, Universidade de Lisboa, Lisbon, Portugal
[134] Institute of Physics of the Czech Academy of Sciences, Prague, Czech Republic
[135] Czech Technical University in Prague, Prague, Czech Republic
[136] Faculty of Mathematics and Physics, Charles University, Prague, Czech Republic
[137] Particle Physics Department, Rutherford Appleton Laboratory, Didcot, UK
[138] IRFU, CEA, Université Paris-Saclay, Gif-sur-Yvette, France
[139] Santa Cruz Institute for Particle Physics, University of California Santa Cruz, Santa Cruz, CA, USA
[140] [a]Departamento de Física, Pontificia Universidad Católica de Chile, Santiago, Chile; [b]Millennium Institute for Subatomic Physics at High Energy Frontier (SAPHIR), Santiago, Chile; [c]Instituto de Investigación Multidisciplinario en Ciencia y Tecnología y Departamento de Física, Universidad de La Serena, La Serena, Chile; [d]Universidad Andres Bello, Department of Physics, Santiago, Chile; [e]Instituto de Alta Investigación, Universidad de Tarapacá, Arica, Chile; [f]Departamento de Física, Universidad Técnica Federico Santa María, Valparaíso, Chile
[141] Department of Physics, Institute of Science, Tokyo, Japan
[142] Department of Physics, University of Washington, Seattle, WA, USA
[143] [a]Institute of Frontier and Interdisciplinary Science and Key Laboratory of Particle Physics and Particle Irradiation (MOE), Shandong University, Qingdao, China; [b]School of Physics, Zhengzhou University, Zhengzhou, China
[144] [a]State Key Laboratory of Dark Matter Physics, School of Physics and Astronomy, Shanghai Jiao Tong University, Key Laboratory for Particle Astrophysics and Cosmology (MOE), SKLPPC, Shanghai, China; [b]State Key Laboratory of Dark Matter Physics, Tsung-Dao Lee Institute, Shanghai Jiao Tong University, Shanghai, China
[145] Department of Physics and Astronomy, University of Sheffield, Sheffield, UK
[146] Department of Physics, Shinshu University, Nagano, Japan
[147] Department Physik, Universität Siegen, Siegen, Germany
[148] Department of Physics, Simon Fraser University, Burnaby, BC, Canada
[149] SLAC National Accelerator Laboratory, Stanford, CA, USA
[150] Department of Physics, Royal Institute of Technology, Stockholm, Sweden
[151] Departments of Physics and Astronomy, Stony Brook University, Stony Brook, NY, USA
[152] Department of Physics and Astronomy, University of Sussex, Brighton, UK
[153] School of Physics, University of Sydney, Sydney, Australia
[154] Institute of Physics, Academia Sinica, Taipei, Taiwan
[155] [a]E. Andronikashvili Institute of Physics, Iv. Javakhishvili Tbilisi State University, Tbilisi, Georgia; [b]High Energy Physics Institute, Tbilisi State University, Tbilisi, Georgia; [c]University of Georgia, Tbilisi, Georgia
[156] Department of Physics, Technion, Israel Institute of Technology, Haifa, Israel
[157] Raymond and Beverly Sackler School of Physics and Astronomy, Tel Aviv University, Tel Aviv, Israel
[158] Department of Physics, Aristotle University of Thessaloniki, Thessaloniki, Greece
[159] International Center for Elementary Particle Physics and Department of Physics, University of Tokyo, Tokyo, Japan
[160] Graduate School of Science and Technology, Tokyo Metropolitan University, Tokyo, Japan
[161] Department of Physics, University of Toronto, Toronto, ON, Canada
[162] [a]TRIUMF, Vancouver, BC, Canada; [b]Department of Physics and Astronomy, York University, Toronto, ON, Canada
[163] Division of Physics and Tomonaga Center for the History of the Universe, Faculty of Pure and Applied Sciences, University of Tsukuba, Tsukuba, Japan
[164] Department of Physics and Astronomy, Tufts University, Medford, MA, USA
[165] Department of Physics and Astronomy, University of California Irvine, Irvine, CA, USA
[166] University of West Attica, Athens, Greece
[167] Department of Physics and Astronomy, University of Uppsala, Uppsala, Sweden
[168] Department of Physics, University of Illinois, Urbana, IL, USA
[169] Instituto de Física Corpuscular (IFIC), Centro Mixto Universidad de Valencia - CSIC, Valencia, Spain
[170] Department of Physics, University of British Columbia, Vancouver, BC, Canada
[171] Department of Physics and Astronomy, University of Victoria, Victoria, BC, Canada
[172] Fakultät für Physik und Astronomie, Julius-Maximilians-Universität Würzburg, Würzburg, Germany
[173] Department of Physics, University of Warwick, Coventry, UK
[174] Waseda University, Tokyo, Japan
[175] Department of Particle Physics and Astrophysics, Weizmann Institute of Science, Rehovot, Israel

[176] Department of Physics, University of Wisconsin, Madison, WI, USA
[177] Fakultät für Mathematik und Naturwissenschaften, Fachgruppe Physik, Bergische Universität Wuppertal, Wuppertal, Germany
[178] Department of Physics, Yale University, New Haven, CT, USA
[179] Yerevan Physics Institute, Yerevan, Armenia

[a] Also at Affiliated with an Institute Formerly Covered by a Cooperation Agreement with CERN, Geneva, Switzerland
[b] Also at An-Najah National University, Nablus, Palestine
[c] Also at Borough of Manhattan Community College, City University of New York, New York, NY, USA
[d] Also at Center for Interdisciplinary Research and Innovation (CIRI-AUTH), Thessaloniki, Greece
[e] Also at Centre of Physics of the Universities of Minho and Porto (CF-UM-UP), Braga, Portugal
[f] Also at CERN, Geneva, Switzerland
[g] Also at CMD-AC UNEC Research Center, Azerbaijan State University of Economics (UNEC), Baku, Azerbaijan
[h] Also at Département de Physique Nucléaire et Corpusculaire, Université de Genève, Geneva, Switzerland
[i] Also at Departament de Fisica de la Universitat Autonoma de Barcelona, Barcelona, Spain
[j] Also at Department of Financial and Management Engineering, University of the Aegean, Chios, Greece
[k] Also at Department of Mathematical Sciences, University of South Africa, Johannesburg, South Africa
[l] Also at Department of Modern Physics and State Key Laboratory of Particle Detection and Electronics, University of Science and Technology of China, Hefei, China
[m] Also at Department of Physics, Bolu Abant Izzet Baysal University, Bolu, Türkiye
[n] Also at Department of Physics, King's College London, London, UK
[o] Also at Department of Physics, Stanford University, Stanford, CA, USA
[p] Also at Department of Physics, Stellenbosch University, Stellenbosch, South Africa
[q] Also at Department of Physics, University of Fribourg, Fribourg, Switzerland
[r] Also at Department of Physics, University of Thessaly, Volos, Greece
[s] Also at Department of Physics, Westmont College, Santa Barbara, USA
[t] Also at Faculty of Physics, Sofia University, 'St. Kliment Ohridski', Sofia, Bulgaria
[u] Also at Faculty of Physics, University of Bucharest, Bucharest, Romania
[v] Also at Hellenic Open University, Patras, Greece
[w] Also at Henan University, Kaifeng, China
[x] Also at Imam Mohammad Ibn Saud Islamic University, Riyadh, Saudi Arabia
[y] Also at Institucio Catalana de Recerca i Estudis Avancats, ICREA, Barcelona, Spain
[z] Also at Institut für Experimentalphysik, Universität Hamburg, Hamburg, Germany
[aa] Also at Institute for Nuclear Research and Nuclear Energy (INRNE) of the Bulgarian Academy of Sciences, Sofia, Bulgaria
[ab] Also at Institute of Applied Physics, Mohammed VI Polytechnic University, Ben Guerir, Morocco
[ac] Also at Institute of Particle Physics (IPP), Toronto, Canada
[ad] Also at Institute of Physics and Technology, Mongolian Academy of Sciences, Ulaanbaatar, Mongolia
[ae] Also at Institute of Physics, Azerbaijan Academy of Sciences, Baku, Azerbaijan
[af] Also at Institute of Theoretical Physics, Ilia State University, Tbilisi, Georgia
[ag] Also at National Institute of Physics, University of the Philippines, Diliman, Philippines
[ah] Also at The Collaborative Innovation Center of Quantum Matter (CICQM), Beijing, China
[ai] Also at TRIUMF, Vancouver, BC, Canada
[aj] Also at Università di Napoli Parthenope, Naples, Italy
[ak] Also at Department of Physics, University of Colorado, Boulder, CO, USA
[al] Also at University of Siena, Siena, Italy
[am] Also at Washington College, Chestertown, MD, USA
[an] Also at Physics Department, Yeditepe University, Istanbul, Türkiye
* Deceased